ROBUST COUPLED OPTIMIZATION OF AIRCRAFT FAMILY DESIGN AND FLEET ALLOCATION FOR MULTIPLE MARKETS

OPTIMISATION ROBUSTE DE LA CONCEPTION DE FAMILLE D'AÉRONEFS ET DE RÉPARTITION DE LA FLOTTE DANS DIVERS MARCHÉS POUR DES SYSTÈMES TOTALEMENT COUPLÉS

A Thesis Submitted to the Division of Graduate Studies
of the Royal Military College of Canada
by

Peter W. Jansen, B.Eng., M.A.Sc.

In Partial Fulfillment of the Requirements for the Degree of
Doctor of Philosophy in Mechanical and Aerospace Engineering

March, 2015

To my family

Acknowledgments

First, I would like to express my gratitude to my supervisor, Dr. Ruben E. Perez, for giving me the opportunity to pursue this research. His guidance and vast knowledge of aircraft design and in the field of optimization were extremely valuable to this work.

I would also like to thank all the past and present members in our grad student office. Their friendship and enthusiasm for discussions made the time at RMC with all its quirks very enjoyable. I also appreciate all the time they spend listening patiently when I discussed some of my ideas and problems with them and thank them for their feedback and insight. The same thanks also extends to several members of the mechanical and aerospace engineering faculty.

Last, but not least, I would like to thank Debbie Fisher for the many hours she spend editing and proof reading some of my documents, including this one, taking care of travel arrangements and filling out the time-sheets.

Abstract

Jansen, Peter Willi. Ph.D. Royal Military College of Canada, March 2015. *Robust Coupled Optimization of Aircraft Family Design and Fleet Allocation for Multiple Markets.* Supervised by Ruben E. Perez, B.Eng., M.A.Sc., Ph.D., P.Eng., Assistant Professor.

Increasing air traffic demand and the resulting climate impact of aircraft are of growing public concern. The requirements for new commercial aircraft can differ significantly for different markets and operators. The design of new aircraft takes into account different markets and operational requirements; the design process is only loosely coupled with the use of these aircraft by operators around the world. The economic and environmental sustainability of commercial aviation requires not only the design of efficient new aircraft, but also closer consideration of the operations and flexibility of these aircraft during the design stage. This can be achieved by coupling the design optimization of multiple aircraft families with the simultaneous allocation of these aircraft in multiple markets. Including operational assignment of aircraft in the design stage can reduce operational inefficiencies, while the design of an aircraft family aims at reducing cost through the use of common components. In order to thoroughly investigate the trade–offs involved in designing efficient, environmentally sustainable aircraft, a coupled robust design optimization involving uncertainties in passenger demand over multiple years of operations was conducted. Results obtained show that the coupled design of aircraft families with the allocation of these aircraft to two distinct markets can significantly reduce fuel burn, operating and acquisition costs compared to existing aircraft. The optimized aircraft also provide higher flexibility and improved performance when compared against aircraft obtained from a robust design optimization approach, where each aircraft is optimized decoupled from the fleet allocation.

Keywords: aircraft families, sustainable aviation, optimization under uncertainty, fleet allocation, aircraft conceptual design.

resume

Jansen, Peter Willi. Ph.D. , Mars 2015. *Optimisation robuste de la conception de famille d'aéronefs et de répartition de la flotte dans divers marchés pour des systèmes totalement couplés.* par Ruben E. Perez, B.Eng., M.A.Sc., Ph.D., P.Eng., Professeur adjoint.

L'augmentation de la circulation aérienne et son impacte sur l'environnement sont une préoccupation croissante du publique. Les critères de conceptions de nouveaux appareils commerciaux varient grandement selon le marché et l'opération. La conception de nouveaux appareils tient compte des marchés et des besoins opérationnels mais le processus de design n'est que faiblement couplé aux emploies de ces appareils par les exploitants d'aéronefs à travers le monde. La durabilité économique et environnemental de l'aviation commerciale exige non seulement un appareil économe mais aussi une plus importante considération de comment ses appareils sont utilisés lors de la conception. Pour parvenir à ceci on doit coupler la conception des familles d'avions aux affectations des appareils dans divers marchés. Inclure l'affectation dans le processus de design peut réduire les inefficiences opérationnelles, alors que la conception de famille d'appareils à pour but de réduire les couts en utilisant de assemblages communs. Pour étudier à fond les compromis requis lors d'une conception d'appareils économiquement et environnementalement durable, une optimisation robuste et totalement couplée utilisant des incertitudes de la demande passagère sur plusieurs années d'opérations fut réalisée. Les résultats démontrent que coupler la conception de familles d'avions avec les affectations de ces appareils à deux marchés distincts peut grandement diminuer la consommation d'essence, les couts d'opérations et d'acquisitions comparés aux appareils existants. Les appareils optimisés permettent une plus grande flexibilité et une meilleure performance que des appareils conçus par une optimisation robuste où chaque appareil est découplé de leur affectation.
Mot clés: Familles d'avions, aviation durable, optimisation et incertitude, affectation de flotte aérienne, conception d'aéronef.

Contents

Acknowledgments **iii**

Abstract **iv**

resume **v**

List of Tables **ix**

List of Figures **xi**

Nomenclature **xv**

1 Introduction **1**
1.1 Motivation 1
1.2 Objectives and Significance 5
1.3 Overview 6
1.4 Contributions 6

2 Literature Review **8**
2.1 Aircraft Design and Environmental Considerations 8
2.2 Coupled Aircraft Design and Network Allocation 11
2.3 Aircraft Family Design 17

3 Aircraft Conceptual Design **20**
3.1 Aircraft Conceptual Design Toolbox 20
3.1.1 Aircraft Definition 21
3.1.2 Weight and Balance 23
3.1.3 Aerodynamics 24
3.1.4 Propulsion 27
3.1.5 Performance 28
3.1.6 The Economics Model 31

3.2 Aircraft Family Design 35
3.2.1 The Modeling of Commonality 39
Commonality Effect on Weight 40
Commonality Effect on Cost 40
3.2.2 Existing Aircraft Families 43

4 Fleet Allocation **45**
4.1 Representative Route Networks 46
4.1.1 North American Network 47
4.1.2 European Network 48
4.1.3 Modelling Future Demand 50
4.2 Fleet Allocation Problem 54
4.2.1 Solving the Allocation Problem 58
4.3 Fleet Allocation Verification 61
4.3.1 Energy Intensity 62
4.3.2 Reference Aircraft Network Performance 63
North American Routes 63
European Routes 66

5 Decoupled Robust Design of Aircraft **71**
5.1 Robust Design Optimization 72
5.1.1 Modeling Uncertainty 72
5.1.2 Uncertainty Propagation 74
5.1.3 Robust Optimization Formulation 75
5.2 Robust Optimization Test Case 76
5.2.1 Aircraft Design Variables 77
5.2.2 Aircraft Design Constraints 78
5.3 Robust Optimization Results 81
5.3.1 Robust Aircraft Network Performance 84
North American Routes 84
European Routes 87

6 Coupled Aircraft Family Design **94**
6.1 Coupled Aircraft Family Design Methodology 94
6.2 Aircraft Family Design Variables 97
6.3 Aircraft Family Test Cases 99
6.3.1 Three Aircraft Families Optimization Results 100
6.3.2 Two Aircraft Families Optimization Results 103
6.3.3 Aircraft Families' Network Performance 107
North American Routes 107

European Routes 112

7 Conclusions and Recommendations **126**
7.1 Conclusions 127
7.2 Recommendations for Future Developments 128

Bibliography **130**

Appendices **140**

A Route Characteristics **141**
A.1 North American Routes 141
A.2 European Routes 146

B Feasible Direction Inspired Particle Swarm Optimizer **151**
B.1 The Particle Swarm Optimizer 151
B.2 Constraint Handling 153
B.3 Algorithm Parallelization 156

C Quality of Performance Response Surface **159**
C.1 Performance with Aerodynamic Polars 159
C.2 Bi-quadratic Performance Response Surface 161
C.3 Aircraft Polars and Bi-quadratic Performance Response Surface 163
C.4 Error Propagation 165

List of Tables

1.1 NASA SFW Project goals summary 2

3.1 Development and production phase cost reduction factors 42
3.2 Aircraft families summary 43

4.1 American network statistics 48
4.2 European network statistics 50
4.3 Turn–around time coefficients 57
4.4 Reference aircraft specifications 62
4.5 Reference aircraft results for operating the North American route network for 15 years 64
4.6 Reference aircraft results for operating the European route network for 15 years 66

5.1 Robust aircraft specifications 76
5.2 Aircraft geometry design variables 77
5.3 Operational design variables 78
5.4 Aircraft Design Constraints 79
5.5 Robust optimization solution aircraft specifications 84
5.6 Robust aircraft results for operating the North American network for 15 years 85
5.7 Robust aircraft results for operating the European network for 15 years 87

6.1 Example of local and global vertical tail design variables for two aircraft 97
6.2 Three families optimization solution aircraft specifications 102
6.3 Two families optimization solution aircraft specifications 106
6.4 Three families results for operating the North American network for 15 years 108

6.5 Two families results for operating the North American network for 15 years . . . 110
6.6 Three families results for operating the European network for 15 years . . . 113
6.7 Two families results for operating the European network for 15 years 114

A.1 Selected Delta Airline routes and average monthly number of passengers from Atlanta . . . 142
A.2 Selected ExpressJet Airlines routes and average monthly number of passengers from Atlanta . . . 143
A.3 Delta Airline routes minimum flight frequencies . . . 144
A.4 ExpressJet Airlines routes minimum flight frequencies . . . 145
A.5 Selected Lufthansa routes and average monthly number of passengers from Munich (MUC) and Frankfurt(FRA) . . . 147
A.6 Selected Cityline routes and average monthly number of passengers from Munich (MUC) and Frankfurt(FRA) . . . 148
A.7 Lufthansa routes minimum flight frequencies . . . 149
A.8 Cityline routes minimum flight frequencies . . . 150

C.1 Timings and error summary when using the aircraft polars in the performance evaluation . . . 161
C.2 Timings and error summary when using the bi–quadratic performance response surface . . . 162
C.3 Timings and error summary when using the aircraft polars and the response surface . . . 164
C.4 Errors in direct operating cost when using the performance response surfaces for Aircraft A1 and Aircraft C2 . . . 165

List of Figures

1.1 Performed domestic departures by representative airlines in July 2011 of Boeing 737 and Airbus A320 family in North American and European markets 4

2.1 Sequential decomposition of the coupled aircraft sizing and fleet allocation optimization problem [1] 12

3.1 Single aircraft conceptual design methodology using `pyACDT` 22
3.2 Example geometric representation for Boeing 777-200 23
3.3 Performance map of parametric turbofan engine 27
3.4 Forces acting on aircraft in straight, steady and symmetric flight . 28
3.5 Quadratic response surface evaluation points for two example aircraft 31
3.6 Example aircraft development cost cash flow 32
3.7 Example aircraft production cost cash flow assuming a three aircraft per month production rate 33
3.8 Example aircraft development and production phase profit cash flow 33
3.9 Example of operating cost breakdown for 150 passenger load and 2420 [nmi] main mission at a fuel price of 2.93 US$ per gallon . . . 34
3.10 Example of direct operating cost breakdown for 150 passenger load and 1000 [nmi] main mission at a fuel price of 2.93 US$ per gallon 35
3.11 Commonality between members of the Embraer E-Jet family . . . 36
3.12 Analogy between multidisciplinary design optimization and aircraft family design [2] 37

4.1 Overview of an airline planning process 45
4.2 Selected Delta Airlines and ExpressJet Airlines routes 48
4.3 Selected Lufthansa and CityLine routes 49
4.4 Passenger demand discrete time simulation 51

4.5 Simulated daily passenger demand for 2012 between Atlanta and Seattle for Delta Airlines with 10% standard deviation of monthly mean . . . 52
4.6 Simulated passenger demand for 15 years of operations with 2.5% increase in mean demand for North American routes and 3.5% for European routes . . . 53
4.7 Simulated revenue passenger miles for 15 years of operations with 2.5% increase in mean demand for North American routes and 3.5% for European routes . . . 53
4.8 Outline of the procedure to solve the allocation problem . . . 58
4.9 Design mission profile following ATC restrictions, takeoff and landing at ISA, no wind . . . 59
4.10 Reference aircraft geometries as modeled in `pyACDT` . . . 61
4.11 Performance of allocated reference aircraft for operating the North American route network for 15 years . . . 65
4.12 Performance of allocated reference aircraft for operating the European route network for 15 years . . . 67
4.13 Route range to design range ratio of performed departures by the reference aircraft on the North American network (43.9% average ratio) . . . 68
4.14 Route range to design range ratio of performed departures by the reference aircraft on the European network (19.1% average ratio) . . . 69

5.1 Histogram of passenger load factor for Delta Airlines and Lufthansa routes (a) and estimated Gaussian probability density function (b) 73
5.2 Lateral and directional degrees of freedom . . . 80
5.3 Robust optimization aircraft geometries . . . 83
5.4 Performance comparison of reference and robust solution for operating the North American route network for 15 years . . . 86
5.5 Performance comparison of reference and robust solution for operating the European route network for 15 years . . . 89
5.6 Route range to design range ratio of performed departures by the robust aircraft on the North American network (26.8% average ratio) 90
5.7 Route range to design range ratio of performed departures by the robust aircraft on the European network (18.5% average ratio) . . . 91
5.8 Frequency of flights performed and energy intensity contours on payload range diagram for the robust aircraft design and operating both networks for 15 years . . . 92

6.1 Decomposition of the coupled aircraft design and allocation optimization problem . . . 96
6.2 Aircraft family geometry design variables and discrete options . . . 98
6.3 Three families aircraft geometries . . . 101
6.4 Aircraft Family D geometries of the two aircraft families solution . 104
6.5 Aircraft Family E geometries of the two aircraft families solution . 105
6.6 Performance comparison of all solutions for operating the North American route network for 15 years . . . 111
6.7 Performance comparison of all solutions for operating the European route network for 15 years . . . 115
6.8 Route range to design range ratio of performed departures by the three family aircraft on the North American network (43.3% average ratio) . . . 117
6.9 Route range to design range ratio of performed departures by the three family aircraft on the European network (26.5% average ratio) 117
6.10 Route range to design range ratio of performed departures by the two family aircraft on the North American network (48.7% average ratio) . . . 118
6.11 Route range to design range ratio of performed departures by the two family aircraft on the European network (30.3% average ratio) 119
6.12 Frequency of flights performed on payload range diagram for the aircraft families A and B designs and operating both networks for 15 years . . . 120
6.13 Frequency of flights performed on payload range diagram for the three aircraft family C designs and operating both networks for 15 years . . . 121
6.14 Frequency of flights performed on payload range diagram for the aircraft family D designs and operating both networks for 15 years 122
6.15 Frequency of flights performed on payload range diagram for the aircraft family E designs and operating both networks for 15 years 123
6.16 Payload range efficiency of three family and robust aircraft . . . 124
6.17 Payload range efficiency of two family and robust aircraft . . . 125

B.1 PSO particle position and velocity update . . . 153
B.2 Dynamic process management PSO parallelization . . . 157
B.3 Asynchronous PSO parallelization . . . 158

C.1 Relative error in fuel burn over the payload range envelope when using the aircraft polars in the performance evaluation . . . 160

C.2 Relative error in fuel burn over the payload range envelope when using the bi–quadratic performance response surface 162
C.3 Relative error in fuel burn over the payload range envelope when using the aircraft polars and the response surface 164

Nomenclature

Roman Symbols

APP	Aircraft purchasing price	[US$]
AR	Aspect ratio	[−]
BH	Flight block hours	[hr]
c_1	Cognitive parameter	[−]
c_2	Social parameter	[−]
C_{AQU}	Aircraft acquisition cost	[US$]
$c_{i,j}$	Cost of assigning fleet-type j to flight leg i	[US$]
C_k	Value of the k^{th} cost contributor	[US$]
CI	Aircraft design commonality index	[−]
D	Drag of the aircraft	[$\mathrm{lb_f}$]
e	Oswald efficiency factor	[−]
E_I	Energy intensity	[$\frac{\mathrm{BTU}}{\mathrm{lb_f\ nmi}}$]
EMH	Ratio of maintenance hours per block hour	[−]
f	Exact function	[−]
$\overline{f}$	Mean value of function	[−]
$f_{i,j,d}$	Flight frequency required by aircraft type j to meet demand of route i on day d	[−]
$f_{i,max}$	Task maximum cost reduction factor	[−]

f_k	Commonality cost reduction factor	$[-]$
$\mathbf{F_N}$	Aircraft thrust vector	$[\mathrm{lb_f}]$
$G_{k,j}$	Number of aircraft of type j overnight at node k	$[-]$
h	Equality constraint function	$[-]$
K	Drag–due–to–lift factor	$[-]$
k_1	Deboarding time index	$[\frac{\mathrm{PAX}}{\mathrm{min}}]$
k_2	Cabin servicing time index	$[\frac{\mathrm{PAX}}{\mathrm{min}}]$
k_3	Boarding time index	$[\frac{\mathrm{PAX}}{\mathrm{min}}]$
L	Aircraft lift	$[\mathrm{lb_f}]$
LHV_{fuel}	Lower heating value of fuel	$[\frac{\mathrm{BTU}}{\mathrm{lb}}]$
m	Aircraft mass	[slug]
$\dot{m}$	Time rate of change of aircraft mass	$[\frac{\mathrm{slug}}{\mathrm{s}}]$
N_j	Number of available aircraft in fleet type j	$[-]$
n_{doors}	Number of doors available for boarding/deboarding	$[-]$
n_{ifc}	Number of infeasible constraints	$[-]$
n_{nodes}	Number of nodes in the network	$[-]$
n_{PAX}	Number of passengers boarding/deboarding	$[-]$
n_{routes}	Number of routes/flights in the network	$[-]$
n_{types}	Number of aircraft types	$[-]$
$\mathbf{p}$	Vector of uncertain parameters	$[-]$
$\mathbf{p}_k^g$	Global best position at iteration k	$[-]$
$\mathbf{p}_k^i$	Particle best position at iteration k	$[-]$
p_i	Proportional cost weighting for task i	$[-]$
R	Flight range	[nmi]
S	Ratio of leading edge suction force	$[-]$

$S_{i,k}$	Arrival/departure count of flight i at node i	$[-]$
S_{ref}	Wing reference area	$[\text{ft}^2]$
S_{wet}	Wetted area	$[\text{ft}^2]$
t	Total block time	[hr]
TH	Turn–around time	[hr]
tol_e	Equality constraint tolerance	$[-]$
tol_i	Inequality constraint tolerance	$[-]$
U_{ann}	Aircraft annual utilization	[hr]
V	Aircraft true airspeed	$[\frac{\text{ft}}{\text{s}}]$
$\dot{V}$	Time rate of change of aircraft true airspeed	$[\frac{\text{ft}}{\text{s}^2}]$
$\mathbf{v}_k^i$	Velocity vector of particle i at iteration k	$[-]$
W	Aircraft weight	$[\text{lb}_\text{f}]$
w	Weighting coefficients	$[-]$
W_{common}	Weight of common components	$[\text{lb}_\text{f}]$
$W_{\text{exclusive}}$	Weight of exclusive components	$[\text{lb}_\text{f}]$
W_{fuel}	Weight of fuel	$[\text{lb}_\text{f}]$
$W_{payload}$	Weight of payload carried	$[\text{lb}_\text{f}]$
x	Local design or decision variable	$[-]$
Y	Side force	$[\text{lb}_\text{f}]$
y	Coupling variable	$[-]$
z	Global design variable	$[-]$
FF	Component form factor	$[-]$
Q_i	Component interference factor	$[-]$
V_{cw}	Crosswind velocity	$[\frac{\text{ft}}{\text{s}}]$

Greek Symbols

α	Angle of attack	[rad]
β	Sideslip angle	[rad]
δ_a	Aileron deflection angle	[rad]
δ_r	Rudder deflection angle	[rad]
$\dot{\gamma}_2$	Climb rate	$[\frac{\text{rad}}{\text{s}}]$
γ_2	Climb angle	[rad]
λ	Taper ratio	[−]
Λ_{LE}	Leading edge sweep angle	[rad]
ϕ	Roll Angle	[rad]
ψ	Yaw Angle	[rad]
σ_f	Standard deviation of function f	[−]
τ	Total value of constraint violations	[−]

Dimensionless Groups

C_{n_T}	Yawing moment coefficient due to asymmetric thrust
C_D	Aircraft drag coefficient
C_l	Rolling moment coefficient
C_n	Yawing moment coefficient
C_w	Weight coefficient
C_Y	Side force coefficient
C_{D_F}	Aircraft skin friction and form drag coefficient
C_{D_i}	Aircraft induced drag coefficient
C_{D_o}	Aircraft parasitic drag coefficient
C_L	Aircraft lift coefficient

Roman Subscripts

d	Day index
i	Vector, matrix row, task, discipline or route index
j	Matrix column or aircraft type index
k	Cost contributor, node or iteration index
l	Design variable lower bound
m	Month index
u	Design variable upper bound
x	Vector component in x-direction
y	Vector component in y-direction or year index
z	Vector component in z-direction or denotes global function

Greek Subscripts

α	Partial derivative with respect to angle of attack $[\frac{1}{\text{rad}}]$
β	Partial derivative with respect to sideslip angle $[\frac{1}{\text{rad}}]$
δ_a	Partial derivative with respect to aileron deflection $[\frac{1}{\text{rad}}]$
δ_r	Partial derivative with respect to rudder deflection $[\frac{1}{\text{rad}}]$

Roman Superscripts

i	Particle index
$\hat{}$	Independent copy of variables

1 Introduction

1.1 Motivation

The continued growth of air traffic over the past decades and the predicted growth for the next several decades have led to increased awareness and concern about emissions produced by commercial aviation. At the same time, fluctuating fuel prices have put increased economic pressure on the airline industry. A current assessment of the environmental impact of aviation, ATTICA (European Assessment of Transport Impacts on Climate Change and Ozone Depletion), estimates that in 2005 the contribution of aviation to total anthropogenic radiative forcing (RF)[1] was 3.5% (range 1.3-10%, 90% likelihood range) and when including estimates for RF rise from aviation–induced cirrus clouds, the contribution increases to 4.9% (2-14%, 90%likelihood range) [4]. Furthermore, the report states that the growth rate in air traffic demand, measured in revenue passenger miles, in 2007 was 6.6% per year and the long–term growth rate from 1972-2007 is 6.23% per year [4], while historically the overall aircraft fuel intensity has only improved 1.2-2.2% a year. These predictions caused international organizations, such as the International Civil Aviation Organization (ICAO), to adopt commercial aviation emission targets. The main target adopted by ICAO is to achieve 2% fleet-wide reductions in carbon dioxide (CO_2) emissions for aviation through 2050 with further investigation of the feasibility of more ambitious medium and long-term goals, including carbon-neutral growth [5]. The goals of the International Air Transport Association (IATA) are to achieve carbon–neutral growth by 2020, with an average improvement in fuel efficiency of 1.5% per year from 2009 through 2020, and a reduction of CO_2 emissions of 50% by 2050, relative to 2005 values [6]. These environmental impact goals are stated for a commercial aviation fleet-wide level.

[1] The net radiation imbalance at the top of the atmosphere due to a perturbation from human activity [3]

On the other hand, the NASA Subsonic Fixed Wing (SFW) project proposes emission and noise targets for individual future aircraft. These goals consider three time frames of increasing improvements corresponding to next technology generations of aircraft. In this context, the "N" generation are aircraft in production today, followed by the N+1, N+2 and N+3 generations, each with a five year timeframe. Table 1.1 summarizes the NASA SFW Project goals for noise, landing and takeoff nitrogen oxides (LTO NO_x) emissions, cruise NO_x and fuel burn.

Table 1.1: NASA SFW Project goals summary [7]

Technology Benefits*	Technology Generations (Technology Readiness Level, TRL, 4-6) N+1 (2015)	N+2 (2020)**	N+3 (2025)
Noise (cumulative below Stage 4)	-32 dB	-42 dB	-52dB
LTO NO_x Emissions (below CAEP/6)	-60%	-75%	-80%
Cruise NO_x Emissions (rel. 2005 best in class)	-55%	-70%	-80%
Aircraft Fuel/Energy Consumption‡ (rel. 2005 best in class)	-33%	-50%	-60%

* Projected benefits once technologies are matured and implemented by industry. Benefits vary by size and mission, N+1 and N+3 values are referenced to a B737-800 with CFM56-7B engines , N+2 values are referenced to a 777-200 with GE90 engines.
** Environmentally Responsible Aviation(ERA) Project's time-phased approach includes advancing "long-pole" technologies to TRL 6 by 2015.
‡ CO_2 emissions benefits dependent on life-cycle CO_2e per MJ for fuel and/or energy source used.

Aspects of sustainability and environmental considerations, such as emissions and noise limits, are playing an increasing role in the development of new transport aircraft [8]. The research emphasis to meet these emission goals has been placed on incorporating technological advancements in new designs and new aircraft configurations, such as blended wing bodies, box-wing or truss-braced wing configurations [7, 9, 10, 11, 12]. Implementing new technologies and configurations carry with them a high risk and require long development time frames. Reductions in aviation emissions may not only stem from technological advancements and new configurations, but also from a closer coupling between the design and operations of new designs. The design of new transport aircraft by original equipment manufacturers and the operational

planning by airline operators are usually done independently of each other, with each focusing on optimizing their respective performance metric. Aircraft manufacturers design new aircraft for design requirements that are based on extensive market research and perceived future needs of operators [13]. The requirements in different markets, such as North America, Europe or China, and even between operators in the same market can be substantially different or even conflicting. The strategic planning process of an airline involves the acquisition and allocation of available aircraft types to specific routes in their network. Airlines usually operate on thin profit margins and try to maximize profit by assigning the most efficient aircraft type for a given route [14]. Due to the disconnect between many operators and few manufacturers, any given aircraft is rarely operated at its design mission. Another consequence is that future environmental impact of air transportation is not solely a function of new aircraft designs and technology but also a function of how these aircraft are used in airline operations [15]. Surveys of performed departures in the US domestic market of single-aisle aircraft from data of the Bureau of Transportation Statistics (BTS) show that most routes covered by these aircraft fall between 30 to 40% of their respective design ranges. Figure 1.1 shows performed departures in the month of July, 2011 of two representative airlines in each market by aircraft in the Boeing 737 and Airbus A320 families. In the European domestic market, most routes are even shorter, falling between 10 to 20% of the respective design ranges. Hence, a tighter coupling between the design of new aircraft and the actual use of these aircraft in the route networks of operators offers an opportunity to determine future aircraft characteristics that allow for a more efficient resource utilization and reduced climate impact of commercial aviation. New aircraft must not only provide improved environmental performance for a single market but also provide the flexibility to cater to different markets and differing expected growth rates depending on the world region. The development cost and time of a single new aircraft program are significant. One way to reduce these costs is to develop a family of aircraft where the individual aircraft of that family share certain components with each other. The design of an aircraft family allows different market needs to be met, with commonality providing operational benefits, increased flexibility and cost savings [16]. Traditionally the design of an aircraft family is done by establishing a baseline aircraft and subsequently modifying it to meet different mission requirements. This approach can often involve substantial redesign efforts, which in many cases results in almost new aircraft and sub–optimal performance [17]. The concurrent design of all aircraft in a family can take greater advantage of commonality in the family, while maintaining high performance values. Commonality between aircraft can also reduce operating

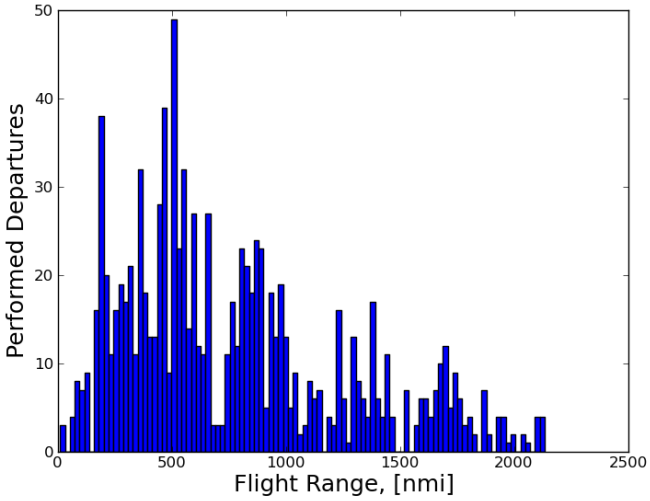

(a) North American market (Delta Airlines)

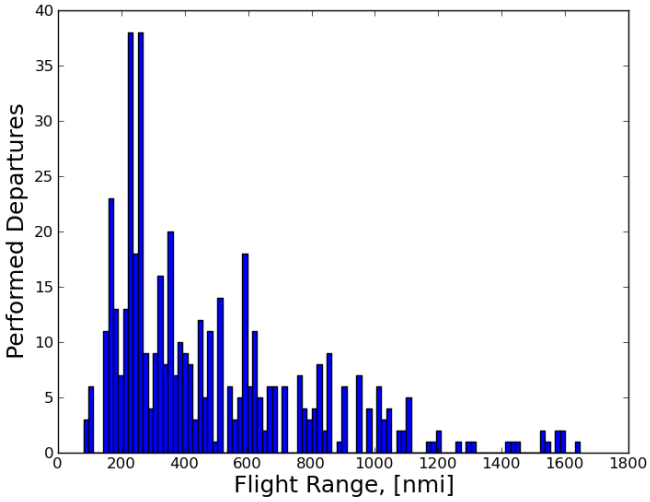

(b) European market (Lufthansa)

Figure 1.1: Performed domestic departures by representative airlines in July 2011 of Boeing 737 and Airbus A320 family in North American and European markets

costs for an operator, because it can simplify fleet maintenance, lower spare part inventories and decrease training costs [2].

1.2 Objectives and Significance

The principal goal of this research is to introduce a system–of–systems framework to combine the multidisciplinary conceptual design optimization of aircraft families with the optimization of the strategic planning of an airline fleet. The design of an aircraft family in itself is a system–of–systems problem, with each aircraft representing an individual system, while the allocation problem represents an additional system. This research study aims to address the following concerns with the design of future transport aircraft:

- The effects and trade-offs involved in the concurrent optimization of aircraft families and aircraft operations on cost and climate impact.
- The trade-offs involved when considering multiple markets in different regions of the world.
- Investigate the economic and environmental sustainability for manufacturers, operators and the public of these aircraft with growing passenger demand.

The main focus will be placed on using a multidisciplinary approach to decompose the problem into subproblems that can be optimized concurrently, accounting for the different trade-offs involved in designing a product family and assigning the individual members efficiently to operators' networks. Additionally, this study aims to enhance the knowledge of solving large system-of-systems problems with uncertainties present. The aim is to develop a framework for the coupled optimization of any type of aircraft and route network. Specific application studies in this work focus to address operational inefficiencies and the sustainability of future narrow–body aircraft. Narrow–body aircraft currently make up approximately 61% of the world's jet transport aircraft and 68% for forecasted deliveries in the next two decades [18]. Furthermore, narrow–body aircraft are used in a wide range of different market segments, while they are usually designed for longer range missions. The disconnect between the design range and the operations of this type of aircraft can result in higher than required takeoff weights and operational inefficiencies.

1.3 Overview

This dissertation is organized as follows. Chapter 2 presents a critical literature review of previous work done in the fields of coupled aircraft design and network allocation, aircraft design with environmental considerations and the design of aircraft families. Chapter 3 introduces the necessary background and description of the tools used for conceptual aircraft design, focusing on the methodology developed to model the design of an aircraft family in the conceptual design stage. Chapter 4 introduces the route networks used in this work, the fleet allocation problem formulation and the modeling of passenger demand uncertainty. The concepts of optimization under uncertainty and how they can be applied to the robust design optimization of aircraft for varying passenger loads and route ranges are the focus of Chapter 5, including a test case of three individually robust optimized aircraft. Chapter 6 describes the problem formulation and methodology for the coupled design of aircraft families and fleet allocation. The results of the fully coupled optimization are also compared against the results of the decoupled robust optimization. Finally, Chapter 7 presents the conclusions derived from the different aircraft optimization approaches used and a discussion regarding possible improvements and recommendations for the future. The standard in aviation in North America is to represent units of measure in the Imperial Measurement System, hence all units will be presented herein using this same standard.

1.4 Contributions

- A methodology to include the effects of sharing common components between members in an aircraft family during the conceptual design phase is introduced.
- A model to simulate the variation in passenger demand, including predicted future growth, for a network of routes and over an extended period of operations is presented.
- The formulation of a fleet allocation problem for the simulated demand characteristics of several years of operations and a solution procedure are described.
- The development of a system–of–systems solution approach to optimize aircraft families coupled with the fleet allocation problem.
- The application of the coupled approach to two distinct markets is presented and the results are used to investigate possibilities this coupled approach has to reduce the environmental impact of commercial aviation, while also providing economic benefits.

- A decoupled individual robust design optimization method was developed to compare against the coupled system–of–systems approach.

2 Literature Review

The coupling of the design of aircraft families and network allocation is a complex problem covering several different areas of research. A comprehensive study of previous research incorporating one or more of the main topics pertaining to the scope of this dissertation has been performed. These topics are the conceptual design of aircraft for environmental considerations, the coupling of the design and allocation of aircraft and the conceptual design of aircraft families. This chapter is divided into three main sections. The first section deals with the design and optimization of new aircraft with environmental considerations. The second section is primarily concerned with previous efforts to combine the design of new aircraft with the allocation of these aircraft in an operator's network, while the third section discusses previous work concerned with the design of aircraft families.

2.1 Aircraft Design and Environmental Considerations

Environmental considerations are of increasing importance in the design of new aircraft. The design of new environmentally friendly aircraft requires a more detailed analysis of inter–disciplinary interactions and higher fidelity analysis methods to assess the impact of new technologies and unconventional configurations. Work performed by Werner-Westphal *et al.* [19] showed the importance of higher fidelity methods in the integrated design of a low noise, efficient, unconventional aircraft. Fuselage weight penalties due to a forward swept canard configuration are captured by higher fidelity aerodynamic and structural analysis. Similarly, Lehner *et al.* [20] introduced an MDO framework for new aircraft design, which stresses the use of higher fidelity methods, such as detailed landing and takeoff analysis for emission and noise models in conceptual aircraft design optimization. The authors also identified three main sources of uncertainty that should be considered. These sources are un-

known performance and costs of future technologies, uncertainties in physical models, such as emissions, and variability in the operations of the designed aircraft. A single–aisle aircraft was optimized with and without the use of advanced technologies, which resulted in aircraft with improved performance. The objective was the predicted ticket costs on a fixed design mission subject to noise and environmental constraints. Counter to the requirement of higher fidelity tools to model new technologies such as extended laminar flow wing designs, only simplified correlation factors were employed for the test case and no uncertainty analysis was performed. Higher fidelity tools are generally still too computationally expensive to be used in the conceptual design optimization of aircraft, where the analysis of a large number of different geometric configurations are required. Additionally, optimization using high fidelity tools usually only allows relatively small changes in the overall geometry of the design of a fixed configuration. Lower fidelity tools do provide the necessary flexibility and they work well for conventional aircraft configurations and current technology levels.

Recent research has also focused on the inclusion of operational considerations, such as climb and cruise trajectories, in the optimization of environmentally friendly aircraft. The effect of incorporating the operations directly in aircraft design was demonstrated by Dallara and Kroo [3]. Their work included a propulsion model for turbofan and propfan engines based on cycle–analysis methods for performance and scaled measurements for noise. To estimate the environmental impact of the aircraft designs, a linear climate model with altitude variation for aviation–induced cloudiness and NO_x was introduced. The aircraft were designed using the conceptual design tool PASS (Program for Aircraft Synthesis Studies) [21], which uses physics–based analysis and semi–empirical formulations. The climate metric employed in this research was the average temperature response (ATR) metric, which estimates the mean temperature change caused by a number of years of sustained operations, for example 30 years, and a discount rate, which is applied for a number of years after the aircraft ceased operations, in this case 0% and 3% discount for 500 years. Using these models, a single–aisle aircraft similar to a Boeing 737-800 was optimized with respect to wing, engine and operational parameters, such as cruise Mach number and initial and final altitude. Additionally, several different technologies meant to reduce the environmental impact of aircraft were investigated; these included the use of propfan engines, natural laminar flow wing design and the use of alternative fuels. The results showed that without additional technologies, climate impact can be reduced by 10-35% when flying lower and slower at a 1% increase in operational cost. Combining new

technologies in the design optimization resulted in reductions of 45% to 70% in climate impact of the new aircraft with operational cost savings of 0.6%. Using the Monte Carlo analysis, a post–optimality study with respect to uncertainties in the emissions model was performed. This study showed that even though the uncertainty is quite large, it is not too large to invalidate the results obtained. Another study included changes in fuel prices from very low to very high prices. Since the environmentally friendly designs fly slower, the flight time is increased; hence for low fuel prices the operating costs are dominated by crew and maintenance costs, while for high fuel prices operating costs are dominated by the fuel cost. The study showed that the obtained results are quite robust with respect to fuel prices and cost savings can be achieved starting at a price of approximately US$ 1.6 per gallon. One more aspect investigated was the effect of operational changes to reduce climate impact for existing aircraft. The results showed that flying exiting aircraft lower and slower and using alternative fuel reductions of 20-60% can be achieved at operational cost penalties of 2-5%.

A similar approach was adopted by Henderson *et al.* [22]. In this study a detailed steady, zero-dimensional thermodynamic propulsion analysis was used to optimize several aircraft types for NO_x emissions at landing and takeoff, fuel burn and direct operating cost. A conceptual aircraft design tool (`pyACDT`) based on semi-empirical formulation and physics–based analysis was used. As for the research discussed above, cruise Mach number and initial and final altitudes were included as design variables in the design optimization. The emissions model calculated the emission index for CO_2 based on the fuel burn, while the emission index of NO_x was calculated by a correlation depending on flow conditions up and downstream of the combustor. Several optimization studies were performed, including a single objective optimization of a narrow–body aircraft with environmental considerations, a multi–objective optimization of the same aircraft and the optimization of a large aircraft for short ranges. Their work showed that low fuel burn designs benefit from high aspect ratio, low sweep wings and fly at low Mach number and altitude. This trend is even more pronounced for minimizing NO_x emissions at landing and takeoff, where high aspect ratio wings allow for smaller engines. Designs for low direct operating cost benefit from higher Mach numbers and hence higher swept, lower aspect ratio wings, which indicate that a low fuel price was used. The result for the large aircraft for short ranges showed a reduction of fuel burn per passenger of 13% when compared to a similar sized aircraft and 5% for smaller aircraft used on similar routes.

Franz *et al.* [8] stress the need to address sustainability aspects in a balanced manner early in the development of future aircraft designs, but addresses the problem of no commonly agreed definition for sustainable aviation. They define sustainability to be based on three broad "pillars" – economic, social and environmental, for which proper indicators have to be selected to allow for a quantitative analysis of any design. The indicators used by the authors were direct operating cost (economic), seat pitch and cumulative equivalent perceived noise level (EPNL) at the three certification points representing a fly-over, sideline and approach position (social) and ATR, LTO NO_x, landing and takeoff field length (environmental). Using these indicators two cases studies were performed using a multi-disciplinary conceptual aircraft design frame work (MICADO), which uses analytical and semi-empirical models. The first was a parameter study of varying cruise Mach number and cruise altitude for an existing 150 passenger aircraft based on a 1960 nautical mile mission. The second included the design of the aircraft, based on wing area, sweep angles and takeoff thrust, within the parameter study. In both cases it was found that, for the given operational mission, reducing the flight level increases the environmental efficiency of the aircraft. Furthermore, when including the design of the aircraft within the framework, the trend to reduce all of the given sustainability indicators was to also reduce the cruise Mach numbers to 0.75 or below.

The studies discussed above showed that significant reductions in environmental impact of aircraft can be achieved by including environmental and operational considerations during the design optimization process. In these cases, a fixed design range and number of passengers were used. These design missions may differ quite significantly from the actual operational use of these aircraft by an airline leading to possible operational inefficiencies that can offset any reductions in emissions, as highly optimized solutions can be very sensitive to minor variations in operational conditions. Hence, the effect of the coupling between the design of new aircraft and the actual operational use of these aircraft need to be explored further.

2.2 Coupled Aircraft Design and Network Allocation

The most extensive research effort to date in coupling the design of new aircraft with the use of these aircraft in airline operations was performed under the supervision of W.A. Crossley from Purdue University. Mane and Crossley [1]

showed in 2005 that incorporating the designed optimization of a yet–to–be designed aircraft in the optimization of a fixed airline transportation network can reduce the daily direct operating costs significantly. They solved the coupled aircraft design and network allocation problem by decomposing the problem similar to a sequential decomposition multidisciplinary design optimization (MDO) approach. The outline of their sequential decomposition can be seen in Figure 2.1. The aircraft design problem and the network allocation prob-

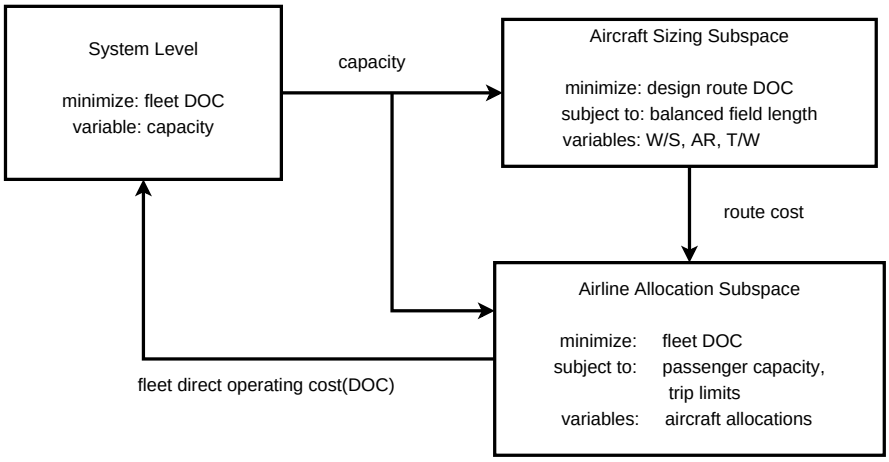

Figure 2.1: Sequential decomposition of the coupled aircraft sizing and fleet allocation optimization problem [1]

lem were considered as disciplines, each solved sequentially by an appropriate optimizer, with the system level optimizer handling the common design variables between the two disciplines. The objective of the coupled optimization was to minimize the network operating costs while meeting a given passenger demand for a simple network. The aircraft design sub–problem consisted of a simple aircraft sizing using the main wing aspect ratio, wing loading, thrust–to–weight ratio and number of passengers as the design variables and subject to a takeoff field length constraint. The reduction in the overall network operating costs resulted from the new aircraft being specifically designed for the given network. They continued their research to illustrate the scalability of the coupled problem for larger airline transportation networks [1]. Starting in 2008, Mane and Crossley [13, 23, 24] extended their research further by incorporating uncertainty in passenger demand. Instead of optimizing the operations of a large airline, they shifted their focus to fractional operation companies that provide on–demand air transportation. As in their previous

work, they decomposed the coupled aircraft design and network allocation problems, but they also included uncertain passenger demand between route pairs and for single routes using a Monte Carlo simulation based on probability distributions. The aircraft design problem was extended by adding total range and cruise velocity as design variables. The results obtained by incorporating uncertainty in passenger demand showed that the overall network operating cost could be reduced by designing an aircraft for a shorter than maximum required range in the network and using chartered aircraft to service longer routes.

Building on the work presented above, Davendralingam and Crossley [25] introduced the addition of a dynamic passenger demand model in the coupled aircraft and network design problem. Incorporating the passenger demand model provides a feedback mechanism to the network optimization problem reflecting changes in ticket price and operations, but no results from a test problem were presented. Davendralingam *et al.* [26] continued the work on dynamic passenger demand models to investigate the effect of introducing new aircraft to an airline network problem. Using dynamic passenger demand, a conceptual four city network problem was solved for three potential new aircraft and compared to two legacy aircraft. In this case, the potential aircraft were not optimized concurrently with the network problem, but modelled on existing new aircraft with a capacity of 50, 180 and 305 passengers, respectively. The results showed that the total estimated revenue was affected by the changes in operation of the different aircraft with revenue increased from the smaller to larger aircraft.

Nusawardhana and Crossley [27] investigated the effect of a yet–to–be designed aircraft on the long–term fleet assignment problem of an airline. Their problem formulation included dynamic aspects, such as annually increasing passenger demand and availability of aircraft due to scheduled maintenance. The objective was to determine when an airline would need to acquire new aircraft to meet future demands and the design of such aircraft. The allocation problems considered were two realistic, large–scale networks consisting of a single hub and 11 and 31 routes, respectively. As for previous work, a simple aircraft sizing tool with the same design variables as above was used. They found that a new large aircraft would be required after six years of operation to meet increasing passenger demand. One main concern with the presented work is that the aircraft sizing problem was solved *a priori* for different numbers of passenger capacities and the longest routes in the given networks. Hence, no direct coupling between the aircraft sizing and fleet allo-

cation problem were considered.

Recent work by Govindaraju and Crossley [28] looked at the effect of including profit-motivated fleet allocation by two airlines for the concurrent design of an aircraft. Instead of solving the allocation problem to minimize cost for the airlines a ticket price model was introduced to allow maximizing profit. Their work showed that when optimizing for a single new aircraft for two large scale networks of different US airlines, there exists a trade–off between the capacity of the new aircraft compared against an optimization for each airline individually. The obtained aircraft has a capacity of 89 passengers, indicating that profit-based allocation leads to smaller aircraft than in their previous work.

Choi *et al.* [29] introduced an approach to include demand uncertainty in the acquisition decision for military airlift operations. The problem to be solved was the introduction of a yet-to-be designed aircraft for the US Air Force Air Mobility Command, which experiences very high uncertainty in the demand of pallets to be delivered. To include this demand uncertainty, a Monte Carlo sampling technique was used in the fleet allocation subproblem. Solving a 22 base problem it was found that to increase the flexibility and reduce operating cost of the existing fleet, a smaller aircraft should be acquired.

Similar to the work done by Crossley *et al.*, research by Taylor and de Weck [30] investigated the effect of concurrent optimization of the design of an aircraft coupled to a package delivery network problem. In this case, the system level optimizer is handling the aircraft design variables, which includes range, capacity, cruise velocity, wing loading, thrust–to–weight ratio and the number of engines. Instead of decomposing the problem into two sublevel optimization problems, only the network optimization problem is solved as a sublevel problem within the system level objective function evaluation. A package delivery network problem consisting of a single hub and six target cities was solved for three existing aircraft and using the coupled approach. They found that integrating the optimization of the flight vehicle design and the transport network allows exploitation of the coupling between the two systems to improve operational efficiency and reduce the daily operational cost of a given network by 10% compared to the existing aircraft.

In an approach by Lehner *et al.* [31] the conceptual design of a new aircraft was coupled with a two stage network design problem. The first stage allocates aircraft between city pairs to minimize operating cost, while in the

second stage, passengers are allocated to the given flights in the route network to optimize a given utility function, such as total fare paid. The main idea behind this two stage approach is to use a small scale representative network to model the large scale real world air transportation problem. Using a five city network and notional 150 and 75 passenger aircraft as the existing fleet introducing a 130 passenger aircraft, with a design range of 1025 nautical miles, can increase the total network operator profit by 10%.

Marwaha and Kokkolaras [32] also coupled the sizing of a new aircraft with the network design and aircraft allocation problems. They used a sequential nested decomposition of the problems, with the aircraft sizing followed by the network configuration and finally the aircraft allocation problem. The test case under consideration was a regional airline in the Canadian west, that expands into the east by adding Toronto and Montreal to the cities served by the airline. To achieve this expansion a new aircraft is required that can fly these longer routes and increased demand. A passenger demand model that includes geographical and language factors was used to estimate the passenger demand between the different city pairs. The sizing of the aircraft was done with the aircraft capacity, design range, wing aspect ratio, thrust–to–weight ratio and wing loading as the design variables. Takeoff field length was the only constraint considered for the aircraft sizing problem. The system level objective was to minimize overall direct operating costs of the fleet. The solution to their first test problem, which consisted of a seven city network, showed significant reduction in direct operating cost, by a factor of almost 3, of designing the network with the aircraft compared to a traditional hub and spoke network. The second test cases, which had an increase in the size of the network to 15 cities, showed that there are still significant reductions when configuring the network. The cost ratio compared to a single-hub network reduces with increasing network size. Another aspect that was highlighted in this work was the multi-modality of the coupled problem, with several observed local minima in the seven city problem and a significant increase in the 15-city problem.

The research works discussed above focused on using high level decision variables, such as capacity, wing loading and thrust-to-weight, for the design of the new aircraft. Hence, the results represent more the operator's point of view on the type of new aircraft required, instead of focusing on the design of these new aircraft. Additionally, the optimizations were mainly carried out with respect to economic considerations in the form of operating costs. Environmental performance considerations were not included either as objectives or constraints.

Work, carried out by Bower and Kroo [33], did include higher fidelity, physics–based analyzes combined with empirical formulations. They performed a multi–objective simultaneous optimization of a single-aisle aircraft design and a specific route network. The objectives selected were operating costs and CO_2 and NO_x emissions. Similar to Taylor and de Weck, the coupled optimization problem was decomposed hierarchically, with the aircraft design problem as the system level optimization and the network problem as a subspace optimization. The aircraft design variables included capacity, wing loading, maximum takeoff weight, wing aspect ratio, taper and sweep angle, thickness–to–chord ratio, ratio of horizontal tail area to wing area, and the location of the wing along the fuselage. The engine design variables included thrust–to–weight ratio, overall and fan pressure ratio and turbine entry temperature. Operational design variables were cruise Mach number and cruise altitude. Carbon dioxide emissions were directly correlated to fuel burn, while the more detailed engine model allowed for an empirical correlation of NO_x emissions. The network selected for the test problem was a simple four city eight segment network with constant passenger demand. Results from the multi–objective optimization showed a strong trade–off between operating costs and NO_x emissions as well as CO_2 and NO_x emissions. For operating costs and CO_2 emissions, there was little trade–off evident, which can be explained by the direct relation of cost and CO_2 emissions on fuel burn. Compared to today's aircraft of the same class, the obtained aircraft designs show a tendency to use higher bypass ratio engines and thicker, higher aspect ratio wings.

Generally, previous research illustrated the possibility of exploiting the coupling between the design of new aircraft and the operational use in a given transportation network to reduce operating costs and possibly emissions. In previous research only single new aircraft are introduced to an existing fleet. A single new aircraft seldom can meet the requirements of multiple markets but incurs high research and development cost. To provide increased flexibility for multiple markets, while lowering research and development cost, the design of several aircraft, which share common components and form an aircraft family, coupled with the use of these aircraft in different markets needs to be explored.

2.3 Aircraft Family Design

Product families, which are groups of related products which share common and distinctive features and meet different design requirements, are widely used in the design of new products [34]. The main advantage of having a line of products with common components is reduced development and manufacturing cost [35]. In the aircraft industry the idea of commonality has been used in successful aircraft families such as the Airbus A320 or Embraer E-Jets product line. The design of an aircraft family allows different market needs and design requirements to be met, while providing operational benefits, increased flexibility and cost savings [16]. From a manufacturer's point of view, product families cater to the varying needs of potential customers by offering a wider selection of aircraft at a lower development and production cost. Commonality between aircraft can also reduce operating costs for an operator, because it can simplify fleet maintenance, lower spare part inventories and decrease training costs [2].

Traditionally the design of an aircraft family is done by designing a baseline aircraft which is subsequently modified to meet varying mission requirements and address different market needs at a later time [17]. This is usually achieved by inserting or removing fuselage frames (plugs), adding wing span and chord extensions and re-engining the aircraft. This approach can often lead to substantial modifications resulting in development costs similar to that of a new aircraft program and sub-optimal performance [17]. Another approach is to design all the aircraft in the family simultaneously while taking into account shared components. This allows taking full advantage of commonality between aircraft while maintaining optimal performance of each aircraft in the family. In both cases the use of common components is generally associated with a weight penalty for some of the aircraft in the family.

Still, little research effort has been performed on the conceptual design of an aircraft family with no recent publications. One of the first works considering the design optimization of an aircraft family was by Willcox and Wakayama [17] in 2003. In this work, the authors investigated the simultaneous optimization of a two aircraft family whose design missions differed significantly. The sample test case was the design of two blended wing aircraft with varying degrees of commonality in the structure of the wing. To account for commonality between aircraft, constant cost reduction factors based on individual component weights and learning curve effects were applied. Minimizing the family simultaneously for maximum takeoff weight produced a lower com-

bined weight when compared to a sequentially optimized family and a weight penalty of 0.05% for the first and 2% for the second aircraft when compared to single point optimization. Performing a cost analysis for the point design and simultaneous optimized aircraft, which included an increased learning curve effect and commonality effects, it was found that due to the weight penalty from the common components, the baseline unit cost of the family was higher. This may be explained by the fact that the cost analysis was performed after the optimization.

In 2006, Allison *et al.* [36] explored the use of MDO decomposition methods in the concurrent design of an aircraft family. The two methods investigated were analytic target cascading (ATC) and collaborative optimization (CO). In both methods, the aircraft family optimization problem is decomposed by optimizing each individual aircraft as decoupled sublevel problems. In ATC the system level problem is solved by a sequence of sub–optimization problems, while in CO the sublevel optimization problems are nested into the system level problem. To explore the validity of both methods, a relatively simple two aircraft family problem was solved, with each aircraft having distinct design missions. The main wing was the common component shared by both aircraft while the objective was to minimize an aggregate of the acquisition and operating costs. Again constant cost reduction factors were used to account for the use of common components. The acquisition costs, which include the development and manufacturing costs, captures the effect of commonality between the aircraft. The performance of the aircraft was evaluated using the conceptual design tool PASS. The two methods arrived at similar solutions, with the CO solution having slightly lower cost indices for both aircraft.

Perez and Behdinan [2] also used a CO–based decomposition approach to optimize a four aircraft family each with distinct missions covering different market segments. A commonality index approach was used to model the effects of commonality on cost. The research and development cost and production costs were affected by the commonality index of each aircraft and by a cost reduction factor for each cost contributor, such as engineering, tooling or support. The commonality index for each aircraft was calculated based on the ratio of the weight of the common components used on that aircraft over the combined weight of the common and exclusive components. The optimization results showed that designing an aircraft family with common components can lead to significant reductions in the cost for a manufacturer by lowering development, tooling and assembly costs. Also some reduction in the direct operating costs was observed when compared to individually optimized air-

craft. These reductions in costs came with a structural weight penalty and higher maximum takeoff weights.

To date, the effects of possible increased structural weight of an aircraft family on fleet wide environmental and economic metrics have not been explored. Additionally, considering design requirements from route networks in different markets or regions of the world for the members of an aircraft family have not been considered explicitly.

3 Aircraft Conceptual Design

The conceptual design of new aircraft is a complex, multidisciplinary task. To properly assess the performance and environmental impact of aircraft, a comprehensive aircraft design framework is required. The framework must provide a level of fidelity in the disciplines that takes into account the interactions and trade–offs of the different disciplines. At the same time, the framework must be flexible and computationally inexpensive, since the conceptual design optimization of aircraft involves the analysis of a large number of different configurations at many different operational conditions. Additionally, the effects of sharing common components must also be considered when designing a family of aircraft and be reflected in the analysis of these aircraft. This chapter presents the main background and the development of the conceptual aircraft design methodology and tools necessary to perform a conceptual design optimization of commercial transport aircraft families. The first part of the chapter provides an overview of the developed aircraft design software split along discipline lines. The second part describes the extension of the aircraft design methodology and analysis tools for aircraft families in the conceptual design stage.

3.1 Aircraft Conceptual Design Toolbox

The main resource for the conceptual design of aircraft to be used for this research is the object–oriented Aircraft Conceptual Design Toolbox (`pyACDT`) written in Python [37]. This toolbox provides a modular, multi–fidelity, multidisciplinary aircraft design framework and has been under development for over ten years. The object–oriented design of the framework provides a modular structure that makes it extremely flexible for multidisciplinary design. The framework uses several high level modules that are used to either define the aircraft, define mission parameters or disciplinary analysis. The object–oriented concepts used in the development of the framework allows for easy

integration of new disciplines and analyses, and rapid use of different levels of fidelity in the analysis. Each discipline is implemented as a stand–alone submodule, while the high level modules ensure seamless interaction between different disciplines.

The general methodology used for an individual aircraft is shown in Figure 3.1. A list of design variables and fixed parameters are used to define the geometry, design payload and design mission for the aircraft. Analysis tools are then used to estimate the weight, propulsive and aerodynamic performance of the design. Based on these performance characteristics, the required fuel for the design mission and design payload are calculated and the maximum take–off weight is updated until convergence in the sizing loop is achieved. After the aircraft is sized, the current design can be assessed based on different criteria such as research and development (RDTE) cost, production cost and/or fuel burn and operating costs for specific missions and payloads. To facilitate the assessment of a given design on many different missions, aerodynamic and performance response surfaces can be generated. Additionally, aircraft design constraints can be evaluated for each discipline.

For this work, each design was started from a white sheet and many different candidate designs were being considered. To provide a rapid assessment of each design, while retaining important interdisciplinary interactions, each discipline used analytical and semi–empirical methods commonly used in conceptual aircraft design. A short description of the analysis modules follows below.

3.1.1 Aircraft Definition

The aircraft definition is handled through several modules. These are the aircraft geometry, systems and payload modules. Different levels of abstraction can be used for these definitions, such as lumped or detailed payloads, to accommodate different design problems. The actual aircraft configuration is defined through the geometry module. The module uses a hierarchical parametric component decomposition with association between joint components. Hence, the aircraft configuration consists of several upper level components, which consist of one or more sublevel components. Where applicable, the module also calculates additional properties, such as wetted areas, internal volumes, an equivalent wing and coordinate locations with respect to a predefined datum, which may be required by different analysis and are directly derived from the parametric inputs. Figure 3.2(a) shows the build–up of in-

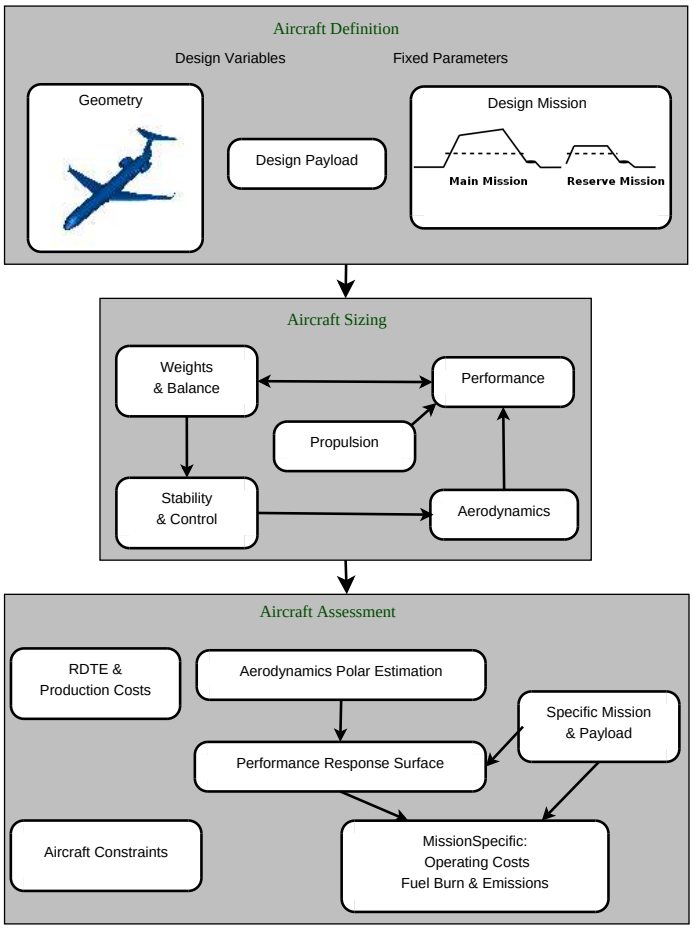

Figure 3.1: Single aircraft conceptual design methodology using `pyACDT`

dividual components for a Boeing 777-200ER, while Figure 3.2(b) shows the integrated geometry of the aircraft. The fuselage is contained in a body surface object, which contains three body segment objects defining the cockpit, passenger compartment and tail section of the fuselage. The input parameters for body segments are radius, width–to–height ratio and shape parameters that are used in a super ellipsoid formulation to generate the outer mold line surfaces. The wing, horizontal and vertical tails are contained in lifting surface objects, which in turn are created from one or more lifting segments. The individual lifting segments are defined by a simple set of preliminary design parameters, such as total area, aspect ratio, taper ratio, leading-edge sweep

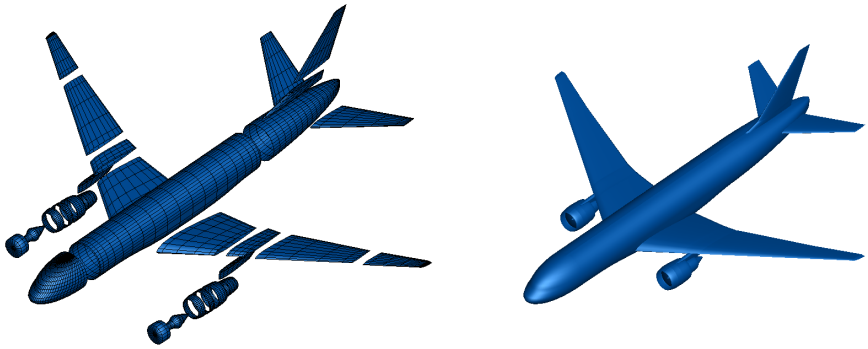

(a) Boeing 777-200ER geometry component build–up

(b) Boeing 777-200ER geometry

Figure 3.2: Example geometric representation for Boeing 777-200

angle, root and tip thickness ratios, dihedral angle, twist distribution and airfoil definitions. Lifting surfaces can contain additional components, control surfaces and wingtips. The geometry of the engines is given by the propulsion module, either from the actual geometry or determined from empirical formulations based on the type of engine and the sea-level static thrust. The nacelles are again modelled as body surfaces and are defined by the geometry of the engines they contain. The use of a parametric definition allows for a greater range of different shapes and aircraft configurations as is desired for conceptual design. The geometry module is also used as a common aircraft definition for the discipline specific analysis modules described below.

3.1.2 Weight and Balance

The weight module estimates the weight of main aircraft component groups using statistical and empirical methods [38, 39, 40]. The maximum takeoff weight is solved using fixed point iterations, since the weight of several components, such as the wing, empennage or landing gear, depends on the maximum takeoff weight with mission fuel weight and payload weight as inputs. The mission fuel required is calculated using the performance module, as discussed in Section 3.1.5. The payload weight is given by the payload definition. The main component groups' weight is given by the summation of the individual component weights. The structures group includes wing,

empennage, landing gear, fuselage and nacelle weights. The propulsion system group includes engine, oil, thrust reverser and starting system weights. The systems group includes the anti-ice, avionics, air-conditioning, electrical, APU, fuel, hydraulic, flight control and instrumentation systems. The furnishings group uses either a statistical estimate based on the number of passengers or, if defined in detail, the weights of individual elements such as seats, lavatories, emergency systems and galleys. Operational items include the weight of attendants and crew and their baggage, the weight of unusable fuel and the empty weight of any cargo containers. Given the weight of each component, the maximum range of the center of gravity (C.G.) for the aircraft configuration is calculated based on the C.G. limit of each component, due to geometric and functional considerations [41].

3.1.3 Aerodynamics

The aerodynamic module is important to properly gauge the performance of a particular design configuration. The module needs to provide the total drag coefficient for a given aircraft geometry either for a given lift coefficient or angle of attack as well as stability derivatives for given flight conditions. Computational efficiency plays an important role since during the conceptual design process, each design must be analyzed at many different flight conditions. High–fidelity computational fluid dynamic (CFD) algorithms can yield very accurate solutions for aerodynamic problems. However, these algorithms do not yet provide the required automated flexibility and computational speed required for the conceptual aircraft design optimization [42]. To provide rapid execution and robustness, analytic and semi-empirical formulations common to conceptual aircraft design are used to evaluate the aerodynamic performance of the aircraft [38, 39, 40, 43, 44].

The total drag of an aircraft can be divided into two main components, parasitic drag and induced drag due to lift. Parasitic drag includes drag from skin friction, pressure, or form drag, interference drag and transonic wave drag due to shock waves. The skin friction and form drag, C_{D_F} are calculated by a detailed component build-up and additions due to fuselage upsweep and base drag, nacelle base drag, and a markup for drag caused by protuberances [43]:

$$\begin{aligned} C_{D_F} &= \sum_i C_{F_i} F F_i Q_i \frac{S_{wet_i}}{S_{ref}} + C_{D_{fuse.upsweep}} \\ &\quad + C_{D_{fuse.base}} + C_{D_{nacellebase}} + C_{D_{protuberance}} \end{aligned} \tag{3.1}$$

where C_{F_i} is the flat–plate skin friction coefficient for component i, FF_i is the form factor to account for pressure drag, Q_i is the comportment interference factor and S_{wet_i}, S_{ref} are the component wetted area and reference area, respectively. Both, the form factor and skin friction coefficient in Equation (3.1), are estimated based on semi-empirical formulations. The skin friction coefficient is calculated based on local Reynolds number, with fixed transition points between laminar and turbulent flow and skin roughness corrections [45]. Schlichting's composition formulation [46] is used to combine skin friction from laminar and turbulent flow, where the Eckert Reference Temperature method [47] is used for laminar flow and the Van Driest II [48, 49] method for turbulent flow. The form factor provides a correction for thickness effects, local surface velocities and pressure drag. Two formulations are used, one for lifting surfaces and one for bodies of revolution, such as the fuselage or nacelles. The lifting surface form factor is a function of Mach number, sweep angle, maximum camber and thickness-to-chord ratio [50, 38], while the form factors for bodies of revolution are based on an empirical function of the fineness ratio, which is the ratio of diameter to length of the body [50, 38]. The transonic wave drag is calculated for each lifting surface carrying lift based on a simple semi-empirical method by Shevell [51]. This method estimates the drag divergence and critical Mach number for a given wing section based on the quarter chord sweep angle, lift coefficient, thickness-to-chord ratio and type of airfoil used. The lift increment and drag due to flaps and spoilers is estimated based on the flap type and deflection of the flap using empirical correlations from NASA and Roskam [45, 40]. The stability derivatives of the aircraft and maximum lift coefficient are estimated using semi–empirical formulations based on work performed by NASA [45] and modified by Roskam [40].

The induced drag is estimated by combining two leading edge suction methods. Both methods estimate the ratio of the actual leading edge suction force to the theoretical maximum suction force, S, to provide a value for the Oswald efficiency factor, e, of the lifting surface, which can then be used to estimate the drag–due–to–lift factor, K, where:

$$K = \frac{1}{\pi ARe} \tag{3.2}$$

which gives the induced drag based on the lift coefficient, C_L, by:

$$C_{D_i} = KC_L^2 \tag{3.3}$$

where AR is the aspect ratio of the lifting surface. The first method uses a polynomial fit to empirical data to estimate the ratio of the suction forces [45]:

$$S_1 = 0.0004K_s^3 - 0.008K_s^2 + 0.0501K_s + 0.8642 \tag{3.4}$$

The second method uses an exponential fit, resulting in the expression [52]:

$$S_2 = 0.974 - 0.0976\exp^{(-0.456K_s)} \tag{3.5}$$

where the parameter K_s is given by:

$$K_s = \frac{AR\lambda}{\cos\Lambda_{LE}} \tag{3.6}$$

with λ the taper ratio and Λ_{LE} the leading edge sweep of the lifting surface. Often one method over-predicts, while the other under-predicts the ratio of the leading edge suction force and *vice versa*. In this study, the two values were averaged to obtained a better estimate for the suction force ratio, S, which is then used to calculate the Oswald efficiency factor:

$$e = \frac{1.0}{\pi\frac{AR}{C_{L_\alpha}}\left[S + (1-S)\right]} \tag{3.7}$$

where C_{L_α} is the lift curve slope of the lifting surface. The induced drag of the aircraft depends on the required lift coefficient, the aspect ratio, taper ratio and leading edge sweep of the wing.

Trim drag is calculated based on a static stability analysis by an integrated stability and control module and the required control surface deflection to achieve a zero pitching moment around the center of gravity of the aircraft. The trim drag calculation assumes a steady state flight condition and, for conventional configurations, the incidence angle of the full horizontal stabilizer is used to achieve the trimmed condition. The analytical aerodynamics module can provide good results very rapidly for standard configuration aircraft.

The aerodynamics module is also used to generate a set of drag polars for a given aircraft geometry and centre of gravity locations. The drag polar is defined as:

$$C_D = C_{D_o} + KC_L^2 \tag{3.8}$$

where the total drag coefficient, C_D, is expressed as a parabolic curve in terms of a lift independent drag coefficient, C_{D_o} and the square of the lift coefficient C_L and a drag–due–to–lift factor, K. It can be noted, that the drag–due–to–lift factor for the aircraft polar includes all effects due to lift for the entire aircraft. The drag polars are generated for a set of altitudes and Mach numbers

for the "clean" or cruise, takeoff and landing configuration. The drag for a given flight condition is then estimated by interpolating between the given drag polar curves. The drag polars are used to further increase the computational speed of the aerodynamic calculations for a given configuration.

3.1.4 Propulsion

The propulsion module uses a parametric turbofan engine model to calculate the net thrust and specific fuel consumption at a given altitude, Mach number and thrust setting. The parametric model is based on the model developed by Bartel and Young [53], which is based on empirical equations and curve fits for two–shaft turbofan engines. The input variables are static sea–level thrust and bypass ratio and the output is the adjusted thrust and fuel consumption for the given flight conditions. A formulation for partial power setting and altitude variation was also added to the parametric model [54]. The original model by Bartel was modified to match available data of existing engine decks. The modified model provides the total installed thrust and its components in any given coordinate system. Additionally, the modified model also predicts the windmilling drag if one or more engines are inoperative [55]. Figure 3.3 shows the variation of thrust and thrust specific fuel consumption (TSFC) with Mach number and altitude for a modeled Turbofan engine. The geomet-

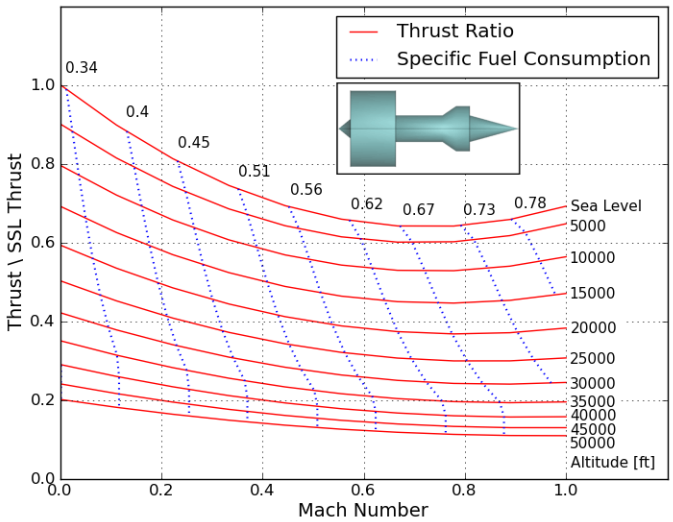

Figure 3.3: Performance map of a parametric turbofan engine at a thrust setting of one (42600 pounds of static sea-level thrust, bypass ratio of 5.8)

ric representation of the engine in the geometry module is also shown. The available thrust decreases with increasing altitude and corresponding decreasing density, and also with increasing Mach number up to the transonic regime. At higher Mach numbers compressibility effects do provide again increasing thrust at lower altitudes. Similarly the specific fuel consumption increases with increasing Mach number.

3.1.5 Performance

The performance module estimates mission fuel burn and flight time, as well as point performance parameters for a given mission profile. The module can also calculate off–design performance for a single mission segment, such as high and hot takeoff performance. Extra performance parameters calculated include takeoff field length, balanced field length, landing field length and second segment climb gradient. The model uses a combination of analytical expressions and numerical simulation in the space domain to calculate the aircraft characteristics for each mission segment. The aircraft is modeled as a point mass system. Figure 3.4 depicts the general forces acting on the aircraft as well as the definitions of the flight path climb angle γ_2. The drag acting

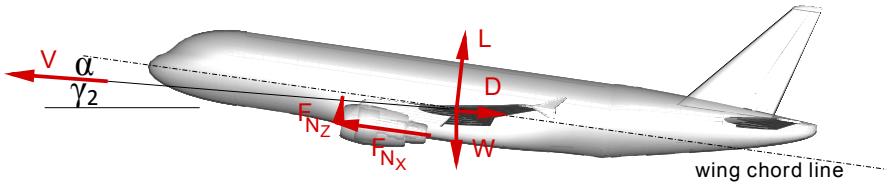

Figure 3.4: Forces acting on aircraft in straight, steady and symmetric flight

on the aircraft is represented by D, while W is the current weight, L is the total lift and V is the true airspeed. The simplified performance equations of motion for the point mass system in the velocity axis system can then be simplified by assuming straight, level and symmetric flight. The general equations of motion are then given by [56]:

$$-D + \sum F_{N_x} - W \sin\gamma_2 = m\dot{V} + \dot{m}V \tag{3.9}$$

$$Y = \sum F_{N_y} \tag{3.10}$$

$$-L + W\cos\gamma_2 + \sum F_{N_z} = mV\dot{\gamma}_2 \tag{3.11}$$

where m is the aircraft mass and $\dot{m}$ the mass flow rate given by the fuel consumption of the engines, Y is the side force and F_{N_x}, F_{N_z} are the net thrust components of each engine in the x and z direction.

The model uses coarse, fixed step numerical simulation for climb and descent, discretized by altitude steps, cruise, discretized by ground distance, and loiter segments, discretized by time steps. At each step the aerodynamic characteristics of the aircraft are either estimated by the full aerodynamics module or the given aircraft polars and the engine characteristics are given by the propulsion module. For takeoff and landing performance, a simplified approach by Powers [57] is used to calculate the ground run performance. The ground run acceleration, or deceleration, is integrated analytically assuming the thrust varies quadratically with the aircraft velocity.

The performance module allows for several options that can be enforced for the different flight segments. For the climb segments, a standard climb schedule can be followed which includes initial climb at a maximum calibrated airspeed (CAS) of 250 knots to an altitude of 10000 feet, as per air traffic control rules (ATC), followed by a level acceleration to a prescribed CAS and climb at constant CAS until the final Mach number is reached, at which point climb continues at a constant Mach number. Similarly, the same procedure in reverse can be applied during descent, including a limit on the rate of descent as given by cabin pressure restrictions due to passenger comfort [58]. The cruise segment can either be performed at constant Mach number and altitude, constant Mach number and constant lift coefficient (cruise–climb), step climb segments or at varying Mach numbers and altitudes.

The computational burden when analyzing the performance of multiple aircraft over a wide range of routes and payloads is substantial. In the current work, the number of points with different payloads and route ranges for which the performance must be evaluated reach the order of half a million points per aircraft when solving the fleet allocation problem. For each set of payload and flight range, the takeoff weight which depends on the fuel required for the mission and the distance traveled during cruise must be determined. The performance module calculates these values by using a two dimensional Newton's method, which requires several performance evaluations to converge on the takeoff weight and length of the cruise segment. To facilitate the analysis of several aircraft in terms of fuel burn, flight time and takeoff weight, a bi–quadratic response surface can be generated. The response surface is constructed using a central composite design with eight points around a ninth

central point of payload and main mission flight range as the independent variables. An estimate of the desired performance output values, such as fuel required or flight time, can then be obtained by solving the quadratic equation [59]:

$$\begin{aligned} \widehat{y} &= a_0 + a_1(x_1 - x_1^0) + a_2(x_2 - x_2^0) + a_3(x_1 - x_1^0)^2 \\ &\quad + a_4(x_1 - x_1^0)(x_2 - x_2^0) + a_5(x_2 - x_2^0)^2 \end{aligned} \tag{3.12}$$

where x_i are the independent variables, in this case payload and main mission flight range, $\widehat{y}$ is the estimate of the exact performance output value, $y = f(\mathbf{x})$, and the coefficients of the polynomial function, $a_0, \ldots a_5$, are given by:

$$\begin{aligned} a_0 &= f(x_1^0, x_2^0) \\ a_1 &= \frac{f(x_1^5, x_2^5) - f(x_1^4, x_2^4)}{(x_1^5 - x_1^4)} \\ a_2 &= \frac{f(x_1^7, x_2^7) - f(x_1^2, x_2^2)}{(x_2^7 - x_2^2)} \\ a_3 &= \frac{f(x_1^5, x_2^5) - 2f(x_1^0, x_2^0) + f(x_1^4, x_2^4)}{2(x_1^5 - x_1^0)^2} \\ a_4 &= \frac{f(x_1^8, x_2^8) - f(x_1^6, x_2^6) - f(x_1^3, x_2^3) + f(x_1^1, x_2^1)}{8(x_1^5 - x_1^0)(x_1^7 - x_1^0)} \\ a_5 &= \frac{f(x_1^7, x_2^7) - 2f(x_1^0, x_2^0) + f(x_1^2, x_2^2)}{2(x_1^7 - x_1^0)^2} \end{aligned} \tag{3.13}$$

where $\mathbf{x}^j$ are the independent variables of point j. An example of the location of the points used is shown in Figure 3.5(a). As can be seen, Point 3 is at the sizing point of the aircraft, with maximum passenger payload and at the design range. The sizing point is used, since the values are known from the sizing of the aircraft and do not need to be reevaluated. Points 1,4 and 6 are defined at the flight range without a cruise segment, hence the aircraft climbs to a specified altitude and then begins the descent. It was observed that for aircraft with low design ranges, generally around 1000 nautical miles, using the sizing point can lead to increased error in the outputs of the response surface. To improve the quality of the response surface, a point at a lower payload can be used, as can be seen in Figure 3.5(b). Employing the response surface to evaluate the performance of an aircraft significantly reduces the evaluation time to an average of 1.4×10^{-4} seconds for different flight ranges and payloads compared to 80 seconds using the full performance model. The average error of the estimated output values from the response surface compared to the full

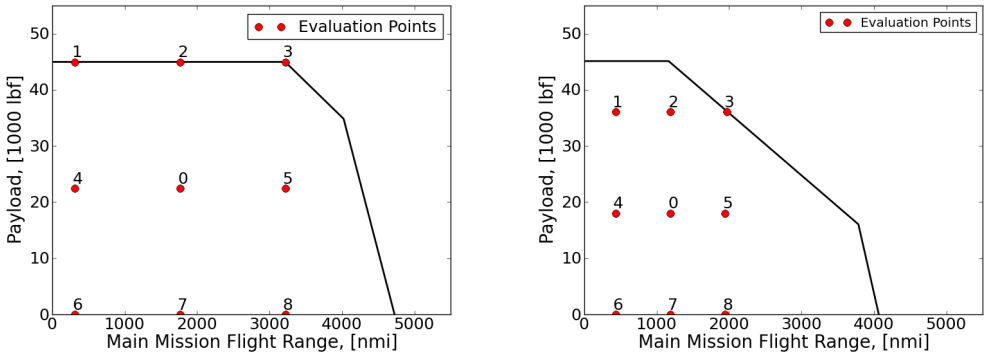

(a) Evaluation points for aircraft with high design range

(b) Evaluation points for aircraft with low design range

Figure 3.5: Quadratic response surface evaluation points for two example aircraft

performance evaluation are less then 1%. An evaluation of the accuracy of the response surface for different aircraft can be found in Appendix C.

3.1.6 The Economics Model

The economics module in `pyACDT` uses individual models to estimate the research, development, testing and evaluation cost, the production cost and the direct and indirect operating costs for each aircraft.

Research and development is mainly a non–recurring effort required to launch an aircraft concept and bring it to production. It includes all phases of design, tooling, testing, quality control and certification. The development cost is based on non–dimensional industry data for typical commercial aircraft [60] and the model given by Roskam [40]. The formulations in the cost model are based on the weight of the aircraft and the number of prototype and test airframes produced. The model predicts the distribution of expenditures during the development process. The cash flow over the development phase is modelled with the use of specific beta probability density functions for each cost contributor and a given time period [61, 2].

The estimation of the production cost is also based on non-dimensional industry data for typical commercial aircraft [60] and the Roskam model [40].

The production cost includes the cost of sustained engineering, manufacturing labor and materials, tooling, quality control and flight-tests. Production costs are recurring and as such are subject to a learning curve effect based on the quantity of aircraft produced. Similar to the development cost, the cash flow for the different cost contributors can be estimated given a rate of production for the aircraft. Figure 3.6 and Figure 3.7 show the cash flow for a representative single-aisle aircraft of the individual cost contributors for the development and production phases, respectively. Figure 3.8 shows the profit cash flow for the same representative aircraft indicating the total investment cost for the aircraft project.

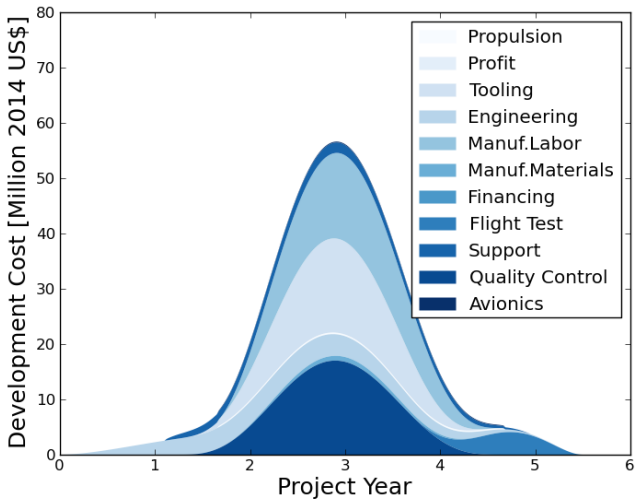

Figure 3.6: Example aircraft development cost cash flow

The operating costs for a given aircraft are calculated based on the number of passengers carried, the annual utilization of the aircraft, as well as the fuel and time required for a given mission and therefore depend directly on the performance of the aircraft for a specific mission. The current model distinguishes between direct and indirect operating costs. The direct operating costs include the cost for flying a specific mission, maintenance, fees and taxes, depreciation and financing. Indirect operating costs include the cost for passenger services, entertainment, insurance, marketing and administration, which are estimated based on industry data and statistics [62]. The breakdown of each cost contributor for an example aircraft can be seen in Figure 3.9. The

main contributor to the direct operating cost for the given mission is the cost of fuel. For shorter range missions, the percentage of the fuel cost decreases, while the contributions from crew cost and fees becomes more significant. For

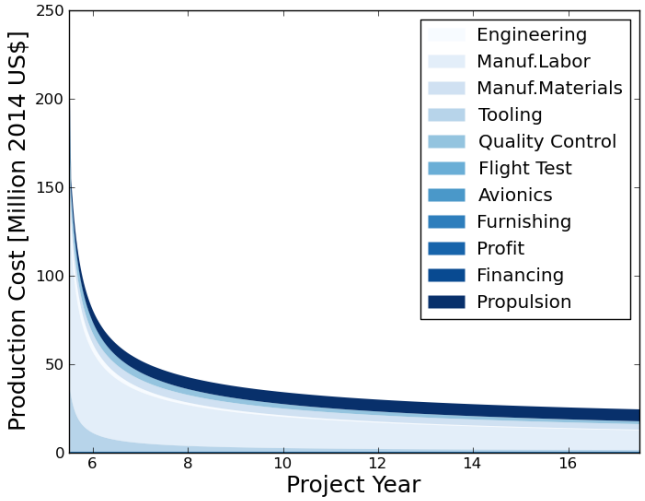

Figure 3.7: Example aircraft production cost cash flow assuming a three aircraft per month production rate

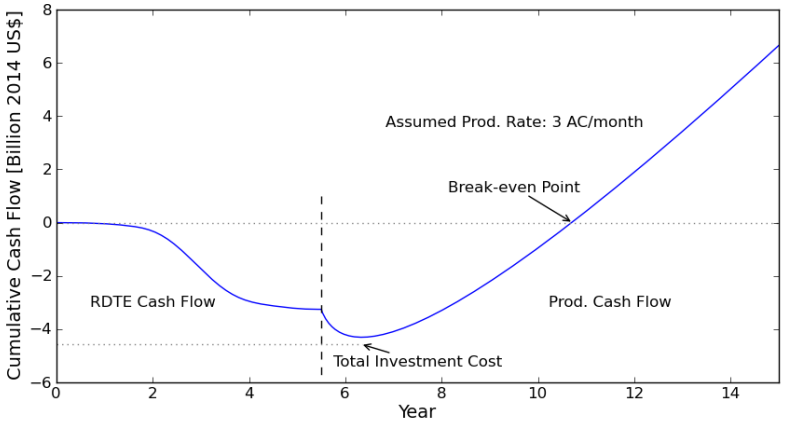

Figure 3.8: Example aircraft development and production phase profit cash flow

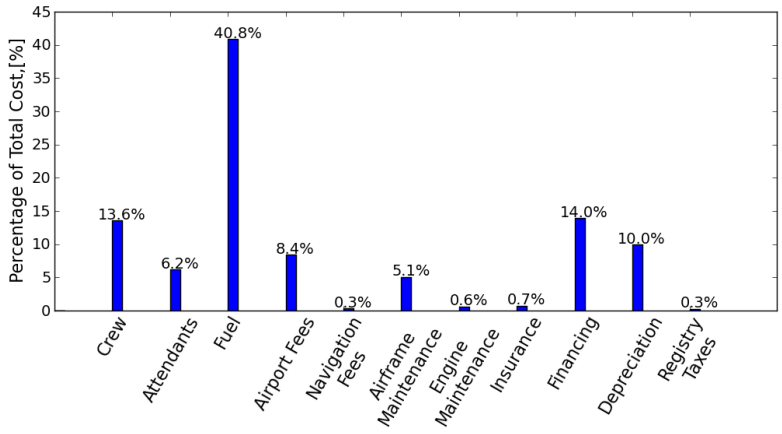

(a) Direct Operating Cost

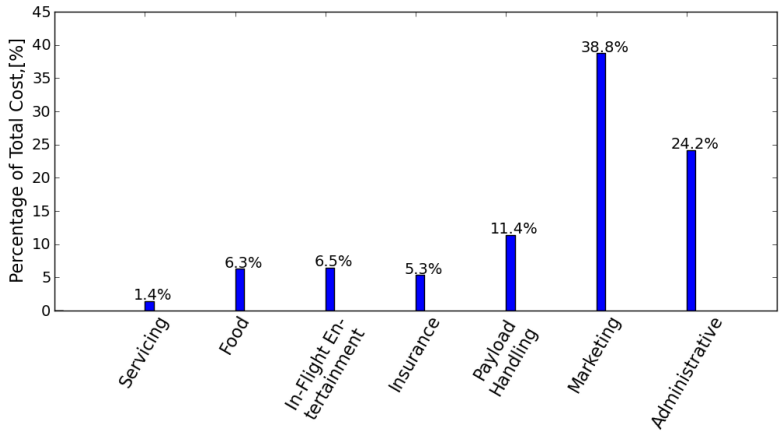

(b) Indirect Operating Cost

Figure 3.9: Example of operating cost breakdown for 150 passenger load and 2420 [nmi] main mission at a fuel price of 2.93 US$ per gallon

a main mission range of 1000 nautical miles and the same aircraft, fuel cost is still the dominant cost contributor, as can be seen in Figure 3.10. It can be noted that the indirect operating cost are independent of the mission range and do not change for the shorter mission.

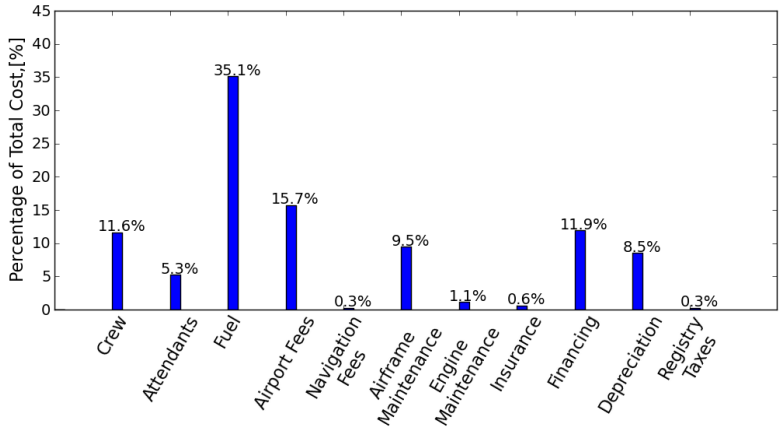

Figure 3.10: Example of direct operating cost breakdown for 150 passenger load and 1000 [nmi] main mission at a fuel price of 2.93 US$ per gallon

3.2 Aircraft Family Design

The design of an aircraft family incorporates balancing the individual design and performance of each aircraft with the design and performance of the other aircraft in the family through the common components. Figure 3.11 shows an example of common components shared by aircraft in the Embraer E-Jet family. The ERJ-170 is the baseline aircraft of the family. The ERJ-175 shares all components of the ERJ-170 but has a higher capacity due to the insertion of fuselage plugs. The ERJ-190 is a further stretched version of the ERJ-170 with additional wing span and chord extensions but with the same empennage geometry, wing leading edge and the winglet. To account for the effect of shared components between aircraft, one requires a measure to determine the level of commonality involved and the corresponding effect on cost and weight. The concurrent design of an aircraft family involves all of the challenges of aircraft design while adding the complexity of balancing the common components with the required individual performance of each aircraft.

A natural framework in which the trade–offs present in the design of product families are considered is given by multidisciplinary design optimization (MDO). In the design of the product family, each individual aircraft can be considered analogous to a discipline in the general MDO process. In an MDO setup, multiple interacting disciplines are optimized with respect to global, $\mathbf{z}$,

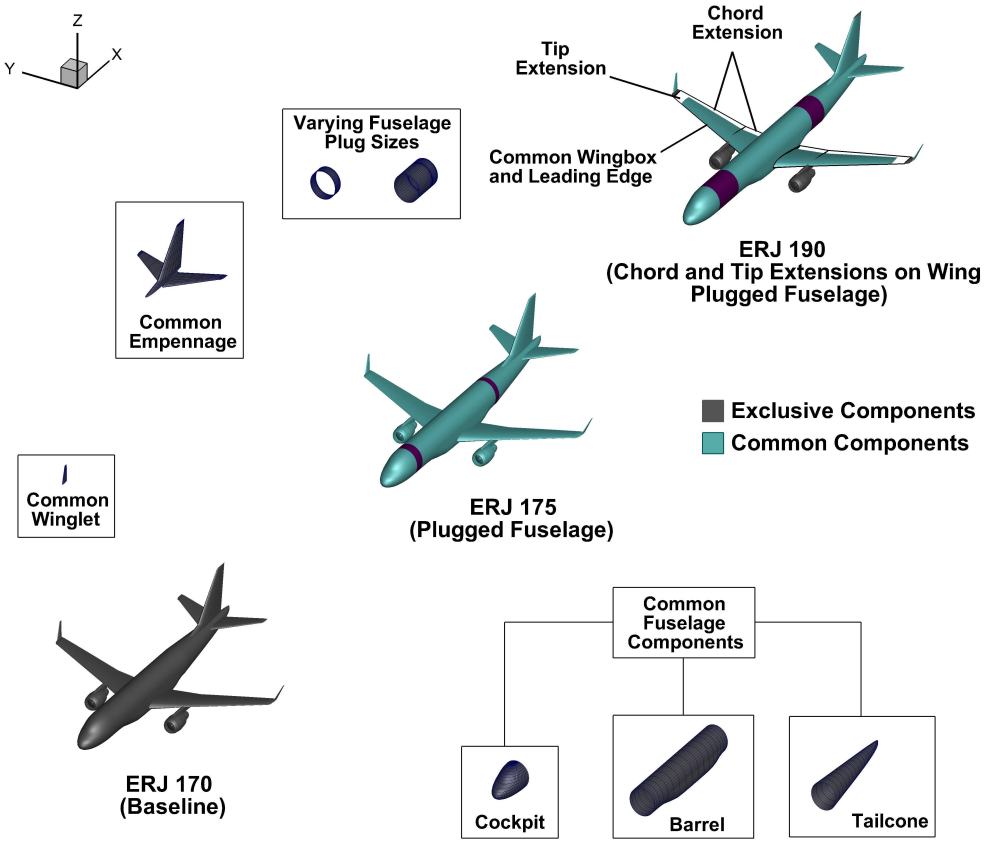

Figure 3.11: Commonality between members of the Embraer E-Jet family

local, $\mathbf{x}_i$, and coupling variables, $\mathbf{y}_i$, for discipline i. Similarly, in the family design problem, multiple aircraft are optimized with respect to common and exclusive components, as can be seen in Figure 3.12.

Several architectures exist to solve an MDO problem, which can be generalized into two main types, monolithic optimization approaches and decomposition optimization approaches. The advantage of a monolithic approach is that the MDO problem is formulated into a single optimization problem and only requires a single optimizer, while a decomposition approach requires an optimizer for each level of decomposition plus a system level optimizer. On the other hand, decomposition approaches can take advantage of weak coupling between disciplines and decompose large complex systems. The first mono-

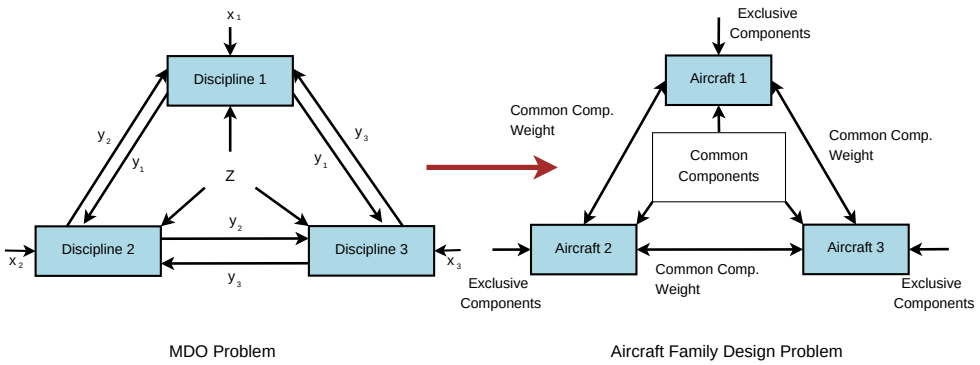

Figure 3.12: Analogy between multidisciplinary design optimization and aircraft family design [2]

lithic MDO architecture was the multidisciplinary feasible approach (MDF), which is formulated for n disciplines as [63]:

$$\min \quad f(\mathbf{x}, \mathbf{y}(\mathbf{x}, \mathbf{y})) \tag{3.14}$$

$$\text{w.r.t} \quad \mathbf{x}$$

$$\text{s.t.} \quad \mathbf{g}_z(\mathbf{x}, \mathbf{y}(\mathbf{x}, \mathbf{y})) \leq 0 \tag{3.15}$$

$$\mathbf{g}_i(\mathbf{z}, \mathbf{x}_i, \mathbf{y}_i(\mathbf{z}, \mathbf{x}_i, \mathbf{y}_{j \neq i})) \leq 0 \quad \text{for } i = 1, \ldots, n \tag{3.16}$$

where $\mathbf{x}$ is the full vector of design variables given by $\mathbf{x} = \left[\mathbf{z}^T, \mathbf{x}_1^T, \ldots, \mathbf{x}_n^T\right]^T$, $\mathbf{g}_z$ is the vector of design constraints depending on more than one discipline and $\mathbf{g}_i$ is the vector of design constraints of discipline i. In this approach a single optimizer provides the global and local design variables to each of the disciplines, but has no knowledge of the coupling variables. The coupling variables are handled within the objective function for every optimizer iteration, usually through iterations of the disciplines until a feasible set of coupling variables is found.

Another monolithic approach is the individual feasible design (IDF) archi-

tecture, which decouples the disciplinary analysis and is formulated as [63]:

$$\begin{aligned} \min \quad & f(\mathbf{x}, \mathbf{y}(\mathbf{x}, \hat{\mathbf{y}})) && (3.17) \\ \text{w.r.t} \quad & \mathbf{x}, \hat{\mathbf{y}} \\ \text{s.t.} \quad & \mathbf{g}_z(\mathbf{x}, \mathbf{y}(\mathbf{x}, \hat{\mathbf{y}})) \leq 0 && (3.18) \\ & \mathbf{g}_i(\mathbf{z}, \mathbf{x}_i, \mathbf{y}_i(\mathbf{z}, \mathbf{x}_i, \hat{\mathbf{y}}_{j \neq i})) \leq 0 \quad \text{for } i = 1, \ldots, n && (3.19) \\ & \hat{\mathbf{y}}_i - \mathbf{y}_i(\mathbf{z}, \mathbf{x}_i, \hat{\mathbf{y}}_{j \neq i}) = 0 \qquad \text{for } i = 1, \ldots, n && (3.20) \end{aligned}$$

where $\hat{\mathbf{y}}$ are independent copies of the coupling variables, sometimes called target variables, which allow the individual discipline analysis to be performed independently [63]. In the IDF approach a single optimizer provides the global and local design variables to each of the disciplines and values for the coupling variables. To ensure inter–disciplinary consistency, a set of equality constraints (Equation 3.20) is introduced to match the coupling variables provided by the optimizer with the coupling variables calculated by the disciplinary analysis. Hence, inter–disciplinary feasibility is only assured at convergence of the optimization. Additionally, the size of the optimization problem is increased, since the coupling variables are included in the optimization problem.

For large MDO problems it may be advantageous to decompose the problem along discipline lines. One such decomposition approach is the collaborative optimization architecture (CO), which decomposes the problem by introducing an additional optimization level. This system level problem is formulated as [63]:

$$\begin{aligned} \min \quad & f(\mathbf{z}, \hat{\mathbf{x}}_1, \ldots, \hat{\mathbf{x}}_n, \hat{\mathbf{y}}) && (3.21) \\ \text{w.r.t} \quad & \mathbf{z}, \hat{\mathbf{x}}_1, \ldots, \hat{\mathbf{x}}_n, \hat{\mathbf{y}} \\ \text{s.t.} \quad & \mathbf{g}_z(\mathbf{z}, \hat{\mathbf{x}}_1, \ldots, \hat{\mathbf{x}}_n, \hat{\mathbf{y}}) \leq 0 && (3.22) \\ & J_i^*(\mathbf{z}, \hat{\mathbf{z}}_i, \hat{\mathbf{x}}_i, \mathbf{x}_i, \mathbf{y}_i(\hat{\mathbf{z}}_i, \mathbf{x}_i, \hat{\mathbf{y}}_{j \neq i}) = 0 \qquad \text{for } i = 1, \ldots, n && (3.23) \end{aligned}$$

where $\hat{\mathbf{z}}_i$ are copies of the global design variables passed to discipline i, and $\hat{\mathbf{x}}_i$ are copies of the local design variables passed to the i^{th} sub-level problem. The objective of the system level problem is the overall design objective, as for the monolithic approaches. Copies of local design variables are only used

if these variables directly affect the global design objective [63]. The equality constraints (Equation 3.23) ensure that the copies of the global, local and coupling variables agree to a single value at convergence. The i^{th} sub-level problem is formulated for discipline i as [63]:

$$\min \quad J_i = \|\hat{\mathbf{z}}_i - \mathbf{z}\|^2 + \|\hat{\mathbf{x}}_i - \mathbf{x}_i\|^2 + \|\hat{\mathbf{y}}_i - \mathbf{y}_i(\hat{\mathbf{z}}_i, \mathbf{x}_i, \hat{\mathbf{y}}_{j\neq i})\|^2 \quad (3.24)$$

$$\text{w.r.t} \quad \hat{\mathbf{z}}_i, \mathbf{x}_i$$

$$\text{s.t.} \quad \mathbf{g}_i(\hat{\mathbf{z}}_i, \mathbf{x}_i, \mathbf{y}_i(\hat{\mathbf{z}}_i, \mathbf{x}_i, \hat{\mathbf{y}}_{j\neq i})) \leq 0 \quad (3.25)$$

The discipline design constraints are treated exclusively in the sub-level problem, while the objective of the sub-level problem is to minimize the error in the global, local and coupling variables to ensure system consistency.

In the case of an aircraft family, the analysis of each individual aircraft is independent, with the exception of the weight of the common components, during the sizing process. The coupling of the aircraft through the weight of the common components can be handled directly in the sizing process of the individual aircraft as described below. Therefore, a monolithic optimization approach, analogous to an MDF architecture is selected to optimize the aircraft family. MDF allows for the implicit coupled analysis of the aircraft, while a single level optimizer handles the global and local design variables, which define the common and exclusive components, for each aircraft project. The MDF approach does not require the addition of design variables or constraints in the aircraft design formulation and, since in this case the coupling is handled directly in the sizing of the aircraft, does also not require an iterative multidisciplinary analysis. Hence, the MDF formulation allows for an efficient solution to the aircraft family design problem.

3.2.1 The Modeling of Commonality

With product families, design for commonality can lead to penalties because common components are not optimal for any single aircraft [64]. Perez *et al.* [2] provided a method to quantify the effect of commonality on weight and cost for the design of an aircraft family. Their methodology assumes that weight and cost are the two disciplines that are the most strongly affected by the use of common components.

Commonality Effect on Weight

When using common components in the design of individual aircraft, it is generally expected that these components will have increased weight and size compared to components designed directly for the given aircraft. This increase in weight is due to the fact that the components have to handle the operational conditions of the aircraft with the most severe conditions. Hence, the common components are oversized for aircraft with less severe operational requirements. To account for this, the weight model allows for fixed weights to be included for certain components when sizing the individual aircraft. This increase in weight also propagates through the analysis of each aircraft and affects other modules, such as aerodynamics and performance and hence the operating cost of the aircraft.

Commonality Effect on Cost

The primary gain of commonality lies in expected cost reductions by savings in the development and production of the common components for the aircraft family. This reduction in cost comes from the common design, manufacturing processes and tooling of these components. Another aspect that can reduce the development cost is the requirement for fewer prototype aircraft and test airframes. A model that includes the effect of commonality on cost requires a method to quantify the design cost savings due to commonality and must take into consideration the varying degree of commonality between the different aircraft in a family. An estimation of the effect of commonality between aircraft in a family is provided by Perez [2], where each cost contributor is multiplied by a constant factor scaled by the level of design commonality:

$$C_k^* = \begin{cases} f_k C_k \frac{1}{CI} & \text{if } CI \geq f_k \\ C_k & \text{otherwise} \end{cases} \tag{3.26}$$

where C_k is the value of the k^{th} cost contributor, such as engineering, labour, *etc*, for the given aircraft, f_k is a commonality cost reduction factor specific to each cost contributor and CI is the aircraft design commonality index.

The commonality index represents a metric to assess the degree of commonality between members of a product family [65]. Hence, the index scales the effect of the cost reduction of each cost contributor. There are many different methods used to determine the commonality index in different industries, for example based on common parts count or even the count of common manufacturing processes [65]. The commonality index used here represents the

degree of original design not required for each of the individual aircraft in the family. The cost model used in this work is mainly dependent on the weight of the aircraft and the components; hence a weight–based commonality index is proposed which relates the weight of the common design components of the overall empty weight of the aircraft:

$$CI = W_{\text{common}} / \left(W_{\text{common}} + W_{\text{exclusive}} \right) \tag{3.27}$$

The weight of components already designed for another aircraft in the family and hence accounted for in that aircraft's development and production costs, is added to the weight of the common components, W_{common}, while the weight of any components design for the specific aircraft are added to the weight of the exclusive components, $W_{\text{exclusive}}$.

Table 3.1 lists cost reduction factors for a typical case, where the cost reduction factor for each cost contributor is estimated by detailing each item as a number of separate tasks. The final cost reduction factor for each cost contributor is the weighted sum of the cost reduction factors for each of its component tasks. Equation (3.28) is used to calculate f_k, the cost reduction factor for the k^{th} cost contributor where $f_{i,max}$ and p_i are the cost reduction factor and the proportional weighting for task i, respectively.

$$f_k = \sum_i f_{i,max} p_i \tag{3.28}$$

This task-structured breakdown incorporates the flexibility to adapt the model to a specific product or project by adjusting the task weighting or available cost savings associated with individual tasks in order to best reflect a particular aircraft family, development project or corporate design and manufacturing environment. The values listed in Table 3.1 are based on an initial estimate refined and validated against available data for the Airbus A320 family of aircraft, and represent the maximum cost reduction realizable for a derivative aircraft sharing previously designed common components with another aircraft.

For the development phase, the greatest cost reductions occur in engineering, tooling and certain flight test tasks (planning and data reduction), where it has been assumed that the engineering effort associated with common components does not need to be repeated. Cost reductions associated with the requirement for fewer prototype aircraft and test articles are also included and can be adjusted to suite the unique features of individual development programs. The next greatest cost reduction predicted is for manufacturing labour

Table 3.1: Development and production phase cost reduction factors

Cost Contributor/Task	Development Phase Fraction [%]	Development Phase Red. Factor	Production Phase Fraction [%]	Production Phase Red. Factor
Engineering	$f_k = 0.075$		$f_k = 0.800$	
Design and system integration	50.0	0.05		
Engineering for mock-ups and models	8.0	0.02		
Engineering for testing	30.0	0.02		
Drawings and specifications	7.0	0.03		
Sustained engineering efforts	5.0	0.80	100.0	0.80
Manufacturing Labour	$f_k = 0.508$		$f_k = 0.854$	
Labour to fabricate (in house)	20.0	0.52	20.0	0.85
Labour to fabricate (contractor)	38.0	0.41	38.0	0.75
Sub- and final assembly	42.0	0.59	42.0	0.95
Manufacturing Materials	$f_k = 0.934$		$f_k = 0.890$	
Raw materials	40.0	0.97	40.0	0.95
Purchased hardware	60.0	0.91	60.0	0.85
Quality Control	$f_k = 0.445$		$f_k = 0.798$	
Receiving inspection	25.5	0.41	32.0	0.75
Production inspection	13.5	0.52	16.9	0.85
Inspection of assemblies	28.3	0.59	35.4	0.95
Inspection of tooling	12.5	0.02	15.7	0.50
Inspection of test articles	20.2	0.50		
Development Support & Testing	$f_k = 0.453$			
Materials and labor for test parts, models and mock-ups	11.8	0.10		
Fabrication of structural test articles and coupons	44.1	0.50		
Structural and systems testing	44.1	0.50		
Tooling	$f_k = 0.061$		$f_k = 0.581$	
Tooling design	25.0	0.02	5.0	0.02
Tooling fabrication	70.0	0.02	60.0	0.50
Tooling maintenance	5.0	0.85	35.0	0.80
Flight Test	$f_k = 0.667$		$f_k = 0.792$	
Engineering Planning	15.0	0.15	15.0	0.35
Instrumentation	20.0	0.60	20.0	1.00
Flight operations	25.0	1.00	25.0	1.00
Data reduction	10.0	0.35	10.0	0.35
Engineering reporting	30.0	0.80	30.0	0.85
Avionics	$f_k = 0.690$		$f_k = 1.000$	
Development and programming	40.0	0.30		
Purchase equipment	60.0	0.95	100.0	1.00

and is based on the assumption that common parts can be acquired from existing product lines and immediately realize cost advantages associated with production quantities and mature manufacturing environments. Cost reduction factors for quality assurance and development support are estimated based on a fixed percentage of manufacturing, tooling and testing labour hours. The cost savings realizable from the production phase are less than for the development phase and are primarily associated with the use of existing tooling

and a reduction in learning curve costs. Table 3.1 does not consider operating costs, although cost reductions could be estimated based on common spare parts inventory and maintenance tasks.

3.2.2 Existing Aircraft Families

The presented cost model and the cost reduction factors were also tested against other existing aircraft families for which data was available. These include the Bombardier CRJ-200, which evolved from the Challenger 600, and the derivative aircraft, which have increased fuselage length by additions of plugs before and aft of the wing, added wing span and chord extensions and a common empennage. Similarly, the Embraer ERJ-145 evolved from the EMB-120 Brasilia, while the ERJ-135 is a shortened version with the same wing and empennage geometry. The ERJ-190 is a stretched version of the ERJ-170 with wing span and chord extensions but with the same empennage geometry. The values for weight and development cost calculated using `pyACDT` in the respective reference year are summarized in Table 3.2 including the values for the Airbus A320 family. The table also lists the relative difference between the reference values from the literature and the calculated values. The listed commonality indices were estimated from the calculated component weights using Equation (3.27).

Table 3.2: Aircraft families summary

Aircraft Family	Maximum Takeoff Weight [lb_f]		Commonality Index[%]	Ref. Year	Development Cost [in Million]	
	Ref. [66]	pyACDT			Ref. [66]	pyACDT
CRJ-200	47700	47715(+0.03[1])	60.6	C$1987	275.0	287.7(+4.63[1])
CRJ-700	73000	70793(-3.02[1])	64.7	C$1995	645.0	665.3(+0.40[1])
CRJ-900	80750	78861(-2.34[1])	98.5	C$1999	200.0	228.1(+2.57[1])
ERJ-145	45635	46898(+2.77[1])	24.7	US$1993	300.0	298.8(-0.41[1])
ERJ-135	42108	42383(+0.65[1])	97.6	US$1997	100.0	108.7(+8.69[1])
ERJ-170	79344	76365(-3.75[1])	NA	US$1999	600.0	614.8(+2.47[1])
ERJ-190	105359	102791(-2.44[1])	80.8	US$1999	150.0	152.3(+1.56[1])
A318-100	130955	123608(-5.61[1])	98.8	US$1996	275.0	279.5(+1.63[1])
A319-100	141978	139574(-1.69[1])	99.4	US$1993	300.0	302.7(+0.90[1])
A320-200	162922	164604(+1.03[1])	NA	US$1984	NA	1329.4(NA)
A321-200	197093	191902(-2.63[1])	92.5	US$1990	660.0	650.4(-1.46[1])

[1] Relative difference w.r.t. reference value.

The values for maximum takeoff weight (MTOW) for the different aircraft agree well with stated values in the literature, with the highest relative differ-

ence of 5.61% for the Airbus A318. The estimated development costs of the individual members of each family also agree well with the reference values. The exception is the ERJ-135, which has the highest relative difference at 8.69%. One reason for this high difference can be given by the fact that the prototypes for the project were two modified ERJ-145s [66]. It can be noted that the same cost reduction factors given in Table 3.1 were used to estimate the cost for all the aircraft. Provided with more information for specific company procedures and aircraft projects, the values could be adjusted further to match specific aircraft projects reducing the error of the predicted cost from the model.

4 Fleet Allocation

The strategic planning of an airline employs complex algorithms to determine the fleet composition and number of aircraft required to operate a given route network to meet demands while making efficient use of resources. The task gets even more complex when considering daily operations in assigning individual aircraft, planning maintenance and scheduling crews. The airline planning process can be decomposed into several sequential steps, as can be seen in Figure 4.1. This approach is a representative approach and may differ from airline to airline [67].

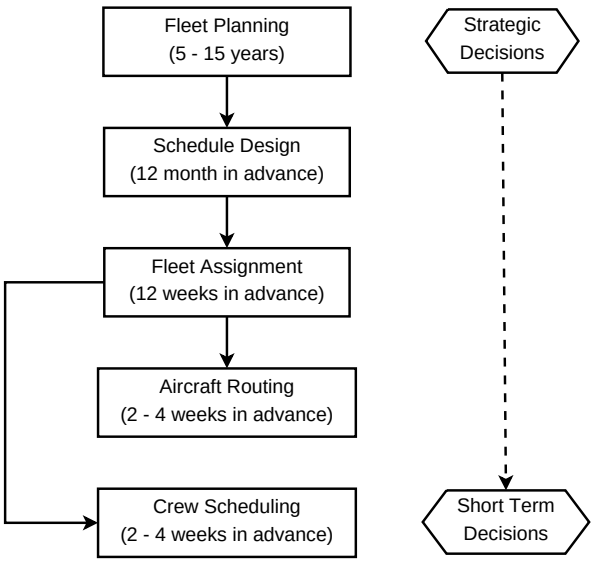

Figure 4.1: Overview of an airline planning process

In *fleet planning* the airline decides on the fleet size and fleet mix to purchase or lease to meet projected market demand. It is generally done infrequently and for a time period between 5 to 15 years. The *schedule design*

typically begins 12 month before it goes into effect and consists of determining the flight legs between specific origin and destination airports and departure and arrival times which maximizes potential revenue [67]. During the *fleet assignment* phase the different types of aircraft in the fleet are assigned to the specific flight legs in the schedule, which is done approximately 12 weeks in advance [68]. Given the types of aircraft for each flight segment the aircraft routing problem can be solved, which assigns the specific aircraft, or tail number, from that fleet type to each specific flight leg in the schedule. Similarly, with the type of aircraft known from the fleet assignment the *crew scheduling* can be performed, which assigns both the cockpit and cabin crews to each of the flight legs. The crew scheduling is dependent on the aircraft types for each use, due to the different type certifications by the crew. Each of these tasks is a complex problem in itself and can either be solved sequentially or simultaneously, with emphasis in resent research on formulating combined problems involving several of the mentioned tasks to provide higher resource utilization and cost reductions [13]. For the presented work the main interest lies in the allocation of individual aircraft types for a given set of routes and passenger demand for a long period of operations, but without a specific flight frequency and timetable for each day of operations.

This chapter presents the representative route networks and the model used to predict varying passenger demand for each route and day of operations. To simplify the planning process, a fleet allocation problem is introduced, which can be considered similar to the fleet planning process with a formulation based on the fleet assignment problem. Finally the solution process for the fleet allocation problem is shown and a test case using aircraft currently in operation is solved.

4.1 Representative Route Networks

The low number of original equipment manufacturers (OEMs) in the world and the global need for commercial transport aircraft results in a high competition in the design of new aircraft. New aircraft need to address not just the requirements for a single market, but for many global markets, each with their own requirements. Similarly, environmental impact of commercial aviation is driven by the global use of the fleets of transport aircraft. Hence to address the sustainability of commercial aviation the requirements of more than one market need to be considered.

Solving an allocation problem for all the routes serviced by airlines in the world for an extended period of time would result in a large and computationally expensive problem. In this dissertation two representative route networks in the North American and European markets are considered. In both networks only passenger flight operations are considered and no cargo operations. The North American market represents an important market for narrow-body aircraft in the foreseeable future, due to its size and the aging fleet of current narrow-body aircraft used. The European market is also a large market with many low cost airlines, which utilize narrow-body aircraft extensively for very short ranges. Additionally, the route structures and route length in the European market can be considered representative for emerging markets, such as China and India. The two route networks selected are described below.

4.1.1 North American Network

The North American network is based on a single hub flight schedule with 48 distinct non-stop routes. These routes are based on routes flown by a wide range of narrow-body aircraft by Delta Airlines and one of Delta Airline's subsidiaries, ExpressJet Airlines, operating from Atlanta (ATL) as the hub. Figure 4.2 shows the different routes selected. The number of passengers for each route and each month was estimated based on the total number of passengers transported and the number of departures performed as obtained from the Research and Innovative Technology Administration (RITA) aviation database [69] for the year 2012.

The selected routes include several long, medium to short range routes in North and South America with varying passenger demand. The longest route, serviced by Delta Airlines, is between Atlanta and Quito with a length of 2057 nautical miles. The highest demand route in every month of the year, also serviced by Delta Airlines, is between Atlanta and Los Angeles with an average of ten flights performed every day. The shortest route, serviced by ExpressJet Airlines, is between Atlanta and Chattanooga with a length of 92 nautical miles. This route is also one of the highest demand routes of the regional airline, with an average of 352 passengers traveling every day.

Table 4.1 summarizes the statistics for the route network for 12 months of operations, where the payload per flight is given by the number of passengers and their baggage with no additional cargo considered. The mean values are calculated based on all departures performed for the year. A detailed list of the routes and the passenger demand can be found in Appendix A.

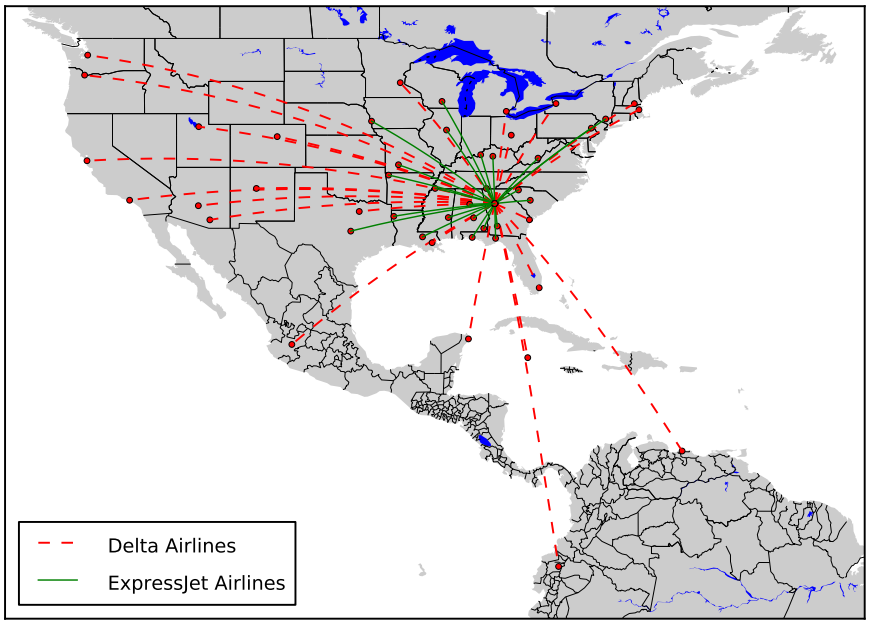

Figure 4.2: Selected Delta Airlines and ExpressJet Airlines routes

Table 4.1: American network statistics

Airline	Range,[nmi]		Passengers (per flight)		Payload, [lbf] (per flight)	
	Mean	Standard Deviation	Mean	Standard Deviation	Mean	Standard Deviation
Delta Airlines	950	518	147	33	32518	7395
ExpressJet Airlines	289	180	53	8	11704	1699

4.1.2 European Network

The second network is based on 48 distinct non-stop routes in Europe serviced by Lufthansa and CityLine from the hubs of Frankfurt (FRA) and Munich (MUC), shown in Figure 4.3. The average demand and monthly variations are estimated based on the types of aircraft operated on each route and general data given by the the Federal Statistical Office of Germany and the annual report published by the Lufthansa Group [70].

The European routes are significantly shorter than the North American

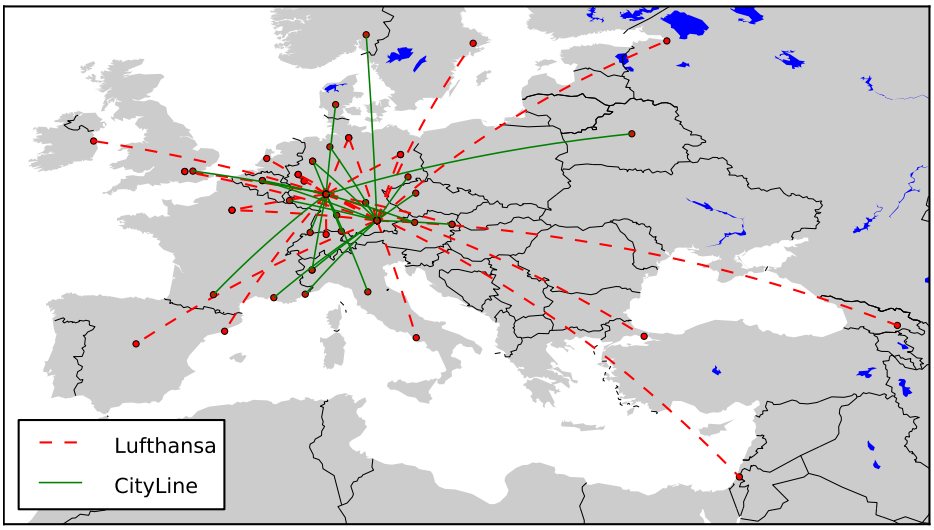

Figure 4.3: Selected Lufthansa and CityLine routes

routes, but with approximately the same amount of passengers traveling every day. The longest route, serviced by Lufthansa, with an average of three flights a day, is between Frankfurt and Tel Aviv at a length of 1596 nautical miles. The highest demand route is also one of the shorter routes between the two hubs of Frankfurt and Munich, with a length of 162 nautical miles and an average of 14 flights provided by Lufthansa every day. Other high passenger demand routes include the routes between Frankfurt and Berlin and Munich and Berlin at a route length of 234 and 259 nautical miles, respectively. The shortest route in this network is offered by Cityline between Munich and Nürnberg at a length of 74 nautical miles and an average of 85 passengers per day.

Table 4.2 summarizes the statistics for the route network for 12 months of operations, where the payload per flight is given by the number of passengers and their baggage with no additional cargo considered. The mean values are calculated based on all departures performed for the year. The detailed list of the routes can be found in Appendix A. The mean range for the routes in the Delta Airlines routes is approximately three times higher than for the Lufthansa routes with double the standard deviation, while the mean range for the two regional airlines is similar in both markets. The mean number of

Table 4.2: European network statistics

Airline	Range,[nmi]		Passengers (per flight)		Payload, [lbf] (per flight)	
	Mean	Standard Deviation	Mean	Standard Deviation	Mean	Standard Deviation
Lufthansa	356	249	117	19	25698	4271
CityLine	269	131	60	16	13142	3517

passengers per flight and variation is also higher for the Delta Airlines routes compared to the Lufthansa routes. The selected routes follow trends observed in the overall European and North American markets and are considered representative for the selected markets.

4.1.3 Modelling Future Demand

The allocation of an aircraft type to specific routes is subject to the route passenger demand characteristics, which is typically an uncertain quantity. From an operator's perspective, the uncertainty characteristics of passenger demand for a given network is an important consideration during the strategic planning phase and when planning new acquisitions of aircraft. Future demand for specific routes and entire markets can only be predicted based on historical data and can show significant fluctuations. Passenger demand for specific routes in an airline's route network can be considered relatively constant on a daily basis [13]. Even so daily fluctuations still exist. More significant fluctuations in the level of demand can be observed in the month-to-month operations. It can be noted, while passenger demand is not necessarily independent from both the type of aircraft and the frequency of the trip offered for a given route [13], it is assumed so in the current analysis.

The uncertainty in the networks needs to be considered when allocating aircraft to specific routes, especially when the sustainability of commercial aviation over a long time frame with predicted overall increases in demand is to be investigated. One method is to use the demand characteristics of an average future day of operations in the allocation problem. This deterministic approach does not address the robustness of the new aircraft with respect to demand fluctuations and predicted increases in the level of demand. Another approach is to use a Monte Carlo sampling technique to generate a set of demand characteristics for each route in a given network [13, 29]. In this work, a discrete time simulation is performed to include the uncertainty characteristics

of trip–demand. The discrete time simulation is closely related to the Monte Carlo sampling technique; the main difference is that discrete time simulation models a system in discrete time steps. Events occurring at each time step can be either independent or dependent on past occurrences and may depend on a given probability or may include parameters that depend on given probability distributions. Discrete time simulation and the closely related discrete event simulation have been used in other works to model boarding and deboarding times from aircraft [71] or operational scheduling [72]. The details of the simulation model algorithm are given in Figure 4.4:

```
Data: route list, monthly average demand(year 0)
initialization;
for route in route list do
    for year in number of years do
        for month in current year do
            monthly average × 1 + rand.gauss(mean% yearly change, %
            yearly standard deviation)
            for day in current month do
                PAX demand = rand.gauss(month average, month
                average×% variation)
            end
        end
    end
end
```

Figure 4.4: Passenger demand discrete time simulation

For each route in the two networks the simulation estimates the passenger demand for each day based on the current monthly mean passenger demand. The model assumes a normal distribution around the mean with a standard deviation of 10% of the given monthly mean value. Figure 4.5 shows the simulated passenger demand based on given monthly mean values for a single year of operations of one of the routes in the US network. For this route the peak demand occurs during the summer months, while the winter months exhibit a lower average demand.

To account for predictions of future increases in passenger demand, the monthly mean passenger demand values are adjusted each year by assuming a normal distribution around a given percentage increase in demand depending on the market under consideration. Future changes in passenger demand de-

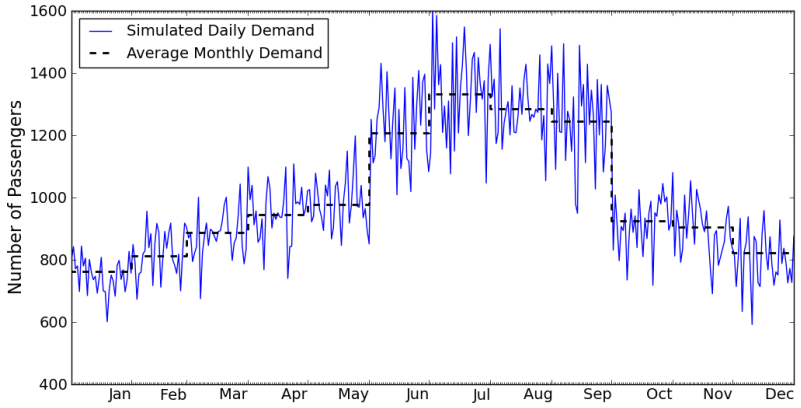

Figure 4.5: Simulated daily passenger demand for 2012 between Atlanta and Seattle for Delta Airlines with 10% standard deviation of monthly mean

pend on a variety of factors, such as the economic performance of a country, and may not follow any standard distributions. The normal distribution is assumed for simplicity of the model. Figure 4.6 shows the simulated passenger demand for both networks assuming an increase of 2.5% for the North American routes and 3.5% for the European routes, both with a standard deviation of 1.5%. These values provide an increase in passenger demand in line with future predictions from OEM forecast reports [73, 74, 75, 76]. Both route networks have approximately the same number of passengers at year zero, but due to the much longer range routes in the North American network, the revenue passenger miles (RPM) are much higher compared to the European market. Revenue passenger miles is given by the total number of paying passengers multiplied by the number of miles that those passengers are transported [77]. This trend can be observed in Figure 4.7, which shows the RPM for the same simulation. The total increase in passenger demand for both networks follows the given mean increases, but the monthly values of individual routes can vary significantly. The RPM increase faster in the North American route network compared to the European network, due to the different route structures and length. The simulation can be run offline for any given number of years of operations. The generated daily passenger demand can then be used in the aircraft allocation problem described below.

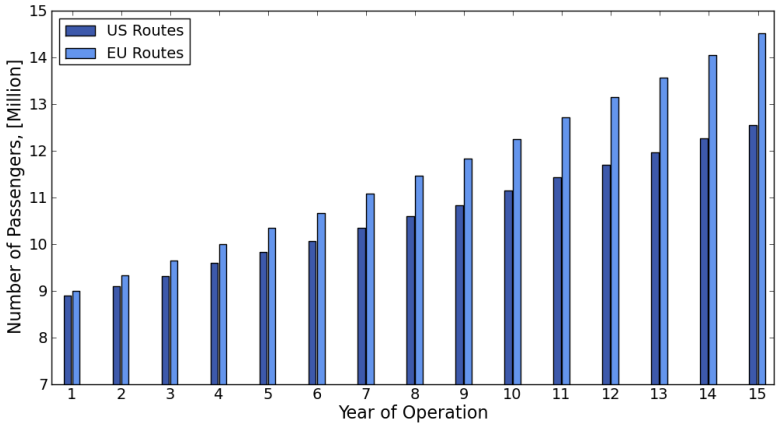

Figure 4.6: Simulated passenger demand for 15 years of operations with 2.5% increase in mean demand for North American routes and 3.5% for European routes

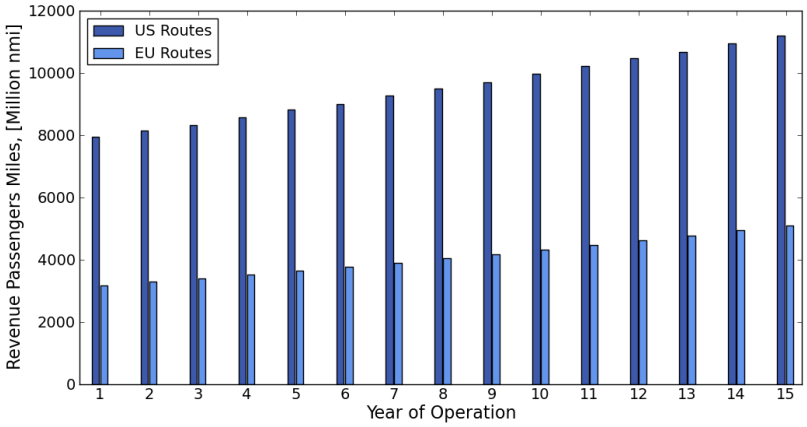

Figure 4.7: Simulated revenue passenger miles for 15 years of operations with 2.5% increase in mean demand for North American routes and 3.5% for European routes

4.2 Fleet Allocation Problem

The general fleet assignment problem tries to assign available aircraft types in an airline's fleet to a given schedule of flights, usually in a 24 hour time window for domestic routes [77]. The fleet assignment formulation by Hane *et al.* [78] is generally referred to as the basic fleet assignment model. The fleet assignment problem is formulated as a constrained integer programming (IP) problem:

$$\text{min} \quad \sum_i \sum_j c_{i,j} x_{i,j} \tag{4.1}$$

$$\text{w.r.t} \quad x_{i,j} = \begin{cases} 1 & \text{if flight } i \text{ assigned to fleet-type } j \\ 0 & \text{otherwise} \end{cases}$$

$$G_{k,j} \in Z^+$$

$$\text{s.t.} \quad \sum_j x_{i,j} = 1 \qquad \text{for } i = 1, \ldots, n_{routes} \tag{4.2}$$

$$G_{k^-,j} + \sum_i S_{i,k} x_{i,j} = G_{k,j} \quad \text{for } k = 1, \ldots, n_{nodes} \text{ and } j = 1, \ldots, n_{types} \tag{4.3}$$

$$\sum_k G_{k,j} \leq N_j \qquad \text{for } j = 1, \ldots, n_{types} \tag{4.4}$$

In this model the objective is to minimize the total cost of assigning the different fleet types to the flight legs in the given schedule, where $c_{i,j}$ is the cost of assigning fleet-type j to flight leg i. The cost for each fleet type consists of direct (DOC) and indirect operating costs (IOC), and spill costs. Spill cost represents the cost associated with lost revenue when the flight leg demand is greater than the capacity of the assigned fleet type. Hence, some passengers have to take either an earlier or later flight, or are recaptured by the airline, but sometimes at a discount, or are lost to a flight from another airline. The problem uses binary decision variables, $x_{i,j}$, to assign fleet type j to flight i and integer decision variables, $G_{k,j}$ to represent aircraft of type j overnight at node k. The equality constraints (Equation 4.2) ensure that each flight leg in the network is covered by one, and only one, aircraft type in the fleet. The balance constraints (Equation 4.3) ensure that the flow through the network is a circulation and can be repeated the next day. The number of aircraft, $G_{k^-,j}$ of type j just before node k plus the sum of arrivals, $S_{i,k}$ equal to one, and departures, $S_{i,k}$ equal to negative one, matches the aircraft overnight at node k. The final set of constraints (Equation 4.4) ensures that the number of assigned aircraft of each fleet type does not exceed the total available

number of aircraft of that type, N_j. There exist several extended versions of the standard fleet assignment problem, such as an itinerary-based assignment problem [14], but each of these formulations require at least average demand data and a detailed flight schedule for a single day of operation.

For the current work the main interest lies in determining the aircraft type for each given route used by an airline for a longer span of operations rather then tracking each aircraft over a detailed flight schedule for a typical day of operations. To account for the longer span of operations the fleet assignment problem is modified into a fleet allocation problem The allocation problem assumes a single monopolistic airline that tries to meet the passenger demand for a given set of routes during a given time of operation. It is assumed that the single airline simulates the overall goal of airlines for a set of representative routes. To reduce the number of decision variables, the demand for each flight is assumed to be symmetric, that is for each day of operations the same amount of passenger demand exists between two city pairs [28]. The modified problem is then given as follows:

$$\min \quad \sum_{i}\sum_{j}\sum_{m}\sum_{d\in m} f_{i,j,d}c_{i,j,d}x_{i,j,m} + \sum_{y}\sum_{j} n_{j,y}C_{AQU_j,y} \tag{4.5}$$

$$\text{w.r.t} \quad x_{i,j,m} = \begin{cases} 1 & \text{if flight } i \text{ assigned to fleet-type } j \text{ for month } m \\ 0 & \text{otherwise} \end{cases}$$

$$\text{s.t.} \quad \sum_{j} x_{i,j,m} = 1 \quad \text{for } i = 1,\ldots,n_{routes} \text{ and } m = 1,\ldots,n_{months} \tag{4.6}$$

where $c_{i,j,d}$ is the cost of assigning fleet-type j to route i for a given day d, and $f_{i,j,d}$ is the number of flights required by fleet-type j to meet the passenger demand of route i on day d, $n_{j,y}$ is the number of aircraft of each type required to operate the network for each year, y, of operations; C_{AQU_j} is the acquisition cost for each aircraft type. The number of aircraft of each type depends on the allocation of aircraft for each year of operation and is a function of the decision variables as described below. It is assumed that the required number of aircraft for each year of operation are leased at the start of each year, given the airline the flexibility to adjust the fleet mix. The flight frequency is determined to ensure the full demand is met for each route based on the capacity of the aircraft, a maximum load factor and the demand for the route for that day. Where load factor represents the number of passengers carried divided by the capacity of the aircraft. The flight frequencies of each aircraft for each day of operations can restrict the use of some of the aircraft types for

certain routes based on a required minimum and maximum flight frequency given by:

$$f_{i,j,d} \geq f_{i,d_{min}} \quad \text{for } i = 1, \ldots, n_{routes} \tag{4.7}$$

$$f_{i,j,d} \leq 24 \quad \text{for } i = 1, \ldots, n_{routes} \tag{4.8}$$

The inequalities in Equation 4.7 limit flight frequency to a minimum daily frequency for each route, which is given in the network data as two thirds of the current flight frequency. The minimum frequency also addresses the problem of using cost as the objective for the network problem by ensuring flexibility for passengers and the airline for connection flights. The maximum frequency inequalities in Equation 4.6 limit the frequency of departures to each destination in a day in order to not overload an airport.

The simplification of the allocation problem reduces the design variables to only binary decision variables, $x_{i,j,m}$, assuming that the same aircraft type is used for all days of operation for a given month. As for the basic fleet assignment problem, the objective of the allocation problem is the sum of the operational cost but with the addition of the acquisition cost of purchasing or leasing the total number of aircraft of each type required for each year of operations. Generally, an airline would assign aircraft to maximize profits; using cost as a surrogate can lead to larger aircraft, since they are more cost–effective [79]. To estimate the revenue for operating a given network, a detailed ticket price and revenue model is required, but revenue management systems strongly depend on individual strategies of each airline and simplified revenue functions usually do not reflect the true complexity of these systems [14]. Including the acquisition cost of the aircraft in the objective prevents the overuse of large aircraft, due to their high acquisition costs compared to smaller aircraft. The balance and fleet size constraints can be removed, since the allocation problem does not require a specific flight schedule to be followed. The equality constraints (Equation 4.6) ensure that each route in the network is covered by one aircraft type in the fleet.

The size of the airline fleet on any day in a month can be calculated based on the allocation of the different aircraft types and the number of flights required to meet the given passenger demand:

$$n_{j,d} = \frac{2 \sum_i f_{i,j} x_{i,j,m} \left[BH_{i,j} \left(1 + EMH_j\right) + TH_j(n_{PAX_{i,d}}) \right]}{24} \tag{4.9}$$

where $BH_{i,j}$ are the block hours of fleet-type j for route i, $TH_j(n_{PAX_{i,d}})$ is the turn–around time as a function of the number of passengers carried, and

EMH_j is the ratio of maintenance hours per block hour. The total sum of time required for each aircraft type is multiplied by two to account for the return trips. The total number of aircraft of each type is then the higher integer value of n_j. A simple model is used to calculate the turn–around time for each aircraft based on estimates of turn–around times in airport planning reports for existing aircraft. The model is developed assuming the critical time path is: engine shutdown, positioning of stairs and opening of doors (2 min), passengers deplaning the aircraft, servicing the interior of the aircraft, passengers boarding the aircraft, removing stairs and pushback (3 min). This assumption is based on the fact that most of the routes are domestic routes and assumes that the time required to refuel the aircraft is shorter than the given time path. The turn–around time for a given aircraft in minutes is then:

$$TH(n_{PAX}) = 2.0 + \frac{n_{PAX}}{k_1 n_{doors}} + \frac{n_{PAX}}{k_2} + \frac{n_{PAX}}{k_3 n_{doors}} + 3.0 \tag{4.10}$$

where n_{PAX} is the number of passengers, n_{doors} is the number of doors used at the gate and k_1, k_2 and k_3 are factors depending on the number of aisles and seats abreast as given in Table 4.3. The number of doors available for moving the passengers is assumed to be one throughout this work.

Table 4.3: Turn–around time coefficients

Aircraft Seat Configuration	Deplane Coefficient (k_1) [Passenger/min]	Servicing Coefficient (k_2) [Passenger/min]	Boarding Coefficient (k_3) [Passenger/min]
2 + 2	24.0	25.09	17.0
3 + 2	24.0	13.05	17.0
3 + 3	21.0	10.95	16.0
2 + 3 + 2	27.0	11.80	18.0
2 + 4 + 2	26.0	11.33	17.0
3 + 3 + 3	26.0	11.50	17.0
3 + 4 + 3	25.0	11.69	17.0

In the allocation problem, it is assumed that a sufficient number of aircraft is available at the beginning of each year of operation. This can result in aircraft sitting idle, due to changing levels of passenger demand for different days and months. Idle aircraft do not only represent lost revenue for an airline but also incur fixed costs, such as insurance and hangar fees. An airline can reduce these losses by either chartering out aircraft or opening up new routes. It is assumed that idle aircraft do incur the full cost by averaging the annual utilization, U_{ann} in hours, for each aircraft type and using this annual utilization in the calculation of the direct and indirect operating costs

for the respective year, y:

$$U_{ann_{j,y}} = \frac{\sum_{m \in y} \sum_{d \in m} 2 f_{i,j,d} t_{i,j,d} x_{i,j,m}}{n_{j,y}} \tag{4.11}$$

where $t_{i,j,d}$ is the total block time by aircraft type j for route i.

4.2.1 Solving the Allocation Problem

The solution of the fleet allocation problem requires two steps, the first is the evaluation of the performance of the different fleet types, the second is the evaluation of the operating cost of each fleet type and the allocation of the different aircraft. An outline of the procedure followed can be seen in Figure 4.8. The flight frequency is determined for each route based on the

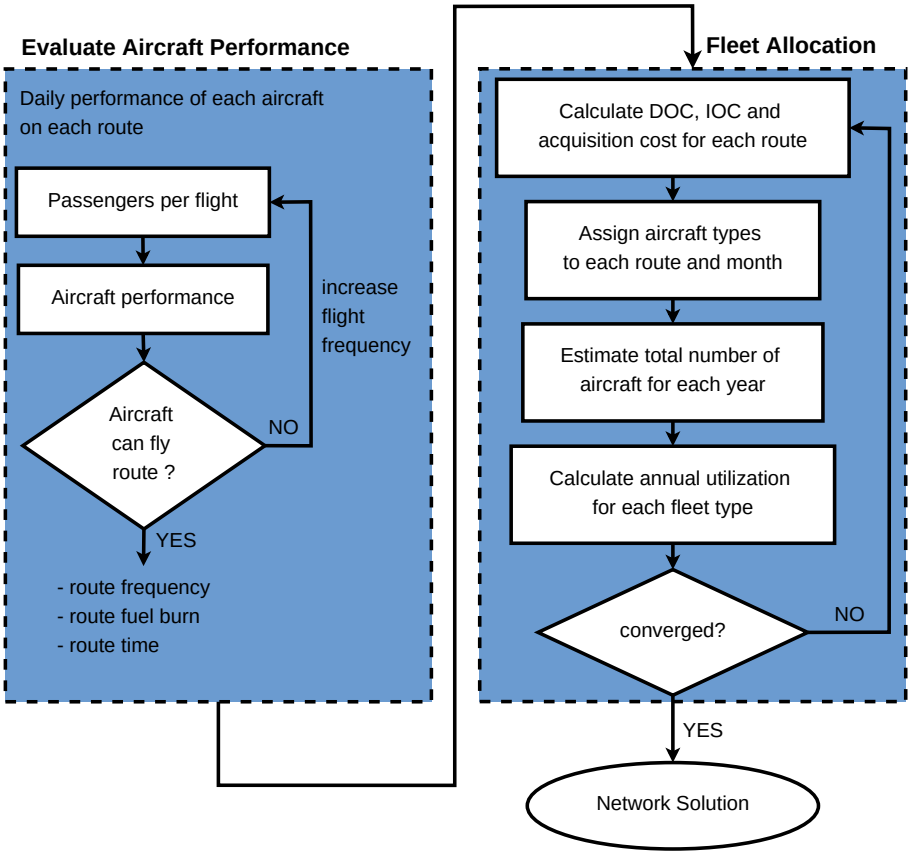

Figure 4.8: Outline of the procedure to solve the allocation problem

capacity of the aircraft, a maximum load factor and the number of flights required to capture all the passengers for each day in the month. If the resulting flight frequency is less than the minimum flight frequency, it is set to the minimum flight frequency. The flight frequency provides the average number of passengers and the payload weight required for the performance evaluation of the aircraft for that route and day. The performance analysis provides the fuel and time required based on the representative domestic mission profile shown in Figure 4.9. The climb schedule includes a constant calibrated air-

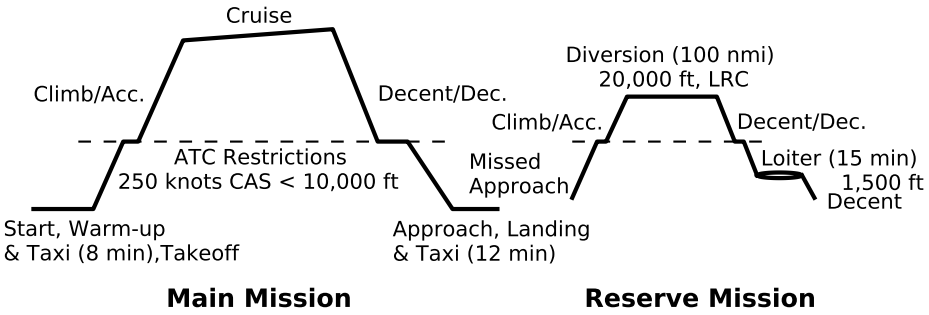

Figure 4.9: Design mission profile following ATC restrictions, takeoff and landing at ISA, no wind

speed (CAS) climb at 250 knots below 10000 feet due to air traffic control (ATC) restrictions, followed by a level acceleration to the climb speed. The remaining climb schedule assumes a constant CAS climb until the cruise Mach number is reached followed by a constant Mach number climb to the initial cruise altitude. The descent rate is limited by cabin pressure considerations and the same ATC restrictions apply as for the climb segment. One relaxation of ATC restrictions is assumed, which is to allow the aircraft to climb during the cruise segment for a more efficient cruise–climb. The mission also includes a 200 nautical mile diversion, consisting of a climb to 20000 feet of altitude, a constant altitude and Mach number cruise segment and descent to 1500 feet altitude with a 15 minute hold. Additionally, 5% fuel reserves based on the fuel required for the main mission are carried throughout the main and reserve mission.

If the aircraft can not achieve the required range of the route at the given payload, the flight frequency is increased, either until the aircraft can achieve the mission or the load factor falls below 30%. In this case, a constant penalty

factor of 1000 is applied to the fuel and time required for the aircraft type and route.

Given the number of passengers, fuel and time required, the direct and indirect operating cost for each aircraft type, day of operation and route can be calculated. The direct operating cost model also provides the required maintenance hours. Together with the turn–around time based on the number of passengers for each flight, Equation 4.10, the number of aircraft required for the network can be estimated based on Equation 4.9. The purchasing price of each aircraft is calculated based on the production cost, RDTE cost amortized over 250 aircraft and a 20% profit margin. The yearly leasing cost for each aircraft, $C_{AQU_j,y}$, are given by [80]:

$$C_{AQU_j,y} = 0.0835 APP_j \tag{4.12}$$

where APP_j is the purchasing price of aircraft type j. The operating and leasing costs of each aircraft type are then aggregated for each month. Since the frequency constraints are directly included in the cost calculation, an aircraft type can now be assigned to each month of operation for each route by selecting the type with the lowest cost. It can be noted that other objectives such as lowest fuel required or lowest time could also be used to assign the aircraft, but it is assumed that an airline would always use the minimum cost aircraft as a surrogate to maximize profits. Also, the direct operating cost do include both flight time, through the cost for the crew, and fuel in its calculation.

Given the allocation of the aircraft type to all the routes, the actual number of aircraft of each type can be determined and the annual utilization can be calculated based on Equation 4.11. Using the updated annual utilization, the operating costs are reevaluated and the process is repeated until the allocation is converged. The final solution of the fleet allocation problem includes the use of the different aircraft types over the years of operation, the total operating and acquisition costs and the total fuel burn to deliver all the passengers to their destinations. This selection process is similar to a shortest path algorithm with the cost of operating the route for a month by the different aircraft types as the path length. This approach was selected, since the large size of the allocation problem for long periods of operation, which reaches up to 51840 decision variables for the coupled optimization test cases, makes it difficult to be solved using other algorithms, such as a branch–and–bound or a simplex algorithm.

4.3 Fleet Allocation Verification

To test the fleet allocation procedure, the allocation problem was solved for four existing aircraft. These aircraft were the Bombardier CRJ-700, the Airbus A319-100, Boeing 737-800 and the Boeing 757-300, together spanning a wide range of capacities and design ranges. Each aircraft was modeled in the `pyACDT` framework; the geometric representation within the framework can be seen in Figure 4.10 and the specification for each can be found in Table 4.4.

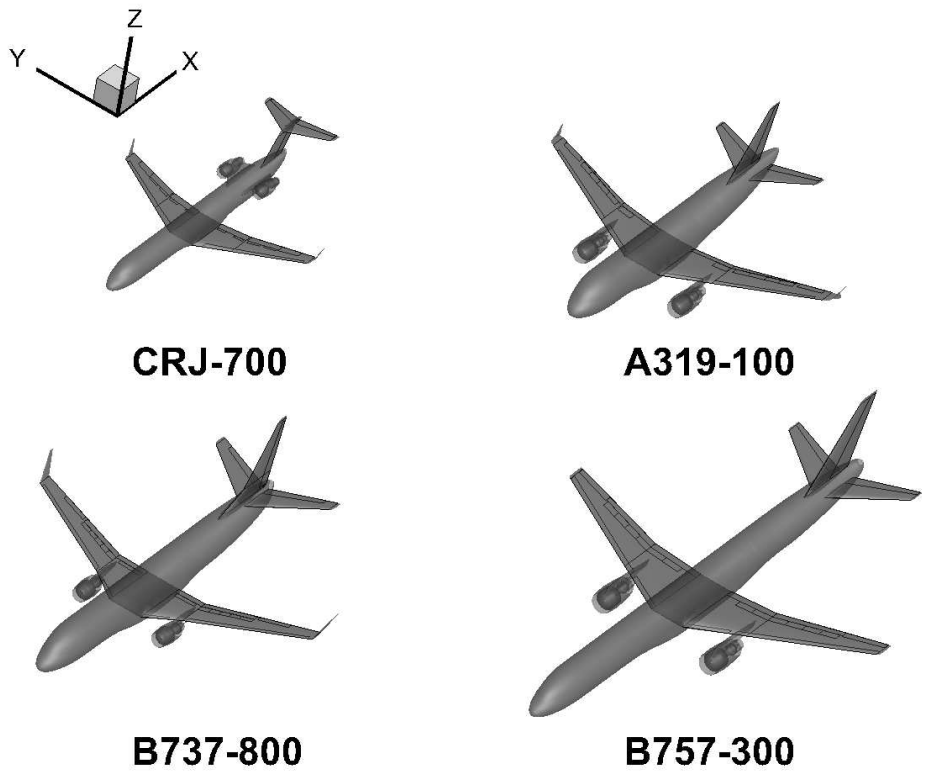

Figure 4.10: Reference aircraft geometries as modeled in `pyACDT`

The capacity is given by a single class layout with a 32 inch seat pitch. The design range is defined as the total flight range, main and reserve mission, at the full single class passenger capacity with baggage. The design commonality index for each aircraft was estimated based on component weights obtained from the weights module and the RDTE and production costs were estimated using the economics module in `pyACDT`.

Table 4.4: Reference aircraft specifications

	CRJ-700	A319-100	B737-800	B757-300
Operation				
Capacity	70	124	175	279
Seat Configuration	2+2	3+3	3+3	3+3
Design Range [nmi]	1218	1650	2700	3050
Geometry				
Wing Projected Span [ft]	76.24	113.43	114.72	124.41
Wing Aspect Ratio	8.81	10.58	11.83	7.79
Wing Reference Area [ft^2]	608.89	1093.91	1018.53	1670.52
Engines				
Maximum Static Thrust [lb_f]	13790	22000	27300	42600
Bypass Ratio	5.1	6.0	5.1	5.8
Flight Condition				
Climb CAS [knots]	290	300	300	300
Cruise Mach	0.74	0.78	0.78	0.79
Cruise Altitude [×1000 ft]	31	35	31	31
Weights and Loadings				
Maximum Takeoff Weight [lb_f]	73000	141978	174700	271000
Operational Empty Weight [lb_f]	43500	87031	94580	141800
Maximum Fuel Weight [lb_f]	19880	42238	46063	76980
Design Fuel Weight [lb_f]	14100	29527	42400	76980
Maximum Wing Loading [lb_f/ft^2]	957.51	1251.64	1522.83	2178.37
Maximum Thrust-to-Weight [lb_f/lb_f]	0.38	0.31	0.31	0.31
Costs				
Design Commonality Index [%]	64.45	99.43	89.39	86.71
Purchasing Price [Mil. 2014 US$]	36.39	61.33	76.93	100.93

The solution of this case can be used to verify the fleet allocation procedure and as reference results to the robust optimization and coupled optimization test cases, which are described in the following chapters. To measure the environmental performance of the aircraft on the two route networks, the metric of energy intensity, E_I, is used, which is introduced below.

4.3.1 Energy Intensity

Energy intensity, E_I, provides a useful measure of aircraft fuel efficiency for given operations and can be used as a metric for an individual aircraft, for aircraft operating on a specific route, or for an aircraft fleet operating in a network [81]. The metric evaluates the energy consumed per pound of payload transported one nautical mile, and for a network is given by:

$$E_I = \frac{\sum_i W_{fuel,i} LHV_{fuel}}{\sum_i W_{payload,i} R_i} \tag{4.13}$$

where $W_{fuel,i}$ is the weight of fuel consumed to operate route i, $W_{payload,i}$ is the payload transported along route i and R_i is the flight range. The lower heating value of fuel, LHV is taken as 18580 [BTU/lb]. The energy intensity does not only include the fuel required to operate the aircraft, and by extension the amount of CO_2 produced [82], but also incorporates the utilization of the aircraft by accounting for the payload and the distance the payload is transported. Considering the utilization of an aircraft is important when comparing performance of aircraft on a given network.

4.3.2 Reference Aircraft Network Performance

Modeling the four aircraft in the `pyACDT` framework, the fleet allocation problem can be solved following the procedure outlined in Section 4.2.1. Each network is solved independently assuming a monopolistic airline. The fuel price was set at 2.93 US$ per gallon and the maximum load factor was set to 90% to allow for the fact that the given capacities are for a single class layout. Following are the results of allocation problem for the two networks when operated for 15 years by the four specified aircraft with the passenger demand provided by the discrete time simulation as given in Section 4.1.3. This results in a total of 34560 binary decision variables and 8640 constraints for each network, respectively. Solving each network following the procedure outlined in Section 4.2.1 took an average of 110 seconds on a single, 3.0 GHz core machine.

North American Routes

Table 4.5 summarizes the performance of the different aircraft for the North American network and also provides the total values for the network. The total values represent the sum of the respective values for the full 15 years of operation. The majority of the routes are covered using the CRJ-700 and Boeing 737-800, with a handful of routes being serviced using the Boeing 757-300. The Airbus A319-100 is not assigned to any of the routes in the network. The CRJ is used mainly on the ExpressJet Airlines routes and on some of the Delta Airlines routes with low demand, resulting in an average range of 301 nautical miles. The short ranges of the assigned routes results in a high average energy intensity, with a high standard deviation. The average annual utilization of the aircraft type is fairly high for the number of short range routes it is assigned to, with 2453 hours. The Boeing 737 is assigned to the majority of routes and days with a wide range of route ranges, including the shortest of the routes between Atlanta and Chattanooga. This results in an average route

Table 4.5: Reference aircraft results for operating the North American route network for 15 years

Aircraft	CRJ-700	A319-100	B737-800	B757-300
Average Load Factor, [%]	78.2	NA	83.7	71.5
Average Route Range, [nmi]	301	NA	1034	908
Average Annual Utilization, [hr]	2453	NA	3008	1936
Max. Number of Aircraft	44	0	117	21
Number of Flights	502966	0	796688	80118
Individual Energy Intensity, [BTU/(lb_f nmi)]	28.95	NA	10.52	12.85
E_I Standard Deviation, [BTU/(lb_f nmi)]	39.15	NA	11.97	12.94
Network Energy Intensity, [BTU/(lb_f nmi)]	11.78			
Total Fuel Required, [Billion lb_f]	19.91			
Total Operating Cost, [Billion 2014 US$]	38.14			
Total Acquisition Cost, [Billion 2014 US$]	14.27			

range of 1034 nautical miles for this aircraft type and a relatively high annual utilization of 3008 hours. The average energy intensity is the lowest of all the assigned aircraft types, but the standard deviation is higher than the mean value. The Boeing 757 is assigned to only five of the routes, which includes the longest route between Atlanta and Quito, and also the relatively short but high demand, route between Atlanta and New Orleans. The average range of the routes assigned to this aircraft is lower than for the Boeing 737, at 908, and the annual utilization is the lowest of the three assigned aircraft types at 1936 hours. The mean and standard deviation of energy intensity is also higher than for the Boeing 737.

The average ranges for all the assigned aircraft are between 25% to 30% of their respective design ranges. The high design ranges of these aircraft results in high takeoff weights and corresponding high empty weight, designing for shorter ranges can reduce the takeoff weight and the empty weight, which can reduce the overall fuel required to operate the routes in the network. The yearly trends of energy intensity, fuel burn, operating cost and load factor for operating the network using the assigned aircraft are shown in Figure 4.11. The network energy intensity consistently decreases over the years by an average of 0.24% per year, resulting in a total decrease of 3.39% in the final year compared to the first year. This reduction in energy intensity is mainly due to

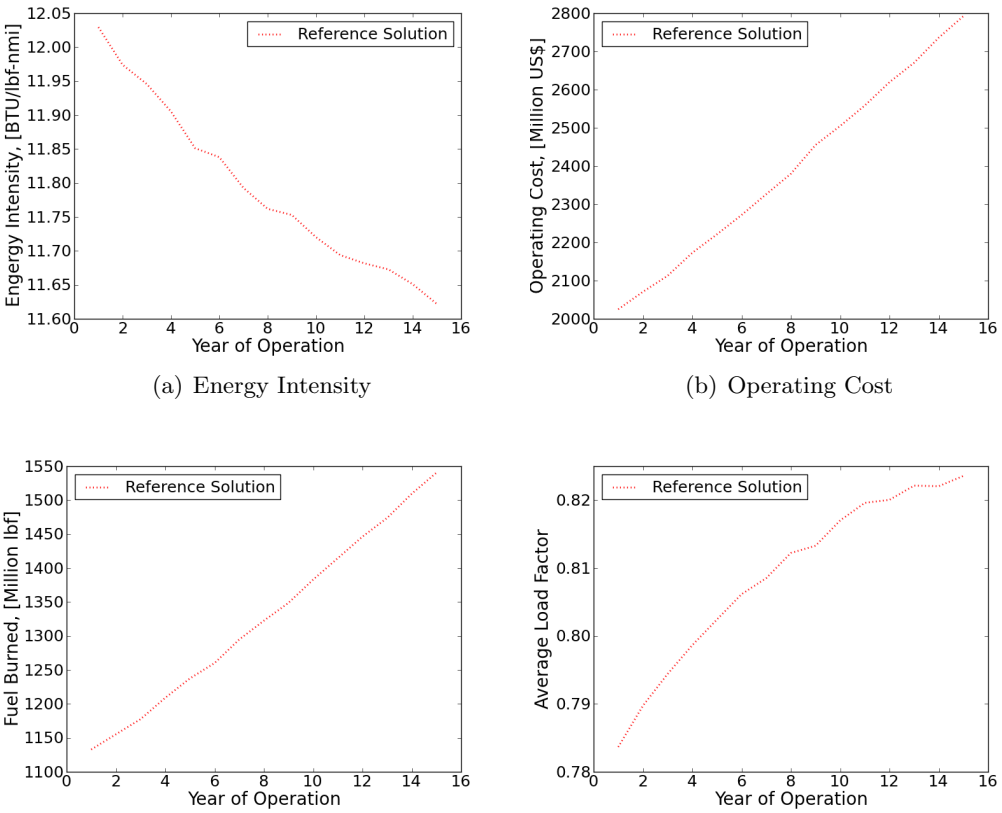

(a) Energy Intensity

(b) Operating Cost

(c) Fuel Burn

(d) Average Load Factor

Figure 4.11: Performance of allocated reference aircraft for operating the North American route network for 15 years

increased utilization of the aircraft by an increase in the load factor over the years, as can be seen in Figure 4.11(d). The total fuel burn increases on average by 2.22% and the operating cost, including direct and indirect operating costs, by 2.32% per year, or by a total of 35.97% and 37.90%, respectively, when comparing the first and final year. These values are slightly lower than the average increase in passenger demand, which increases on average by 2.5% resulting in a total of 41.13%, and revenue passenger miles, which increase by 2.47% per year or a total of 40.73%. With the energy intensity decreasing over the years, due to increasing load factors, the increases in fuel burn and cost are slightly lower than the increases in demand growth.

European Routes

For the European network, the routes are dominated by several very low range but high demand routes, such as the route between the two hubs of Frankfurt and Munich. Table 4.6 summarizes the performance of the solutions for the European network. All types of aircraft are allocated to some of the routes in

Table 4.6: Reference aircraft results for operating the European route network for 15 years

Aircraft	CRJ-700	A319-100	B737-800	B757-300
Average Load Factor, [%]	78.4	76.6	81.6	81.5
Average Route Range, [nmi]	232	334	374	316
Average Annular Utilization, [hr]	1596	1760	1878	1292
Max. Number of Aircraft	41	22	124	18
Number of Flights	234989	67080	970664	71751
Individual Energy Intensity, [BTU/(lb_f nmi)]	33.61	20.26	15.93	17.27
E_I Standard Deviation, [BTU/(lb_f nmi)]	43.83	25.83	19.13	18.09
Network Energy Intensity, [BTU/(lb_f nmi)]	17.05			
Total Fuel Required, [Billion lb_f]	12.21			
Total Operating Cost, [Billion 2014 US$]	31.51			
Total Acquisition Cost, [Billion 2014 US$]	13.11			

the European network, but as for the North American network, the majority of flights are performed by the CRJ-700 and the Boeing 737. The average route range for all the aircraft types are significantly lower than for the North American network, especially for the two Boeing aircraft, with low annual utilization. This results in high mean and standard deviations of energy intensity for each aircraft and the network as a whole; even so the total fuel burn is lower than in the previous case. The Boeing 757 is not assigned to any of the routes until year seven, at which point it is assigned to some of the very high demand but short routes, such as the route between Frankfurt and Berlin. This again raises the possibility of improved network efficiency with high capacity aircraft designed for shorter ranges and corresponding lower takeoff and empty weight.

Figure 4.12 shows the change in energy intensity, fuel burn, load factor and operating cost per year when operating on the network with these four aircraft allocated for minimum cost. The energy intensity generally decreases over the

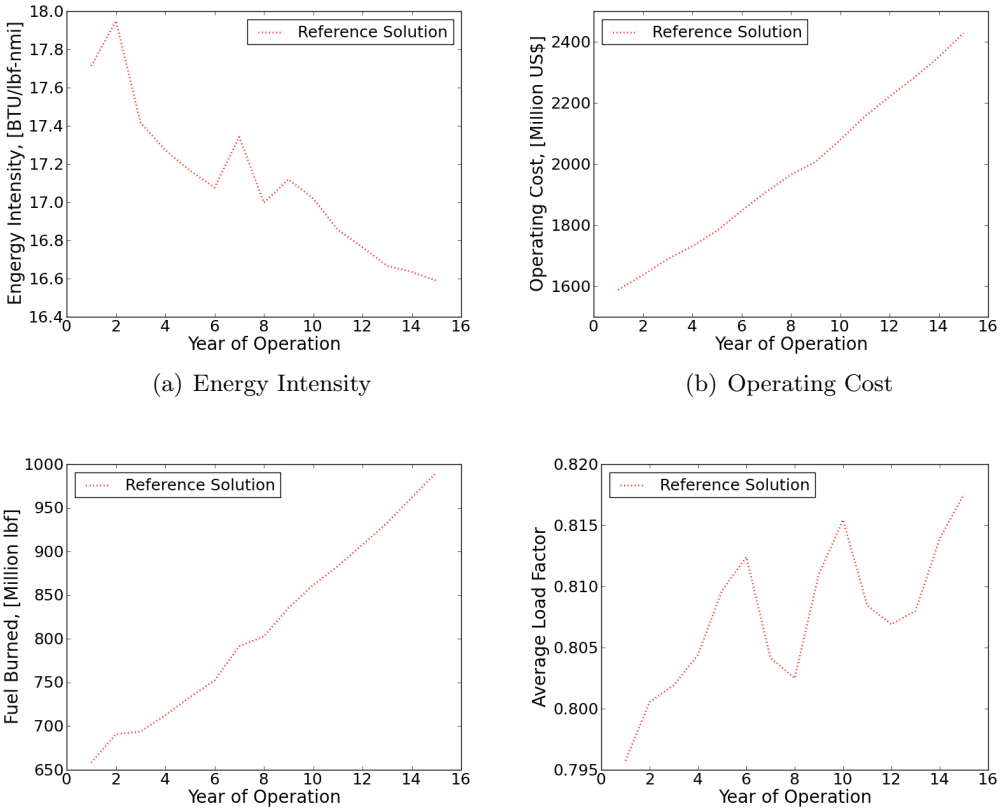

(a) Energy Intensity

(b) Operating Cost

(c) Fuel Burn

(d) Average Load Factor

Figure 4.12: Performance of allocated reference aircraft for operating the European route network for 15 years

years, but with some years with noticeable fluctuations. The average load factor follows a similar trend with several severe reductions in the average load factor. One of these low load factor years can be directly linked to the start of allocating the Boeing 757 in year seven, which has a significantly higher capacity as the next smaller aircraft. The reduction in load factor in year seven results in an increased energy intensity for the network in this year, due to the lower utilization of available capacity. The second valley in the average load factor is the result form switching routes assigned to the Airbus A319 to the higher capacity Boeing 737. This switch does not result in an increase in energy intensity, since the change in available capacity and corresponding

efficiency of the two aircraft is not as large as for the previous case. Overall, the energy intensity decreases by 6.34% between the first and final year, which represents almost double the reduction as for the North American network. The fuel burn and operating cost increase consistently over the years by 2.97% and 3.08% per year, respectively. The total increases from the first to the last year are 50.41% and 52.83% in terms of fuel burn and operating cost, which are higher than for the North American network. Considering the increases in passenger demand and revenue passenger miles, which increase by 3.47% and 3.44% or totals of 61.13% and 60.66%, the relative increases in fuel burn and operating cost are lower than for the North American network solution.

Figure 4.13 shows the ratio of the route range to the main mission design range of performed departures in log scale by the reference aircraft during the 15 years of operating the North American network. The departures are distributed between 10 to 90% of the respective design ranges, with an average range ratio of 43.9%. The highest number of departures occurs around 25% of the design ranges of the reference aircraft.

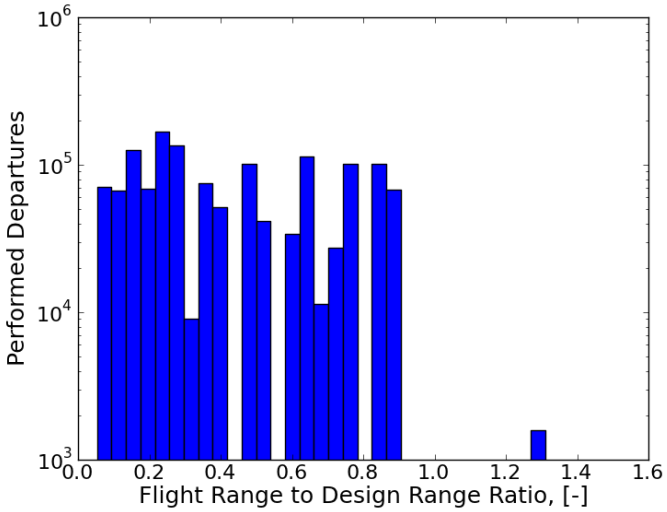

Figure 4.13: Route range to design range ratio of performed departures by the reference aircraft on the North American network (43.9% average ratio)

Figure 4.14 shows the range ratio of the performed departures for the European network. For the European network the main number of departures

occur between 10 to 50% of the respective aircraft design ranges, resulting in an average range ratio of 19.1%. This again demonstrates the difference in the routes for the two networks, with the European network dominated by high demand short range routes, while the North American routes are more distributed with respect to passenger demand and route ranges. Aircraft designed for a single market suffer from operational inefficiencies when operated on routes in a market with a different route structure.

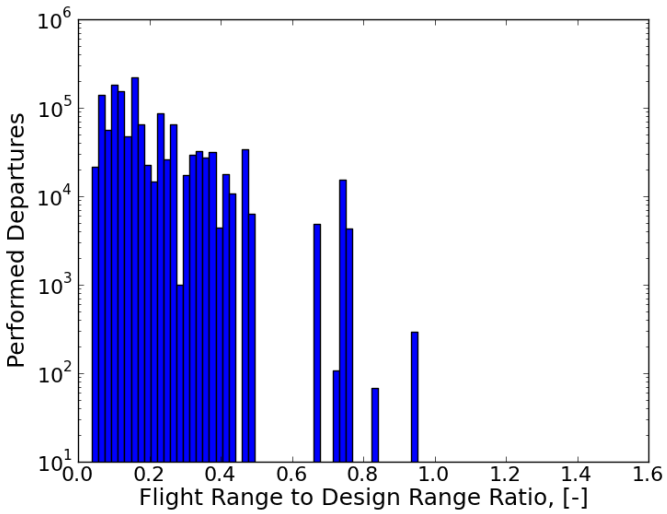

Figure 4.14: Route range to design range ratio of performed departures by the reference aircraft on the European network (19.1% average ratio)

In both networks the yearly increase in fuel burn and operating cost are lower than the increases in passenger demand, due to better utilization of the aircraft, through higher load factors. The better utilization of the aircraft also results in decreasing yearly energy intensities. In spite of this, the increases in fuel burn and costs are only slightly lower then the increases in passenger demand, which was expected given estimates from business as usual scenarios. This also indicates an unsustainable scenario for commercial aviation for the future. The allocation of the existing aircraft and their operational use in the two given networks follows the same trends as the use of narrow–body aircraft in the North American and European markets from available data. This verifies that the selected route networks and the formulated allocation problem

is representative. Additionally, the values obtained act as a "business as usual" case for the optimization test cases solved in the following two chapters.

5 Decoupled Robust Design of Aircraft

In this work the main focus is on the robustness of the environmental performance of new aircraft designs when allocated to routes of an airline with varying passenger demand. The fully coupled design of aircraft with the fleet allocation is a complex system–of–systems problem. One approach to reduce the complexity is to perform decoupled robust design optimizations of individual aircraft with respect to varying operational flight ranges and passenger loads.

Robust design optimization is part of the field of stochastic optimization, or optimization under uncertainty, and takes into account the effects of uncertainties present during the design process. In robust design optimization, the main goal is to reduce the sensitivity, or increase the robustness, in performance of the solution to variations in design parameters. Many different sources of uncertainties exist. Some common sources of uncertainties in aircraft design include geometrical uncertainties, such as manufacturing tolerances, modeling uncertainties, such as errors in the analysis models used, uncertain external parameters and variations in the operational environment [83]. Japanese engineer Genichi Taguchi is one of the first designers to acknowledge that the performance of any design can be significantly affected by variations in variables outside the control of the designer and that a good design must be insensitive to such variations [84]. In most cases, increased robustness comes at the expense of a decrease in nominal performance of a design [59].

The decoupled robust design optimization of individual aircraft removes the complexity of solving the fleet allocation problems during the design process, while still accounting for variations in operational range and passenger loads given by the route networks of the two markets. Following is a descrip-

tion of the robust optimization approach used to perform a decoupled robust aircraft design optimization. The solutions of a three aircraft test case are also presented, including the performance of the aircraft when allocated to the route networks introduced in Chatpter 4 and which can then be used as reference results to compare to the fully coupled aircraft design method introduced in Chapter 6 in terms of sustainability in operating the two route networks.

5.1 Robust Design Optimization

Robust design optimization aims to formulate a design optimization problem in such a way that the effect of uncertain input variables and parameters are accounted for in the solution. Three main steps are involved in the optimization under uncertainty [59]:

1. Identification, modeling and representation of the uncertainties under consideration during the design process.
2. Propagation of the uncertainties through the analysis models to quantify their impact on the design performance.
3. Formulating and solving a robust optimization problem which results in a robust optimal solution.

Many different methods exist on how to implement each of these steps to perform a robust design optimization. The methodology for each of the steps used here is discussed below.

5.1.1 Modeling Uncertainty

The uncertainties present in an engineering system can be classified into two general groups based on their origin as *aleatory* and *epistemic* uncertainties [85]. Aleatory uncertainties are the inherent variations, and as such irreducible, present in a physical system, input parameters or operating conditions, while epistemic uncertainties arise from the lack of knowledge during any phase of the modeling process of the system [85]. Epistemic uncertainties are not an inherent property of the system and can be reduced or removed by increasing the knowledge of the system or increasing the fidelity of the analysis used to model the system. The modeling of uncertainties can be divided into probabilistic and non–probabilistic approaches, where probabilistic are generally used for aleatory uncertainties with known distribution and non–probabilistic approaches are often used for epistemic parameters with scarce

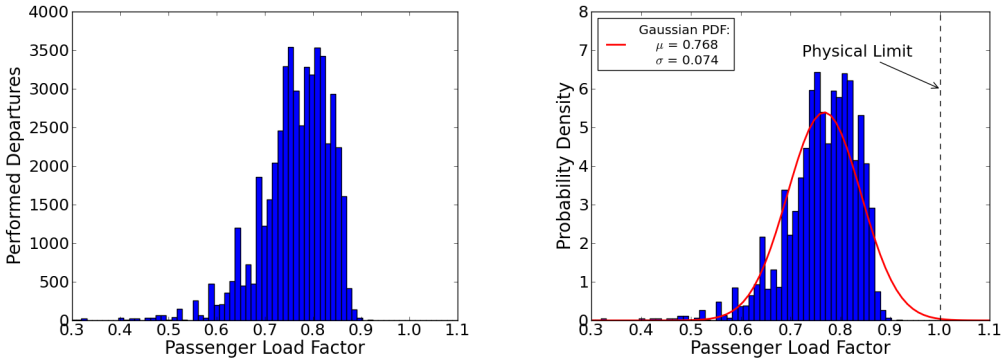

(a) Passenger Load Factor Histogram

(b) Probability Density Function

Figure 5.1: Histogram of passenger load factor for Delta Airlines and Lufthansa routes (a) and estimated Gaussian probability density function (b)

data.

For the current work the two uncertain external parameters that are being considered are the operational flight range and payload for each aircraft, which are aleatory uncertainties. Hence, the probabilistic approach is used, which is commonly used for these types of uncertainties [85]. The probabilistic approach makes use of a probability density function to model the uncertain parameter. The probability density function can either be known if sufficient data is available to generate it, or a distribution function, such as Gaussian, beta, log-normal, or exponential, can be assumed and matched to the data that is available [83]. Often the available data can not be matched to any given distribution function and a Gaussian distribution is assumed for simplicity. The use of the Gaussian distribution function can be justified by virtue of the central-limit theorem, which states that the sum of any number of independent random variables with different distributions tends to have a Gaussian distribution if no single variable contributes significantly [59].

Here, both uncertain parameters are assumed to have a Gaussian distribution; Figure 5.1 shows the passenger load factor for each departure of the Delta Airlines and Lufthansa for the routes specified in Section 4.1 for the year of 2011. The load factors were estimated based on single class cabin configurations for the respective aircraft that performed the flight. It can be

noted, that the load factor for each departure is only an average approximation, since the available data is aggregated monthly data, hence the high peaks that fall outside of the Gaussian approximation of the distribution could be more distributed than shown here. Care has to be taken when using a Gaussian distribution which spans from $[-\infty,\infty]$. As shown in Figure 5.1(b) a load factor greater than one or below zero is unrealistic.

5.1.2 Uncertainty Propagation

The propagation of uncertainty is needed to evaluate the statistical parameters of objectives and constraints with respect to uncertainties in parameters and design variables. The two most common methods are simulation methods, such as the Monte Carlo simulation (MCS), and methods based on the sensitivity of the output to variations in the input. It generally involves the re–evaluation of the design during the optimization process either to calculate sensitivities or perform numerical simulations [86].

The approach used in this work makes use of sensitivity information to estimate the effect of small perturbations around expected parameter values. Using a Taylor series expansion of the output function $f(\xi)$ around the point ξ^0, which are the mean values of n uncertain variables:

$$\begin{aligned} \widehat{f}(\xi) &= f(\xi^0) + \sum_{i=1}^{n} \frac{\partial f}{\partial \xi_i} \left(\xi_i - \xi_i^0\right) \\ &\quad + \frac{1}{2} \sum_{i=1}^{n} \sum_{j=1}^{n} \frac{\partial^2 f}{\partial \xi_i \partial \xi_j} \left(\xi_i - \xi_i^0\right) \left(\xi_j - \xi_j^0\right) + \dots \end{aligned} \tag{5.1}$$

Neglecting the second and higher order terms the first–order approximation of the mean and variance of $f(\xi)$ is given by:

$$\overline{f} \approx f(\xi^0) \tag{5.2}$$

and the variance of the output function,σ_f^2, is:

$$\sigma_f^2 \approx \sum_{i=1}^{n} \left(\frac{\partial f}{\partial \xi_i}\right)^2 \sigma_{\xi_i}^2 + \sum_{i=1}^{n} \sum_{j=1}^{n} \frac{\partial f}{\partial \xi_i} \frac{\partial f}{\partial \xi_j} cov_{\xi_i,\xi_j} \tag{5.3}$$

Equation (5.3) is further simplified if the random variables, ξ_i are independent and uncorrelated, hence the second term can be removed. The approximation of the mean and variance of the output requires only the mean and variance

of the uncertain input variables.

One drawback of sensitivity based methods is that they provide a local approximation of the statistics of the output values and hence their accuracy can be poor for increased variance of the input variables [59]. On the other hand, the computational burden depends only on the way the sensitivities are calculated and is generally significantly lower than any simulation based method.

5.1.3 Robust Optimization Formulation

Given the statistics of the output values of the system with the uncertain input parameters of operational ranges and payload as external parameters, the robust aircraft design optimization problem can be formulated. This can either be achieved by adding robustness considerations as additional objective(s), trying to minimize the sensitivity of the design performance, or as constraints, trying to achieve a certain low level of variability of the design performance. In this case the increase of robustness is considered a wish attribute and is added to the objective of the optimization. The robust optimization problem for an individual aircraft is then given as:

$$\min \quad E_I(\mathbf{x}, \overline{\mathbf{p}}) + \sigma_{E_I}(\mathbf{x}, \sigma_{\mathbf{p}}) \tag{5.4}$$

$$\begin{aligned} \text{w.r.t} \quad & x_i \in \{\mathbb{R}^n, x_{l_i} \leq x_i \leq x_{u_i}\} \quad i = 1, \ldots, n \\ & x_i \in \{\mathbb{Z}^m, x_{l_i} \leq x_i \leq x_{u_i}\} \quad i = n+1, \ldots, n+m \end{aligned} \tag{5.5}$$

$$\text{s.t.} \quad g_i(\mathbf{x}) \leq 0 \quad i = 1, \ldots, n_{con} \tag{5.6}$$

where $\mathbf{x}$ are the bounded continuous, n, and discrete, m, aircraft design variables listed in Section 5.2.1, $\overline{\mathbf{p}}$ are the mean values of the uncertain parameters, in this case a mean operational range and load factor, which are considered independent from each other. The variance of the objective function is obtained using the sensitivities of the objective around the mean parameter values using Equation (5.3) and the forward difference method to calculate the partial derivatives. The main objective of the optimization is the energy intensity as evaluated at the mean operational range and payload, $E_I(\mathbf{x}, \overline{\mathbf{p}})$, and the standard deviation of the energy intensity around the mean, σ_{E_I} with the coefficients w_1 and w_2 that can be used to prescribe the relative importance and determine the desired trade–off between the two objectives. The inequality constraints, $g_i(\mathbf{x})$, are the aircraft design constraints listed in Section 5.2.2,

which do not depend on the variations in operational range or load factor. The resulting optimization problem can either be solved as a single objective problem using the weighting coefficients for each of the objectives or as a multi–objective problem.

5.2 Robust Optimization Test Case

The robust optimization test case uses the traditional robust optimization formulation described above in Section 5.1. The solutions of this case can be used as reference results to compare the robustness of the coupled optimization cases on the route networks for the two markets, in terms of variation of performance and the performance itself. Additionally, the robust optimization test case uses the same technology level as the coupled optimization cases in the following chapter. Three aircraft are optimized independently by minimizing simultaneously for the energy intensity and its variance around a mean operating range and payload. The fleet allocation problems for the two networks are not solved during the optimization process. One drawback of this approach is that the capacity and design range of each aircraft must be selected beforehand. The capacity and design ranges for the three aircraft are given in Table 5.1, along with their respective mean operational ranges, payloads and the respective variances. The selected aircraft are representative of new aircraft coming into the market in the near future, such as the upgraded E-Jet family (Embraer), the C-Series (Bombardier), the B737MAX (Boeing) and A320neo (Airbus). The design capacity is defined as the capacity using

Table 5.1: Robust aircraft specifications

	Aircraft R1	Aircraft R2	Aircraft R3
Design Range, [nmi]	2100	3100	3500
Design Capacity	86	135	192
Operational Range, [nmi]			
mean value	280	492	624
standard deviation	160	294	492
Operational Load Factor, [%]			
mean value	73.23	75.03	76.83
standard deviation	8.81	8.10	7.40

a single class cabin layout with a seat pitch of 32 inches. The design range is defined as the total range, main mission and reserve mission, at a payload of maximum passenger capacity and baggage. The statistics of the operational values were determined using the data for the North American and European networks. A Gaussian distribution is assumed for each of the parameters.

5.2.1 Aircraft Design Variables

The design variables are separated into aircraft geometry and operational variables for each aircraft. The design variables were selected to provide a high level of flexibility to the optimizer in designing the respective aircraft. For example the discrete variable for the location of the engines, either under the wing or on the aft fuselage, determines if a conventional or T-tail configuration is used. Fixed parameters also affect the design; for example the single class capacity of each aircraft and the discrete design variable of the number of seats abreast define the number of aisles, length and width of the fuselage. The geometry design variables, including their upper and lower bounds, are listed in Table 5.2.

Table 5.2: Aircraft geometry design variables

Design Variable Name	Lower Bound	Upper Bound
Seats Abreast	4	6(10)[1]
Wing Semi-Span, [ft]	35.0	60.0(100.0)[1]
Wing Root Chord, [ft]	12.0(18.0)[1]	24.0(45.0)[1]
Wing Crank Location, [% Semi-Span]	20.0	40.0
Wing Leading Edge Sweep, [deg]	10.0	40.0
Inner Wing Segment Taper Ratio	0.4	0.8
Inner Wing Segment Tip Thickness Ratio	0.11	0.14
Outer Wing Segment Taper Ratio	0.2	0.6
Outer Wing Segment Tip Thickness Ratio	0.08	0.11
Wing Dihedral, [deg]	-2.0	7.5
Wing Root Leading Edge Location, [%]	0.25	0.75
Winglet Span [ft]	0.0	10.0
Winglet Cant Angle [deg]	0.0	90.0
Winglet Chord Offset [%]	0.0	0.6
Winglet Taper Ratio	0.2	0.7
Horizontal Tail Semi-Span, [ft]	12.0(14.0)[1]	25.0(35.0)[1]
Horizontal Tail Root Chord, [ft]	8.0(13.0)[1]	16.0(26.0)[1]
Horizontal Tail Taper Ratio	0.2	0.7
Horizontal Tail LE Sweep, [deg]	15.0	50.0
Horizontal Tail Dihedral, [deg]	-3.0	8.0
Vertical Tail Semi-Span, [ft]	8.0(13.0)[1]	28.0(40.0)[1]
Vertical Tail Root Chord, [ft]	10.0(12.0)[1]	23.0(30.0)[1]
Vertical Tail Taper Ratio	0.2	0.9
Vertical Tail LE Sweep, [deg]	15.0	50.0
Engine Static Sea Level Thrust [lb_f]	9500.0	65000.0
Engine Bypass Ratio	5.0	9.0
Engine Incidence Angle, [deg]	0.0	3.0
Engine Tow–in Angle, [deg]	-3.0	3.0

[1] Values in brackets are the bounds for Aircraft R3.

The operational design variables are the cruise Mach number, initial cruise altitude and the constant CAS climb speed, which are given with their respective bounds in Table 5.3. This results in a total of 30 design variables for each

Table 5.3: Operational design variables

Design Variable Name	Lower Bound	Upper Bound
Cruise Mach Number	0.5	0.9
Initial Cruise Altitude [×1000 ft]	20	38
Constant Climb CAS [knots]	250	350

aircraft, of which three are integer design variables, namely the number of seats abreast, the engine location, and the initial cruise altitude.

5.2.2 Aircraft Design Constraints

Selecting a set of appropriate constraints is crucial for the conceptual design optimization of any aircraft. The design of aircraft is strongly driven by constraints, more even than the extrema of the objective function. Additionally, any design solution that violates constraints is unlikely to be certified as a commercial transport aircraft. The design of each individual aircraft is constrained by limits on geometry, weights, aerodynamics, stability and control and performance, which are listed in Table 5.4. Many of the constraints are either based on rules developed from existing aircraft and/or from the Federal Aircraft Regulations (FAR25) certification requirements.

The minimum Mach number constraint is given by ATC minimum flight speed restrictions between 20000 ft and 30000 ft. The geometry constraint limits the overall wing span to meet airport gate constraints [87] and prevent the loss of elevator effectiveness due to shock formation on the horizontal and vertical stabilizer, before a significant drag rise on the wing. The tip–back angle and takeoff rotation angle constraints ensure adequate placement of the wing and main landing gear. The fuel volume constraint ensures sufficient space in the wings to meet the design mission fuel requirements and reserves.

The weight constraints put a lower and upper bound on the center of gravity location as measured from the leading edge of the mean aerodynamic chord, which is based on good design of exiting aircraft. The aerodynamic constraints avoid negative compressibility effects on the wing, horizontal and vertical stabilizers.

Table 5.4: Aircraft Design Constraints

Constraint	Value
Flight Condition	
Cruise Mach Number	$\geq$ Mach Number (280 [kts] CAS at cruise ALT)
Geometry	
Wing Span, [ft]	$\leq 118(260)^1$
Wing LE Sweep, [deg]	$\leq$ HT LE Sweep
Wing LE Sweep, [deg]	$\leq$ VT LE Sweep
Tip–back Angle, [deg]	$\geq 15.0^\circ$
Rotation Angle, [deg]	$\geq 10.0^\circ$
Wing Fuel Volume, [cubic ft]	$\geq$ Required Fuel Volume
Weights and Balance	
Forward Center of Gravity Location, [% MAC]	≥ 5
Aft Center of Gravity Location, [% MAC]	≤ 55
Aerodynamics	
Wing Mach Divergent Drag Number	$\geq$ Cruise Mach Number
HT Mach Divergent Drag Number	$\geq$ Cruise Mach Number
VT Mach Divergent Drag Number	$\geq$ Cruise Mach Number
Stability and Control	
Minimum Static Margin, [%]	≥ 10
Trim HT Lift Coefficient	≤ 1.0
Maximum Aileron Deflection (OEI TO), [deg]	$\leq 10^\circ$
Maximum Rudder Deflection (OEI TO), [deg]	$\leq 15^\circ$
Maximum Roll Angle (OEI TO), [deg]	$\leq 5^\circ$
Crosswind Vel. @ 10 deg Aileron Deflection (APR), [kts]	≥ 25
Crosswind Vel. @ 18 deg Rudder Deflection (APR), [kts]	≥ 25
Crosswind Vel. @ 5 deg Roll Angle (APR), [kts]	≥ 25
Static Roll Stability, [1/rad]	$-0.20 \geq C_{l_\beta} \leq 0.05$
Static Yaw Stability, [1/rad]	$0.03 \geq C_{n_\beta} \leq 0.15$
Performance	
Takeoff Field Length, [ft]	$\leq 6000\ (7500)^1$
Engine-Out Climb Gradient II	≥ 0.024
Landing Field Length, [ft]	$\leq 5000\ (6000)^1$

[1] Values in brackets are the bounds for Aircraft R3.

The stability constraints ensure adequate longitudinal and lateral–directional static stability based on existing aircraft. The constraints on the maximum trimmed lift coefficient ensure adequate remaining control authority. The constraint is evaluated during takeoff, when the aircraft has the slats and flaps in the takeoff configuration, during cruise, when the aircraft is in a clean configuration, and during landing, when the slats and flaps are at their maximum deflection. The appropriate size and positioning of the vertical tail is strongly affected by the lateral controllability under one engine inoperative takeoff conditions and crosswind landing conditions. The constraints for both

conditions are evaluated by solving the lateral-directional force and moment equations for steady flight. Figure 5.2 shows the degrees of freedom and the definition of the axis definition for the stability analysis.

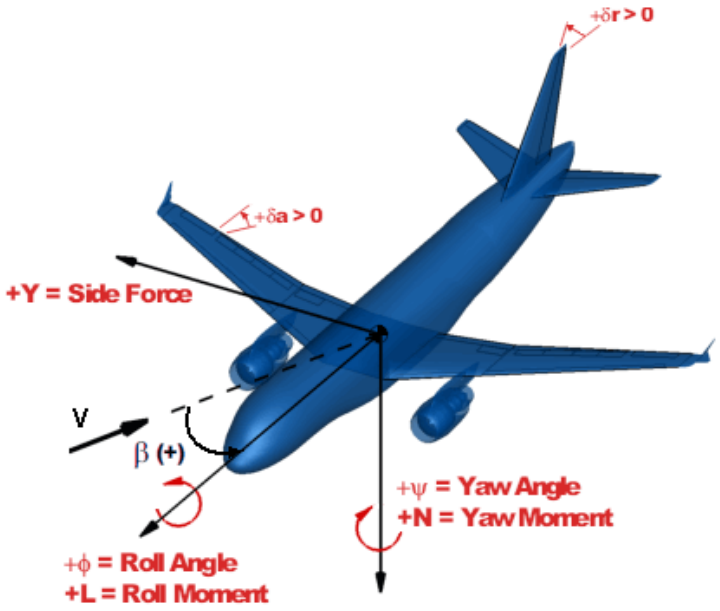

Figure 5.2: Lateral and directional degrees of freedom

The first condition under consideration is the case of one engine failing during takeoff. The size of the vertical tail, in combination with the overall geometry of the aircraft, and the deflection limits of the control surfaces must provide sufficient control authority to either continue or abort takeoff safely. During takeoff condition with one engine inoperative and the other engine at maximum thrust, the lateral-directional force and moment equations can be simplified to:

$$\begin{bmatrix} C_{Y_{\delta_a}} & C_{Y_{\delta_r}} & C_W \\ C_{l_{\delta_a}} & C_{l_{\delta_r}} & 0 \\ C_{n_{\delta_a}} & C_{n_{\delta_r}} & 0 \end{bmatrix} \begin{Bmatrix} \delta_a \\ \delta_r \\ \phi \end{Bmatrix} = - \begin{Bmatrix} C_{Y_\beta} \\ C_{l_\beta} \\ C_{n_\beta} \end{Bmatrix} \beta - \begin{Bmatrix} 0 \\ 0 \\ C_{n_T} \end{Bmatrix} \tag{5.7}$$

where C_Y,C_l and C_n are the side force, roll moment and yaw moment coefficients for aileron deflection, δ_a, rudder deflection, δ_r, sideslip angle, β, and asymmetric thrust, T. For steady level flight, the weight coefficient, C_W, is equal to the lift coefficient of the aircraft. The constraints are evaluated by

requiring that the sideslip angle is zero ($\beta = 0$) in the equation above and solving for the roll and control surface deflection angles required to maintain the aircraft straight.

The crosswind landing constraints are based on FAR 25.237 and evaluated with the aircraft in the landing configuration at an altitude of 30 ft above the ground using the lateral-directional force and moment equations:

$$\begin{bmatrix} C_W & C_{Y_{\delta_a}} & C_{Y_{\delta_r}} \\ 0 & C_{l_{\delta_a}} & C_{l_{\delta_r}} \\ 0 & C_{n_{\delta_a}} & C_{n_{\delta_r}} \end{bmatrix} \begin{Bmatrix} \phi \\ \delta_a \\ \delta_r \end{Bmatrix} = - \begin{Bmatrix} C_{Y_\beta} \\ C_{l_\beta} \\ C_{n_\beta} \end{Bmatrix} \beta \tag{5.8}$$

Solving the set of equations and setting the roll angle, aileron deflection and rudder deflection to their respective maximum values provides the maximum sideslip angle. The maximum values for the control surface deflections assume a two-third maximum control input, leaving one-third control available for gust recovery. The maximum crosswind velocity, V_{cw}, can be obtained based on the maximum sideslip angle by:

$$V_{cw} = V_\infty \sin(\beta) \tag{5.9}$$

where V_∞ is the free steam velocity, or total airspeed of the aircraft. For the analysis of the maximum crosswind constraints, it is assumed that the aircraft remains aligned with the runway but allows the aircraft to roll to a maximum of five degrees. This sideslip approach is the most conservative crosswind landing approach. Pilot crosswind landing techniques, such as "crabbing" where the aircraft is turned into the crosswind and only aligned with the runway just before touchdown, can significantly increase the crosswind capability of an aircraft.

The performance constraints are based on an off-design takeoff, at standard day sea-level and maximum takeoff weight, and landing, at maximum landing weight, and a minimum climb gradient during takeoff with one engine inoperative as per FAR requirements. The takeoff field length strongly depends on the thrust–to–weight ratio of the aircraft, while the landing field length depends on the wing loading of the aircraft.

5.3 Robust Optimization Results

The design space for a multidisciplinary conceptual aircraft design optimization is very complex with 30 continuous and discrete design variables, 27

non–linear constraints, discontinuities and possibly multiple local minima for each individual aircraft. Due to these requirements a gradient–free global optimizer was selected to solve the robust aircraft design optimization problem. As mentioned above the feasibility of the aircraft design solution is paramount, but one disadvantage of most global optimization algorithms is the handling of constraints, which are usually handled by the addition of a penalty function to the objective. Therefore, the robust aircraft design cases are solved using a feasible direction inspired, asynchronous constrained particle swarm optimization algorithm `FDPSO`, integrated as part of the Python object–oriented optimization framework `pyOPT` [88]. A detailed description of the optimization algorithm can be found in Appendix B. Due to the heuristic nature of the optimization algorithm several runs for each of the aircraft were performed on 48 cores, each 3.0 GHz, of a 120 core Beowulf cluster. The evaluation of 1000 iterations for a single aircraft by the optimizer required on the order of 20 hours of computational time. Additionally, several runs were performed with different weighting schemes between the mean energy intensity and the standard deviation of energy intensity as the objective. It was found that the main difference in solutions was with respect to different cruise altitudes and cruise Mach numbers, where a lower cruise altitude and lower cruise Mach number were preferred for solutions with slightly higher robustness, and only minor variations in overall geometry of the aircraft were observed. Figure 5.3 shows the geometry of the three aircraft obtained with equal weighting of the mean performance and robustness. All the aircraft obtained are fully feasible. Table 5.5 lists selected specifications and parameters of the three aircraft.

Aircraft R1 uses a T-tail configuration with four seats abreast like other aircraft in its class. The wing span and area is higher than similar aircraft with a comparatively high aspect ratio, resulting in a low wing loading and low induced drag. The low climb speed and high aspect ratio result in low thrust engines and a design for a more fuel efficient climb. The low thrust engines also provide a lower thrust–to–weight ratio compared to similar aircraft. Aircraft R2 and Aircraft R3 operate at similar cruise Mach numbers and altitudes compared to existing aircraft in their class, but as Aircraft R1, the climb speeds are lower. Aircraft R2 uses a five seat abreast cabin and Aircraft R3 a six seat abreast cabin configuration. All three aircraft have higher span and area wings, while maintaining the same or achieving slightly higher aspect ratios as other aircraft in their respective classes.

The performance of these aircraft was then analyzed by solving the fleet allocation problem for the two given networks. The results of these post

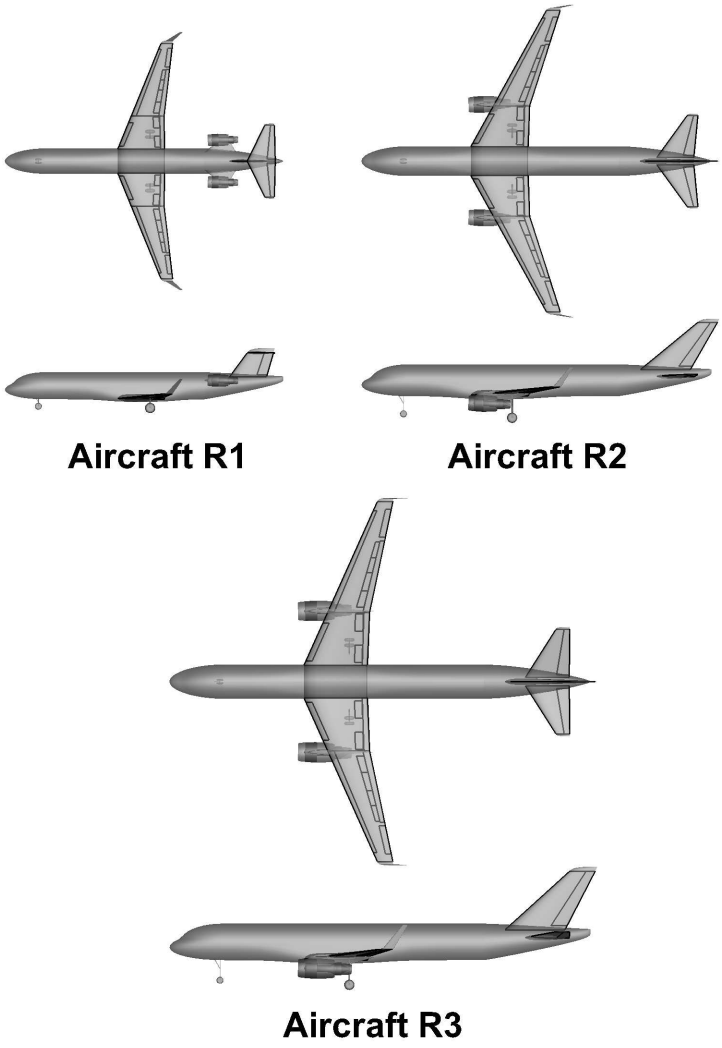

Figure 5.3: Robust optimization aircraft geometries

optimality analyzes can be found in Section 5.3.1, where they are compared against the reference solutions described in Section 4.3.2. It was observed that the solutions with equal weighting of the mean and standard deviation of energy intensity provided the best solutions for the two networks.

Table 5.5: Robust optimization solution aircraft specifications

	Aircraft R1	Aircraft R2	Aircraft R3
Operation			
Capacity	86	135	192
Seat Configuration	2+2	2+3	3+3
Design Range [nmi]	2100	3100	3500
Geometry			
Wing Projected Span [ft]	94.18	113.98	133.87
Wing Aspect Ratio	10.56	11.46	11.95
Wing Reference Area [ft^2]	779.18	1148.71	1592.22
Engines			
Maximum Static Thrust [lb_f]	12660	23238	35672
Bypass Ratio	6.7	7.5	8.0
Flight Condition			
Climb CAS [knots]	265	270	280
Cruise Mach	0.70	0.75	0.75
Cruise Altitude [×1000 ft]	30	35	37
Weights and Loadings			
Maximum Takeoff Weight [lb_f]	82559	146290	218774
Operational Empty Weight [lb_f]	44422	77992	117904
Maximum Fuel Weight [lb_f]	25482	41831	66030
Design Fuel Weight [lb_f]	18016	36705	55896
Maximum Wing Loading [lb_f/ft^2]	876.63	1283.51	1634.27
Maximum Thrust-to-Weight [lb_f/lb_f]	0.31	0.32	0.33
Costs			
Design Commonality Index [%]	0.00	0.00	0.00
Purchasing Price [Mil. 2014 US$]	47.11	69.64	91.93

5.3.1 Robust Aircraft Network Performance

Given the aircraft obtained, the fleet allocation problem for each of the networks can be solved using the method described in Chapter 4. Following are the results of the two networks when operated for 15 years by the three design solutions to the robust aircraft design optimization problem with the same passenger demand characteristics given by the discrete time simulation as shown in Section 4.1.3. The maximum load factor was set at 90% and the fuel price was set at 2.93$/US Gallon.

North American Routes

Table 5.6 summarizes the allocation and performance of the robust aircraft for operating the North American network for 15 years with the simulated passenger demand as outlined in Section 4.1.3. The same seed for the random number generator was used to obtain the same demand profiles as for

the reference case to better compare the performance of the different aircraft. The allocation of aircraft is similar to the reference case, with Aircraft R1 and

Table 5.6: Robust aircraft results for operating the North American network for 15 years

Aircraft	Aircraft R1	Aircraft R2	Aircraft R3
Average Load Factor, [%]	73.6	NA	83.8
Average Route Range, [nmi]	339	NA	1052
Average Annual Utilization, [hr]	2432	NA	2837
Max. Number of Aircraft	49	0	127
Number of Flights	552491	0	777904
Individual Energy Intensity, [BTU/(lb_f nmi)]	17.14	NA	9.29
E_I Standard Deviation, [BTU/(lb_f nmi)]	23.89	NA	10.00
Network Energy Intensity, [BTU/(lb_f nmi)]	9.92 (-15.75%[1])		
Total Fuel Required, [Billion lb_f]	16.77 (-15.76%[1])		
Total Operating Cost, [Billion 2014 US$]	37.63 (-1.34%[1])		
Total Acquisition Cost, [Billion 2014 US$]	16.17 (2.99%[1])		

[1] Relative difference w.r.t. reference aircraft solution.

Aircraft R3 covering all of the routes with approximately the same number of total flights. As for the reference case, the medium capacity aircraft, Aircraft R2 is not allocated to any of the routes in the network. This gives similar average ranges and annual utilization for these two aircraft as for the CRJ-700 and Boeing 737-800, but due to the smaller engines with higher bypass ratios, lower wing loadings and climb speeds, the average energy intensity is lower. This is especially true for Aircraft R1, which has approximately half the average energy intensity compared to the CRJ. As mentioned before, the lower wing loading results in lower lift coefficients, especially during climb, and hence lower induced drag, which allows for smaller engines. This results in an overall 15.8% lower energy intensity and fuel burn for the entire network. This significant reduction in fuel required does not translate into significant reductions in operating cost, while the acquisition cost are 3% higher. The small decrease in operating cost is due to increases in flight times from the slower climb speeds and corresponding higher crew cost. The higher acquisition cost are due to the fact that the robust aircraft do not benefit from any commonality with other aircraft, resulting in higher purchasing prices.

The yearly changes in energy intensity, fuel burn per year and operating cost per year follow the same trends as for the reference case, Figure 5.4, with the exception of the average load factor, which starts lower in the first year but increases more rapidly to match the load factor of the reference case in the final years. The network energy intensity consistently decreases over the

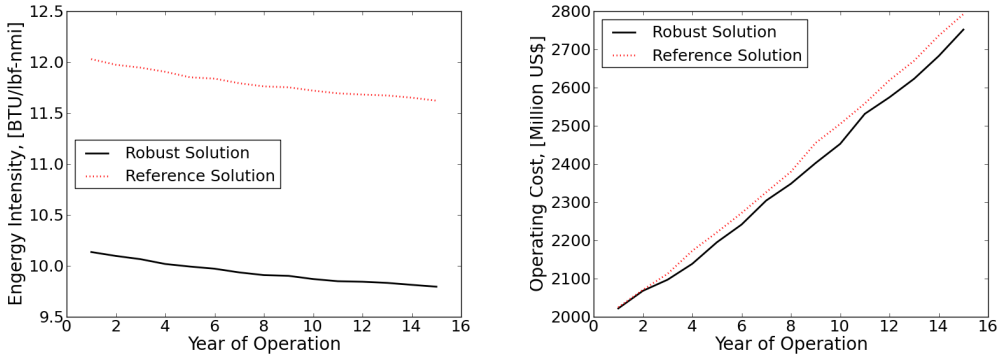

(a) Energy Intensity

(b) Operating Cost

(c) Fuel Burn

(d) Average Load Factor

Figure 5.4: Performance comparison of reference and robust solution for operating the North American route network for 15 years

years by an average of 0.24% per year, resulting in a total decrease of 3.36% in the final year compared to the first year. The total fuel burn increases on average by 2.22% or by a total of 36.02%, maintaining a 15% reduction compared to the reference case each year. The operating cost increases by 2.23% per year, or a total of 36.11% when comparing the first and final year.

Compared to the reference case the difference in operating cost is negligible in the first couple of years, until the difference increases to approximately 2% in the final years. As for the reference case, the increases in fuel burn and cost are slightly lower than the increases in demand growth, following the same yearly trends. Around the ninth year the fuel required to operate the network by the robust aircraft matches year one of the reference case, which indicates that even with the significant reductions in fuel burn the growth in passenger demand will result in overall higher fuel burn and CO_2 emissions well within the lifetime of these aircraft.

European Routes

Table 5.7 summarizes the performance of the robust aircraft solutions for the European network.

Table 5.7: Robust aircraft results for operating the European network for 15 years

Aircraft	Aircraft R1	Aircraft R2	Aircraft R3
Average Load Factor, [%]	82.8	87.3	87.3
Average Route Range, [nmi]	404	282	226
Average Annual Utilization, [hr]	2553	1452	1557
Max. Number of Aircraft	134	79	63
Number of Flights	1476663	467562	79767
Individual Energy Intensity, [BTU/(lb_f nmi)]	13.68	16.43	20.27
E_I Standard Deviation, [BTU/(lb_f nmi)]	17.47	17.71	21.59
Network Energy Intensity, [BTU/(lb_f nmi)]	14.69 (-13.85%[1])		
Total Fuel Required, [Billion lb_f]	10.54 (-13.65%[1])		
Total Operating Cost, [Billion 2014 US$]	32.91 (4.46%[1])		
Total Acquisition Cost, [Billion 2014 US$]	15.25 (5.77%[1])		

[1] Relative difference w.r.t. reference aircraft solution.

All three robust aircraft are assigned to the European network, but a large proportion of the daily routes is covered by Aircraft R1, while the other two aircraft are mainly used for the very high demand but short range routes within Germany, such as the routes between Munich, Frankfurt and Berlin. The resulting average ranges for the larger two aircraft are very low, at 282 and 226 nautical miles, respectively, and corresponding low annual utiliza-

tion around 1500 hours and high average energy intensities, which are only marginally lower than the reference aircraft's values. The lower operating range design for Aircraft R1 significantly reduces the average energy intensity for this aircraft, resulting in an overall reduction in energy intensity and fuel burn for the European network by 13.85% and 13.65% respectively. The standard deviation of the energy intensity for all of the aircraft is lower compared to the reference aircraft, especially for Aircraft R1. The capacity of Aircraft R3 is significantly lower than the single class capacity of the B757-300, which results in an overall significant increase in the number of flights required to meet all the demand in the network; even so the allocation maintains high average load factors for all the aircraft. The consequence is that despite the reductions in fuel burn, the operating cost driven by fees and maintenance for the high number of takeoffs and landings, are 4.46% higher for this set of aircraft. There is also an increase in the number of aircraft of each type required, which increases the total acquisition cost for the network by 5.77%.

The yearly variations in energy intensity, fuel burn, operating cost and load factor when operating on the European route network for the robust and reference sets of aircraft are shown in Figure 5.5. The energy intensity of the robust aircraft is essentially constant over the years, with only minor variations and a total decrease of less than one percent. As the energy intensity for the reference cases decreases so does the difference between the two solutions, which starts at a relative difference of 16.49% in the first year but reduces to 11.53% in the final year. The load factor and energy intensity do show less fluctuations for the robust case. The fuel burn follows a similar trend, with an average of 3.39% per year increase and a total of 59.4%, which corresponds to an 16.29% difference in the first year and only a 11.31% difference in the final year compared to the reference case. An additional effect is that the fuel burn of the robust solution exceeds the fuel burn of the first year reference solution earlier than for the North American network, in the seventh year. The operating cost starts at approximately the same level but due to increases in passenger demand and the resulting increases in the required number of flights, the operating cost increases at a higher rate for the robust case, at an average of 3.64% and a final difference of 9.68% in the final year compared to the reference solution. This high rate of increase in cost also means a total increase in operating cost of 64.80% from the first to the final year, which is higher than the increase in passenger demand and revenue passenger miles. The yearly trends in energy intensity and fuel burn follow the same expected trends as the reference solution. The yearly average load factor does not show similar variations as the reference case, since the switches to larger capacity

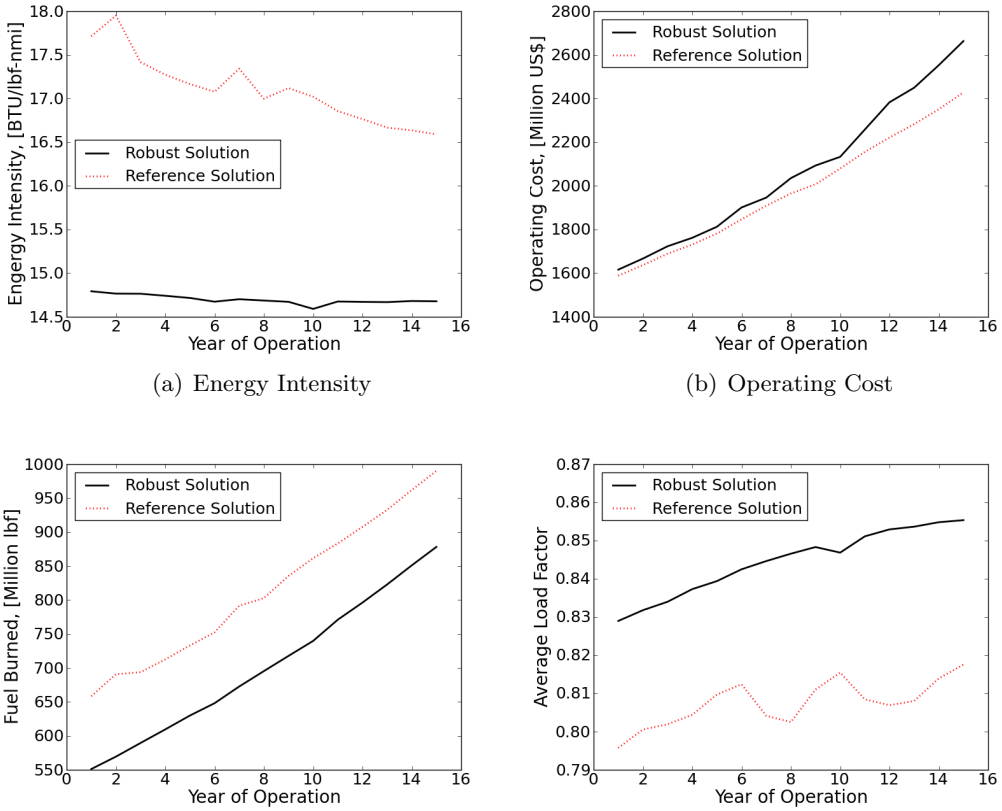

(a) Energy Intensity

(b) Operating Cost

(c) Fuel Burn

(d) Average Load Factor

Figure 5.5: Performance comparison of reference and robust solution for operating the European route network for 15 years

aircraft required to accommodate the increases in passenger demand are more gradual. The robust solutions, with their relatively high design ranges, perform better on the North American network than the European network, with similar decreases in fuel burn and energy intensity but an increase in operating cost compared to the reference solution on the European network, while the operating cost for the North American network is slightly lower.

It can be noted that the objective of the robust design optimization was the energy intensity and its robustness, and not the operating cost of the aircraft. As such the robust solution does exhibit lower energy intensity for both net-

works. What the solution also demonstrates is the effect of different markets; even so the robust solution performs well on the North American network. The reduced flexibility of just three representative aircraft does show higher sensitivity to the growth in the European network. The European network is dominated by high demand short range routes, while the design ranges for the robust aircraft are still significantly higher than required. This leads to aircraft with higher than required maximum takeoff weight, and corresponding structural weight, which is carried for every mission. Figure 5.6 shows the ratio of the route range to the main mission design range of performed departures in log scale by the robust aircraft during the 15 years of operating the North American network. Similarly to the reference aircraft the departures are mainly distributed between 10 to 90% of the respective design ranges but with a higher concentration of performed departures below 30% of the design range compared to the reference aircraft. This results in an average range ratio of 26.8%, which is significantly lower than the average range ratio of the reference aircraft of 43.9%.

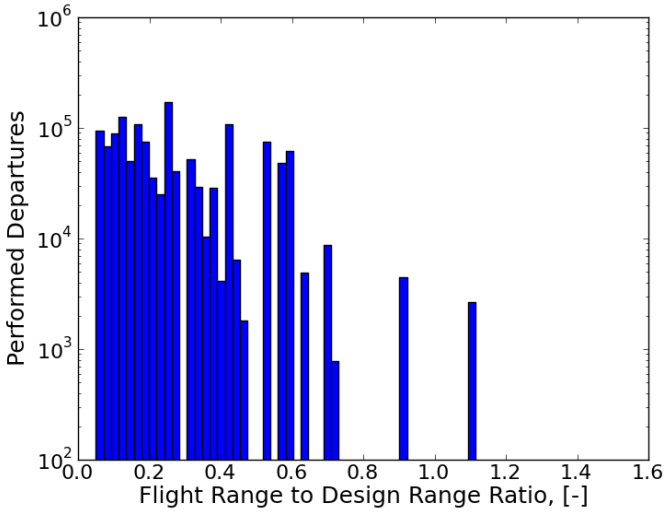

Figure 5.6: Route range to design range ratio of performed departures by the robust aircraft on the North American network (26.8% average ratio)

The same trend can be observed for the European network, as shown in Figure 5.7, with a higher number of departures at range ratios below 20% of the respective aircraft design range, compared to the reference case. The av-

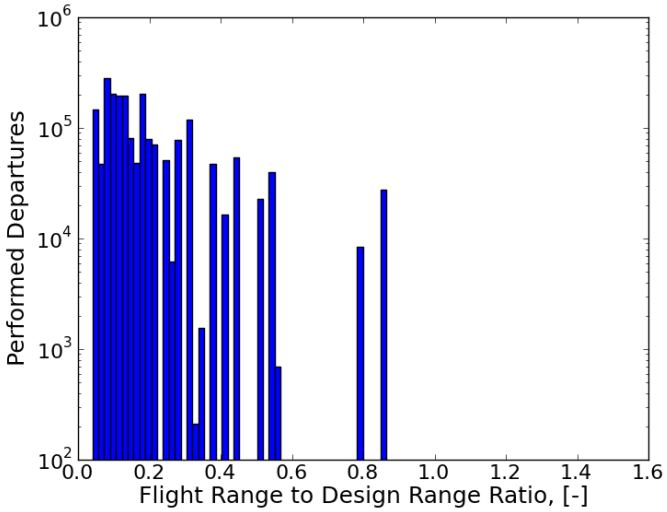

Figure 5.7: Route range to design range ratio of performed departures by the robust aircraft on the European network (18.5% average ratio)

erage range ratio for the European network is also lower with a value of 18.5% of the respective aircraft design range, but the shift is insignificant compared to the shift in the North American market.

The overall performance of the robust aircraft with respect to energy intensity and fuel burn is improved over the reference, despite the shift to lower range ratios for the robust aircraft. This is due to the increased fuel efficiency and robustness of the aircraft with respect o operational range and load factor. Figure 5.8 shows the payload range diagrams for the three robust aircraft. On these diagrams the constant energy intensity contours are shown as well as the frequencies of the performed departures for operating both networks for the given 15 years. It should be noted that only the main mission flight range is shown; the full flight range also includes the 200 nautical mile reserve mission. The energy intensity contours follow similar distributions for all the aircraft. Close to the design range the energy intensity is the lowest and the bands of increasing E_I are large. As range and/or payload decrease so does the width of the contour bands and the energy intensity. For the three aircraft, the highest frequency of flights occurs in the region of the payload range diagram with high energy intensity at relatively high payloads but low flight ranges, while few flights occur in the low E_I region close to the respective design ranges.

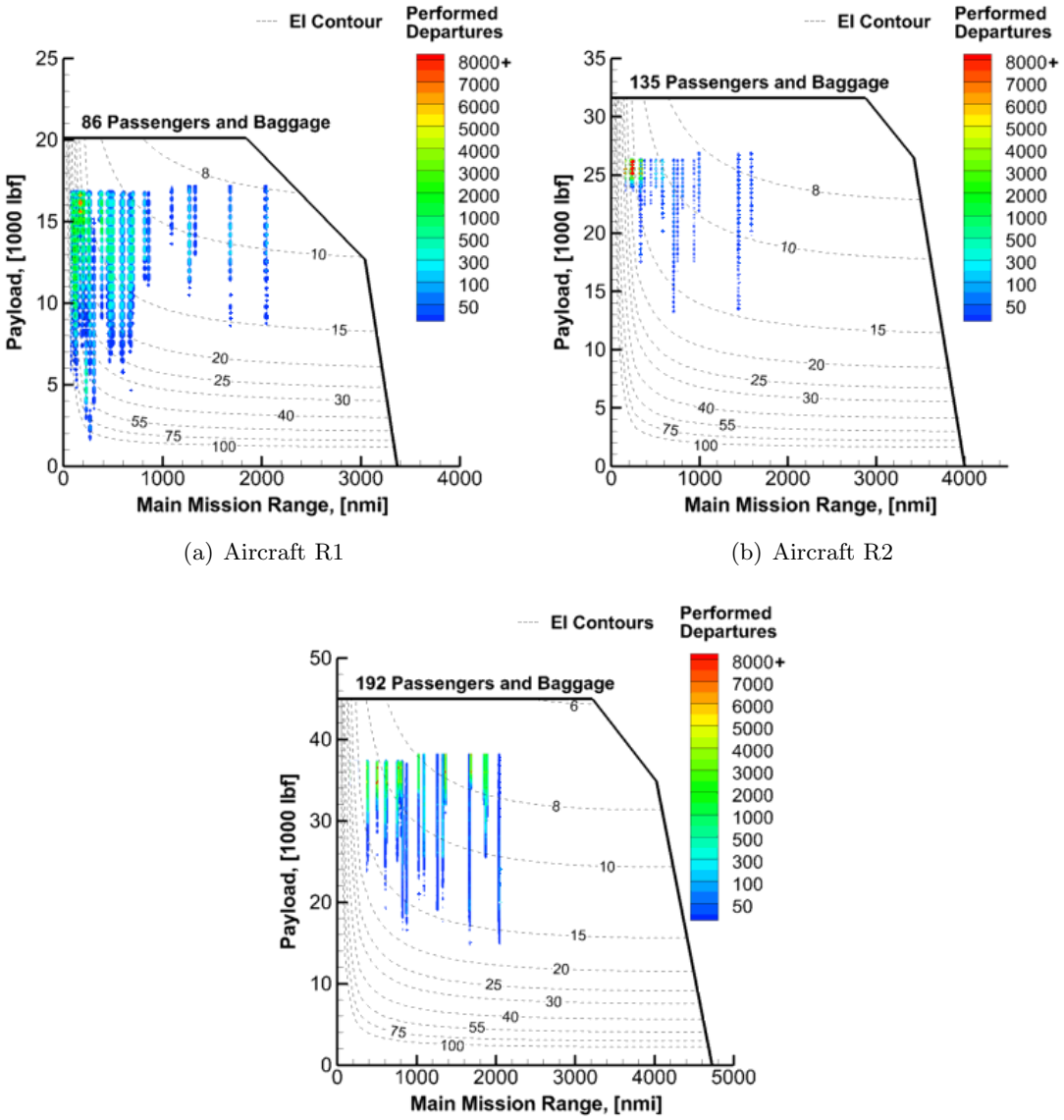

(a) Aircraft R1

(b) Aircraft R2

(c) Aircraft R3

Figure 5.8: Frequency of flights performed and energy intensity contours on payload range diagram for the robust aircraft design and operating both networks for 15 years

Reducing the design range could shift a larger portion of the performed flights into lower energy intensity regions of the respective payload range envelopes, but without coupling the design of these aircraft directly with the network allocations the actual values of these design ranges is not known.

Additionally, the capacities of the robust aircraft were fixed, but as the use of the Boeing 757-300 shows, a high capacity aircraft may address the increases in passenger demand in the European and North American markets. Hence, coupling the design of a number of aircraft closer to operational use in both markets can take advantage of selecting appropriate capacities and design ranges in combination with increased flexibility provided by aircraft families to not only further reduce fuel burn and energy intensity but also operating and acquisition costs.

6 Coupled Aircraft Family Design

The decoupled robust aircraft optimization results in the previous chapter showed significant reductions in fuel burn and energy intensity compared to existing aircraft, but the design range and capacity for each aircraft must be selected beforehand. Even so available data can be used to guide this selection; the design of each aircraft is still decoupled from the actual operations. Closer coupling with the operations of these aircraft during the design process can reduce operational inefficiencies. Additionally, since two markets are being considered, a single aircraft in each class cannot meet all the requirements, in terms of capacity and range, of each market. To increase the flexibility of aircraft provided, while reducing the research and development cost, a family of aircraft in each class can be considered.

The following chapter introduces the approach used to simultaneously design several aircraft families coupled with the fleet allocation problem for both markets considered. Two test cases are presented, one with three aircraft families and one with two aircraft families and the performance of each case on both route networks is compared with the robust and reference solution.

6.1 Coupled Aircraft Family Design Methodology

The coupled problem has several sub-problems that need to be considered, namely: the concurrent optimization of all aircraft in a family, the optimization of several aircraft families and the coupling of the aircraft with the fleet allocation in both markets. One strategy is to decompose the coupled optimization problem sequentially into a bi–level optimization strategy. In this case the aircraft family optimization and fleet allocation problems are both handled by sub-level optimizers, while a system level optimizer handles the

coupling variables and constraints and the system level objective. The strategy proposed here is closely related to a hierarchical optimization strategy [89] as shown in Figure 6.1, with the allocation problems nested as sub-level problems in the system level optimization of the aircraft families.

The system level optimization problem consists of the aircraft families design optimization and the overall system objective following the MDF formulation introduced in Section 3.2:

$$\min \quad E_I(\mathbf{x}, \mathbf{z}) \tag{6.1}$$

$$\begin{aligned} \text{w.r.t} \quad & x_i \in \{\mathbb{R}, x_{l_i} \leq x_i \leq x_{u_i}\} \quad i = 1, \ldots, n \\ & x_i \in \{\mathbb{Z}, x_{l_i} \leq x_i \leq x_{u_i}\} \quad i = n+1, \ldots, n+m \\ & z_i \in \{\mathbb{R}, z_{l_i} \leq z_i \leq z_{u_i}\} \quad i = 1, \ldots, l \\ & z_i \in \{\mathbb{Z}, z_{l_i} \leq z_i \leq z_{u_i}\} \quad i = l+1, \ldots, l+k \end{aligned} \tag{6.2}$$

$$\text{s.t.} \quad g_i(\mathbf{x}, \mathbf{z}) \leq 0 \quad i = 1, \ldots, n_{con} \tag{6.3}$$

where $\mathbf{x}$ are the local bounded continuous, n and discrete, m, aircraft design variables exclusive to each aircraft and $\mathbf{z}$ are the global bounded continuous, l and discrete, k, aircraft design variables of common components, described in Section 6.2. The inequality constraints, $g_i(\mathbf{x}, \mathbf{z})$, are the design constraints for each aircraft listed in Section 5.2.2. The system level optimization problem is solved by a single optimizer. For a given set of design variables all the aircraft are sized and the constraints are evaluated. Then the sub-level optimizations solve the fleet allocation problems of both networks from the given performance and operating cost of each aircraft following the formulation from Section 4.2. The discrete time simulation used in the network allocation problems is run offline to determine the daily passenger demand for each network as given in Section 4.1.3. The system level objective is the energy intensity of the current designs on both networks, which is calculated from the allocation of the aircraft on the two networks for the full time of operations. Both optimization levels are coupled by the performance and operating cost of each aircraft for each route and the allocation of each aircraft, where the network solution provides the total network operating cost and fuel burned for all simulated days of operation for both networks, which can then be used to assess the system level objective function value. The main advantage to performing the network optimization as a sub-level optimization inside the main optimization objective function is that the system level optimizer solves

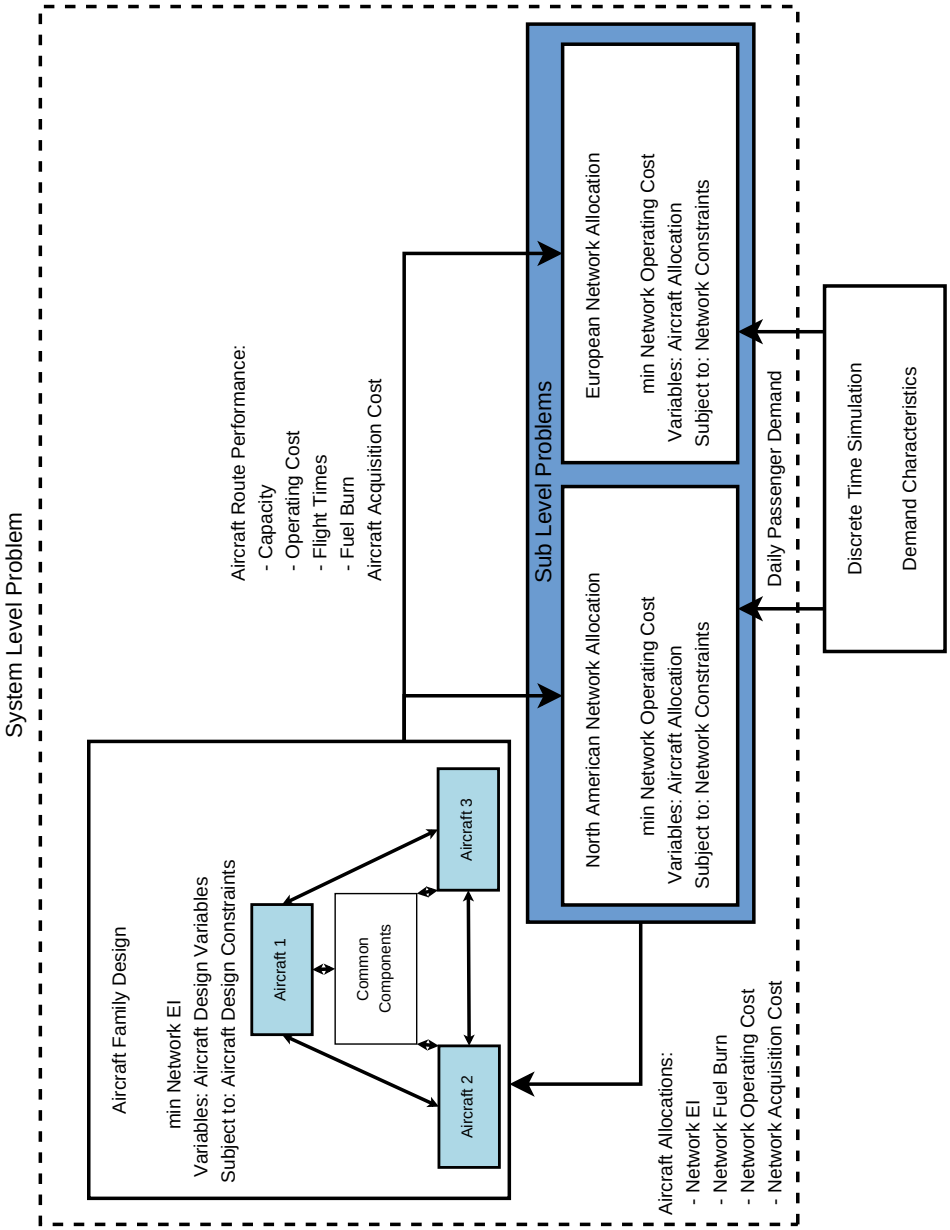

Figure 6.1: Decomposition of the coupled aircraft design and allocation optimization problem

only the aircraft design optimization problem, while the sub-level optimizers only solve the network optimization problems. This approach works well in this case, since the solution of the network problems is obtained relatively quickly compared to the analysis of all the aircraft in the families.

6.2 Aircraft Family Design Variables

To couple the designs to the requirements of each network the capacity and design range are added to the set of local design variables for each aircraft listed in Section 5.2.1. Additional binary design variables for the number of seats abreast, the horizontal and vertical tail are also introduced as global design variables for each family. These binary design variables provide to the optimizer the flexibility of selecting the level of commonality between the aircraft in a family. For each binary design variable a value of zero represents that the component is not shared between the two aircraft, while a value of one represents that the component is shared. In the case where a component is common, the set of design variables determining that component becomes part of the global set of design variables, while the same sets of local variables for each of the aircraft sharing that component become inactive. Table 6.1 shows the status of the set of design variables for the vertical tail for the example of two aircraft, Aircraft A1 and Aircraft A2. The wing is assumed to

Table 6.1: Example of local and global vertical tail design variables for two aircraft

Commonality Variable	Not Common		Common	
$VT_{comm_{A1 \leftrightarrow A2}}$	0		1	
Design Variable	Type	Status	Type	Status
Aircraft A1				
Vertical Tail Semi-Span, [ft]	$local_{A1}$	active	$local_{A1}$	inactive
Vertical Tail Root Chord, [ft]	$local_{A1}$	active	$local_{A1}$	inactive
Vertical Tail Taper Ratio	$local_{A1}$	active	$local_{A1}$	inactive
Vertical Tail LE Sweep, [deg]	$local_{A1}$	active	$local_{A1}$	inactive
Aircraft A2				
Vertical Tail Semi-Span, [ft]	$local_{A2}$	active	$global_{A1 \leftrightarrow A2}$	active
Vertical Tail Root Chord, [ft]	$local_{A2}$	active	$global_{A1 \leftrightarrow A2}$	active
Vertical Tail Taper Ratio	$local_{A2}$	active	$global_{A1 \leftrightarrow A2}$	active
Vertical Tail LE Sweep, [deg]	$local_{A2}$	active	$global_{A1 \leftrightarrow A2}$	active

be shared between each member of the family, but additional local variables are introduced for each derivative aircraft. These represent span and chord

extensions on the root and tip, as shown in Figure 6.2. When the vertical

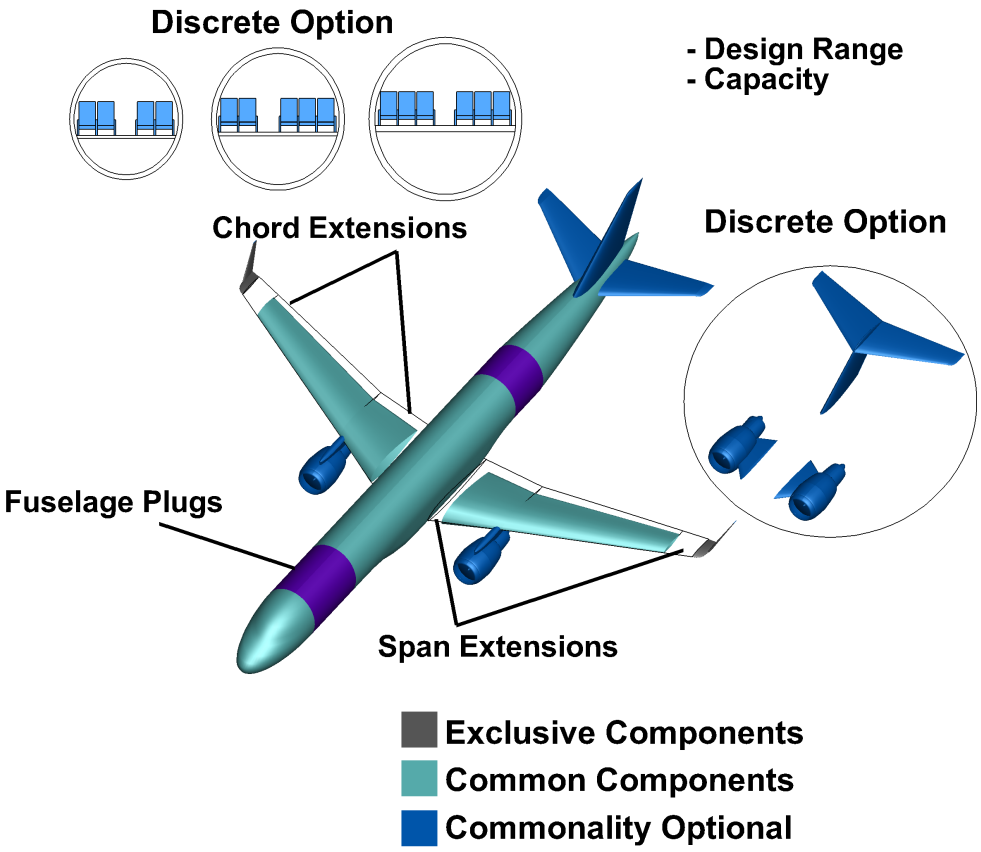

Figure 6.2: Aircraft family geometry design variables and discrete options

tail is common, the set of local design variables defining the vertical tail of Aircraft A2 become the global set of design variables defining the vertical tail for both, Aircraft A1 and Aircraft A2. The local design variables for Aircraft A1 become inactive. In the MDF formulation of the problem the optimizer does not distinguish between local and global variables explicitly, which makes this change in the type of design variables possible without reformulating the optimization problem. The design variable of the static sea-level thrust of the engine is left independent for each aircraft, but it is assumed that the engines share commonality when the value of the thrust falls within 15% of each other. When evaluating the objective function of the system level optimization problem, the aircraft are sized from the largest aircraft in each family to the

smallest. In the case of common components, such as horizontal and vertical tail, the weight of that component of the larger aircraft is used during the sizing of the smaller aircraft in the family. This accounts for the fact that common components must be sized for the most critical conditions of all aircraft that share that component. For the purpose of calculating the design commonality index for each member of the family, the smallest aircraft of the family is still considered the originally designed aircraft for the fuselage and wing, while the larger members are considered derivative aircraft. Hence, the weight of the fuselage and wing structure are not included as common component weights for the smallest aircraft. For the larger members in the family, the weight of the fuselage and original primary wing structure is included in the weight of common components for the design commonality index. Similarly, the reverse approach is used for a common horizontal or vertical tail, where the weight is considered as common component weights for the smaller aircraft but not the aircraft for which they were sized.

6.3 Aircraft Family Test Cases

The coupled aircraft family and fleet allocation problem was solved for two test cases. The first test case assumed three aircraft families, with two aircraft in each family, while the second test case assumed two aircraft families with three aircraft in each family, resulting in a total of six aircraft in each case. As described above, the optimizer has the flexibility to adjust the level of commonality between the aircraft in each family through the global binary design variables. The only commonality that is assumed to be fixed between each member of the respective families is the primary structure of the wing and the fuselage cross section. The feasibility of each aircraft is assessed based on the same set of design constraints listed in Section 5.2.2. This results in a total of 195 mixed, integer and continuous, design variables for the three aircraft family test case and 192 design variables for the two aircraft family test case, each with 172 constraints.

The system level optimization of the coupled problem was solved using the `FDPSO` optimization algorithm, while the two route networks were solved independently following the procedure outlined in Section 4.2.1. As for the robust case the system level optimization problem is a mixed integer optimization problem with discontinuities in the design space. One additional reason for using the global `FDPSO` is the switch of some of the design variables from active to inactive, depending on the value of the binary commonality design

variables. During the optimization process the network allocation problem was solved for 15 years of operation with the combined energy intensity as the system level objective. Each test case was solved five times, due to the heuristic nature of the PSO algorithm and the best solutions to both cases are shown below. It can be noted that the best solutions showed only minor variations in the designs and were all fully feasible. The evaluation of 500 iterations by the system level optimizer with 47 particles required on the order of 240 hours of computational time on 48 cores, each 3.0 GHz, of a 120 core Beowulf cluster.

6.3.1 Three Aircraft Families Optimization Results

The first solution is for the case of three aircraft families, each with two aircraft which share common components. The geometries of the six obtained aircraft can be seen in Figure 6.3 with the common components shared between each aircraft shaded in blue. Table 6.2 lists selected specifications and parameters of the aircraft. All the aircraft share the fuselage, horizontal and vertical tails, but none of the engines fall within the 15% range of static sea-level thrust and are hence not shared between any of the aircraft within the three families. The aircraft in Family A use a T-tail configuration with four seats abreast. The capacities of both aircraft are the same as the CRJ-700 and CRJ-900 family from Bombardier, with similar design ranges. Compared to the CRJs, the wing span and aspect ratio are significantly higher with an approximately 20 feet higher wing span and lower wing area. Both aircraft still fall within the Group III gate constraint. The climb speed, cruise Mach number and initial cruise altitude are low. The lower cruise Mach number allows for a lower wing sweep to support the higher aspect ratio wing at no or very low weight penalty. This results in low thrust requirements for the engines, higher fuel efficiency and hence lower maximum takeoff weight and wing loading.

Aircraft Family B uses a five seat abreast configuration with capacities of 129 and 146, respectively. As for Aircraft Family A, both aircraft have high wing spans, with aircraft B2 almost reaching the Group III gate constraint of 118 feet, and high aspect ratios. The design ranges are approximately half of the design range of the reference Aircraft B, while the climb speed is low at 260 knots CAS. This, in combination with the low induced drag due to the high aspect ratio wings, allows again for relatively low thrust–to–weight ratios and lower maximum takeoff weights.

Aircraft C1 has the same capacity and fuselage configuration as the ref-

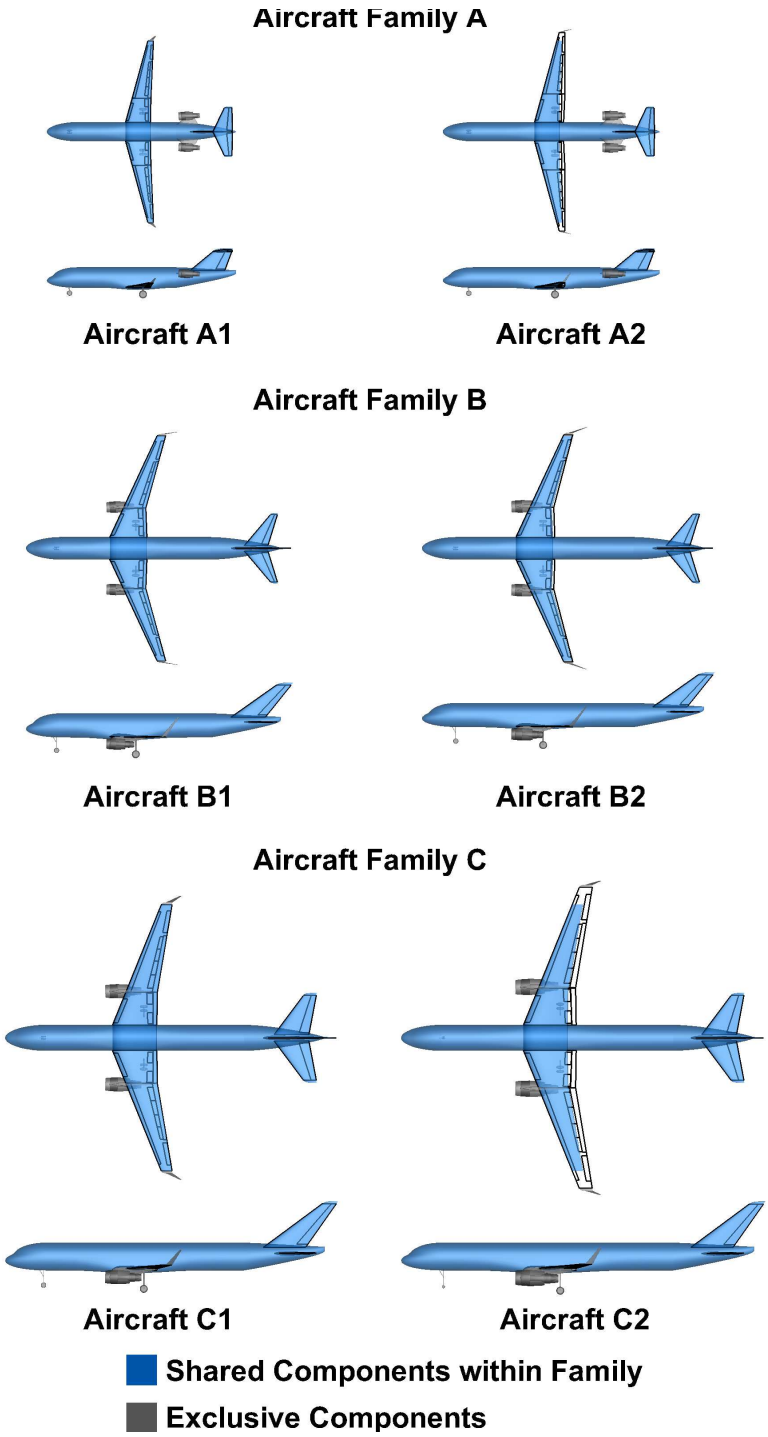

Figure 6.3: Three families aircraft geometries

Table 6.2: Three families optimization solution aircraft specifications

	Aircraft Family A		Aircraft Family B		Aircraft Family C	
	Aircraft A1	Aircraft A2	Aircraft B1	Aircraft B2	Aircraft C1	Aircraft C2
Operation						
Capacity	71	88	129	146	192	233
Seat Configuration	2+2	2+2	2+3	2+3	3+3	3+3
Design Range [nmi]	1243	1318	1504	1668	1458	2343
Geometry						
Wing Projected Span [ft]	91.79	98.34	111.89	116.24	136.22	150.72
Wing Aspect Ratio	13.06	12.98	14.59	14.09	12.35	11.61
Wing Reference Area [ft^2]	564.08	745.40	918.72	988.57	1434.32	1943.78
Engines						
Maximum Static Thrust [lb_f]	10640	12800	17500	21890	28350	38040
Bypass Ratio	6.7	6.9	7.3	7.5	7.9	8.3
Flight Condition						
Climb CAS [knots]	260	260	260	260	260	274
Cruise Mach	0.70	0.71	0.74	0.75	0.75	0.75
Cruise Altitude [×1000 ft]	27	30	35	35	35	36
Weights and Loadings						
Maximum Takeoff Weight [lb_f]	63458	77727	114820	132886	177607	236036
Operational Empty Weight [lb_f]	36604	45095	67256	77611	107070	137463
Maximum Fuel Weight [lb_f]	12716	18429	28453	31937	54491	79148
Design Fuel Weight [lb_f]	10180	12060	17159	21002	25419	43609
Maximum Wing Loading [lb_f/ft^2]	691.31	790.38	1026.18	1143.25	1303.84	1566.07
Maximum Thrust-to-Weight [lb_f/lb_f]	0.34	0.33	0.30	0.33	0.32	0.32
Costs						
Design Commonality Index [%]	4.39	59.35	4.64	62.61	4.62	56.36
Purchasing Price [Mil. 2014 US$]	39.85	42.74	58.89	61.58	79.65	90.88

erence Aircraft C, but a 58% lower design range, and three feet higher wing span. Even so the horizontal and vertical tail are larger and heavier, since they are shared components with the 233 capacity Aircraft C2. The low design range allows for smaller engines and an overall 18.8% lower maximum takeoff weight. The second aircraft in the family uses span extensions to increase the wing span by 14.5 feet and a 4 foot root chord extension to increase the wing area. Compared to other similar aircraft, namely the Boeing 757-200 and 757-300, the aircraft has a high aspect ratio and low wing loading. In addition the design range is lower at 2343 nautical miles, resulting in a lower maximum takeoff weight. The "baseline" aircraft only have the empenage as common components, resulting in low design commonality indicies between 4 to 5%. The design commonality index of the three derivative aircraft are also relatively low between 50 to 60%.

6.3.2 Two Aircraft Families Optimization Results

The second solution is for the case of two aircraft families, each with three aircraft in the respective family. The geometries of the six obtained aircraft can be seen in Figures 6.4 and 6.5. Selected specifications and parameters of the six aircraft are listed in Table 6.3.

The capacities of the first two aircraft in Family D are similar to Family A in the previous case. The third aircraft in the family has a capacity of 98 passengers. The aircraft use a T-tail configuration with four seats abreast in the cabin. All the aircraft in the family share the horizontal and vertical tail. The wing is complete shared between Aircraft D1 and Aircraft D2 and only a 1.29 foot root chord extension is added to Aircraft D3. The projected spans vary slightly due to different cant angles of the winglets. The aspect ratio is higher than that of other aircraft in their class, but lower than the aspect ratios of the aircraft in Family A of the previous case. The design range is highest for the smallest aircraft, at 1492 nautical miles, and decreases to 1276 nautical miles for the highest capacity member of the family. This results in very similar thrust requirements for the three aircraft and hence the engines are also shared across this family. Similar to the previous results, all the aircraft perform low speed climbs followed by cruising at a Mach number of around 0.70.

The second family of aircraft in this test case has significantly higher capacities than the aircraft in Family D, with a 185 passenger capacity of Aircraft E1 to 224 passengers of Aircraft E3. All the aircraft share the same fuselage

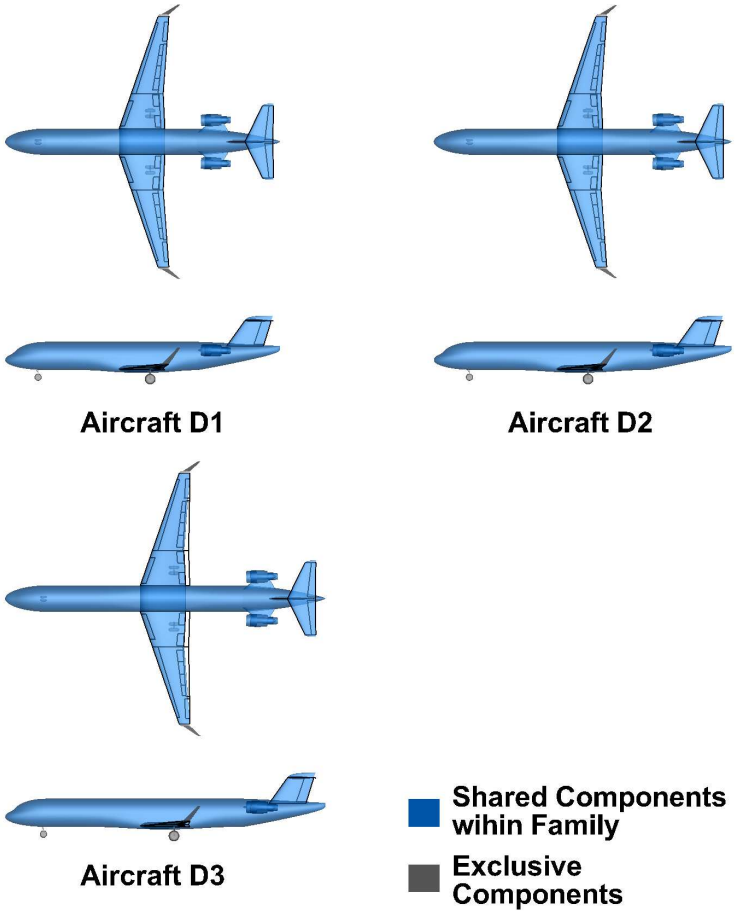

Figure 6.4: Aircraft Family D geometries of the two aircraft families solution

layout, with six seats abreast, a conventional configuration with engines under the wings, the horizontal tails and the wing with only minor span and chord extensions by Aircraft E2 and E3. The vertical tail is only shared between the two larger aircraft, while Aircraft E1 has a scaled down version of the same tail. The design ranges are comparative to the design ranges of the aircraft in the previous case, with Aircraft E1 having a design range of 1811 nautical miles, Aircraft E2 a lower design range of 1596 nautical miles and Aircraft E3 an increased design range of 2263 nautical miles. The aspect ratios of each of the aircraft are also quite high for aircraft in their class, while the preferred climb speed is low. This in combination with the lower design ranges results in aircraft with lower MTOW compared to existing aircraft with similar ca-

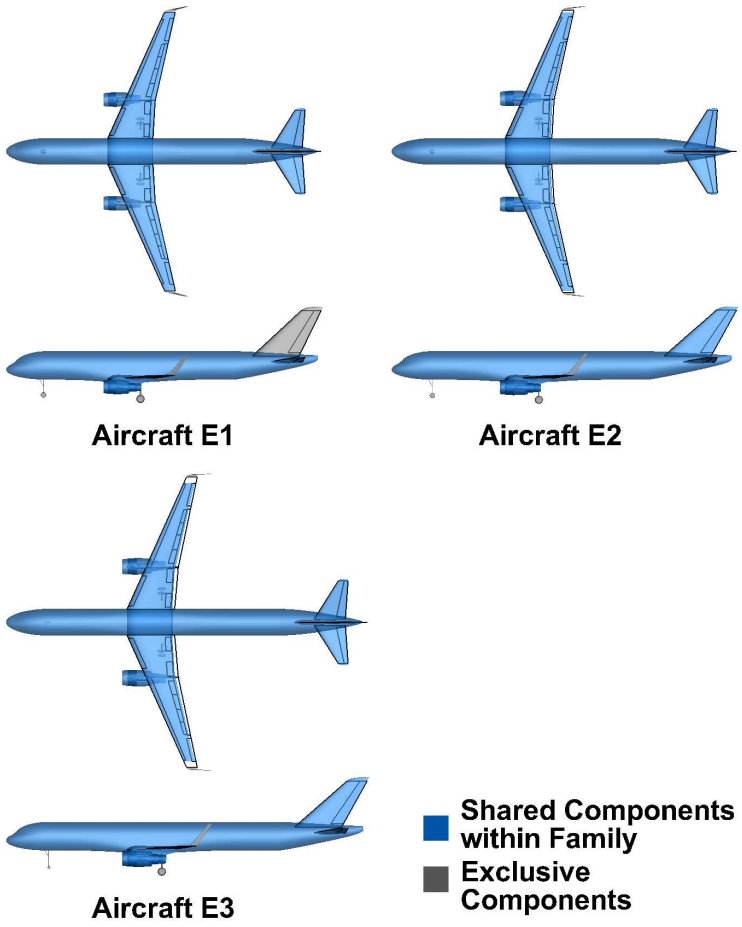

Figure 6.5: Aircraft Family E geometries of the two aircraft families solution

pacities.

As for the case of three aircraft families and to some degree the robust optimization results, all the aircraft have relatively high spans and reference areas, resulting in lower wing loadings, and low initial climb speeds. Hence, the aircraft spend more time in the constant CAS climb segment of the mission profile. During climb the lift coefficient is generally higher resulting in higher induced drag, but this higher induced drag is mitigated by the higher aspect ratio wings. The relatively low maximum wing loading also allows for lower maximum thrust engines, which in this case have high bypass ratios, resulting in lower fuel consumption. All these factors combined, from the lower design

Table 6.3: Two families optimization solution aircraft specifications

	Aircraft Family D			Aircraft Family E		
	Aircraft D1	Aircraft D2	Aircraft D3	Aircraft E1	Aircraft E2	Aircraft E3
Operation						
Capacity	76	89	98	185	204	224
Seat Configuration	2+2	2+2	2+2	3+3	3+3	3+3
Design Range [nmi]	1492	1306	1276	1811	1596	2263
Geometry						
Wing Projected Span [ft]	96.04	95.57	96.22	135.40	135.58	138.56
Wing Aspect Ratio	11.57	11.57	10.43	13.17	12.95	13.10
Wing Reference Area [ft^2]	745.07	745.07	821.06	1425.39	1508.38	1591.17
Engines						
Maximum Static Thrust [lb_f]	11248	12283	12332	28718	32932	37741
Bypass Ratio	6.7	6.8	6.8	7.9	8.1	8.3
Flight Condition						
Climb CAS [knots]	260	260	264	263	260	260
Cruise Mach	0.71	0.69	0.70	0.76	0.75	0.75
Cruise Altitude [×1000 ft]	32	29	30	35	35	37
Weights and Loadings						
Maximum Takeoff Weight [lb_f]	69433	76859	84167	177587	192422	222292
Operational Empty Weight [lb_f]	39340	44080	47799	104726	115779	129125
Maximum Fuel Weight [lb_f]	23130	23130	26419	53812	58891	61925
Design Fuel Weight [lb_f]	12256	11962	12651	29474	28742	40528
Maximum Wing Loading [lb_f/ft^2]	722.95	804.24	874.71	1311.53	1419.28	1604.29
Maximum Thrust-to-Weight [lb_f/lb_f]	0.32	0.32	0.29	0.32	0.34	0.34
Costs						
Design Commonality Index [%]	25.35	69.92	84.12	24.96	66.64	80.85
Purchasing Price [Mil. 2014 US$]	38.87	41.22	42.83	73.54	77.55	83.89

ranges to the lower thrust engines, result in aircraft with lower maximum takeoff weight. In addition, due to the relationship between the research and development and production cost of aircraft and their MTOW in combination with the higher design commonality indicies within the families, this results in lower acquisition costs.

6.3.3 Aircraft Families' Network Performance

The results of the two test cases when operated for 15 years on the two networks are described below. It can be noted that the combined performance, in terms of energy intensity and fuel burn, of each set of families is very similar, even so each represents a unique set of aircraft. This showcases the multi–modality of the coupled optimization problem.

North American Routes

The performance of the three family solutions for the North American network is summarized in Table 6.4, while the performance of the two family solutions is summarized in Table 6.5. In the case of the three aircraft family solutions, all aircraft except the smaller of the medium capacity aircraft, Aircraft B1, are allocated to the network. The majority of routes and days are serviced by the two regional jet family aircraft, Family A, and by the high capacity, highest design range large aircraft, Aircraft C2. As with the previous cases, the average ranges are similar, with around 300 nautical miles for the two regional jet type aircraft and 1000 nautical miles for Aircraft C2, with the other two aircraft falling in between. The annual utilization is above 2000 hours, with the exception of Aircraft C1, which is used on relatively few days and routes. It can be noted that for Family A a switch occurs; in the first seven years of operations Aircraft A1 is used almost exclusively for mainly the ExpressJet routes, after which Aircraft A2 is used almost exclusively for the same routes. This switch can be explained by the increase in passenger demand over the years, at which point the switch to the larger capacity aircraft is more economical than performing multiple flights with the smaller of the two aircraft.

The generally lower design ranges of all the aircraft result in lower takeoff weight and hence smaller engines. This, combined with higher efficiency design for shorter ranges results in lower energy intensity mean and standard deviation values for all the aircraft compared to the previous cases. The overall result on the network is a significant decrease in energy intensity and fuel burn by 21% compared to the reference aircraft and over 6% compared to the

Table 6.4: Three families results for operating the North American network for 15 years

	Aircraft Family A		Aircraft Family B		Aircraft Family C	
	Aircraft A1	Aircraft A2	Aircraft B1	Aircraft B2	Aircraft C1	Aircraft C2
Average Load Factor, [%]	75.9	76.0	NA	82.8	75.6	82.3
Average Route Range, [nmi]	314	352	NA	667	894	1071
Average Annual Utilization, [hr]	2241	2347	NA	2569	1579	2764
Max. Number of Aircraft	45	52	0	52	19	111
Number of Flights	190944	384737	0	31125	5628	623304
Individual Energy Intensity, [BTU/(lb_f nmi)]	17.46	15.50	NA	9.93	10.16	8.65
E_I Standard Deviation, [BTU/(lb_f nmi)]	22.88	21.08	NA	10.92	10.48	9.32
Network Energy Intensity, [BTU/(lb_f nmi)]	9.30 (-21.04%[1], -6.28%[2])					
Total Fuel Required, [Billion lb_f]	15.71 (-21.08%[1], -6.31%[2])					
Total Operating Cost, [Billion 2014 US$]	35.95 (-5.73%[1], -4.45%[2])					
Total Acquisition Cost, [Billion 2014 US$]	14.40 (-8.29%[1], -10.95%[2])					

[1] Relative difference w.r.t. reference aircraft solution.
[2] Relative difference w.r.t. robust aircraft solution.

robust solution. The operating costs are also lower, by 5.7% and 4.5%, as are the acquisition costs, by 8.3% and 11%, respectively. The lower operating costs are provided by the lower fuel required and the extensive use of the high capacity aircraft, which results in a lower number of flights and hence lower fees. At the same time, the operating cost are not reduced as significantly as the fuel burn, due to the increased flight times, which are a result from the lower climb speeds. The increases in flight time result in corresponding higher crew cost. The use of high capacity aircraft also results in a lower number of aircraft required and the reduced aircraft purchasing prices through the use of shared components reduce the acquisition costs.

The two aircraft family solution only uses four of the six available aircraft on the North American network. The first two aircraft of Family D and the two higher capacity aircraft of Family E. Aircraft D2 is used significantly more than Aircraft D1, which is designed for a higher design range, but the routes Aircraft D2 are assigned to are generally shorter, resulting in a low average range of under 300 nautical miles, while the average range for Aircraft D1 is almost 600 nautical miles. The average ranges for the two larger aircraft are close in value to each other at over 1000 nautical miles. As for the three family case, the largest capacity aircraft is used extensively throughout the network. The mean values and standard deviation of the energy intensity for all the assigned aircraft are low compared to other solutions, especially for the two members of Family E, while the annual utilization is high for all the aircraft. The obtained fuel burn and energy intensity are slightly lower than for the three family case at 22.4% compared to the reference case and 7.9% compared to the robust solution. Extensive use of the two larger capacity aircraft provides lower operating cost, by 6.8% and 5.5%, and lower acquisition cost, by 14.8 and 17.3% compared to the reference and robust solutions.

Figure 6.6 shows the change in energy intensity, fuel burn per year and operating cost per year when operating on the North American route network for the four test cases. The average load factor for each year of operation is also shown. The performance of the two family test cases is very similar, with the two family solution providing consistently lower results in terms of energy intensity, fuel burn and operating cost. The two family solution does show a higher number of fluctuations over the years of operations, which can be attributed to a lesser number of switches in the aircraft types allocated compared to the three family case, which changes aircraft within each family more frequently to match demand. The average increase in fuel burn is 2.36% and 2.32% for the three and two family solutions, or a total change of 38.6%

Table 6.5: Two families results for operating the North American network for 15 years

	Aircraft Family D			Aircraft Family E		
	Aircraft D1	Aircraft D2	Aircraft D3	Aircraft E1	Aircraft E2	Aircraft E3
Average Load Factor, [%]	70.4	73.7	NA	NA	82.8	82.1
Average Route Range, [nmi]	572	288	NA	NA	1034	1068
Average Annular Utilization, [hr]	2432	2201	NA	NA	2941	2826
Max. Number of Aircraft	27	42	0	0	121	111
Number of Flights	68883	472436	0	0	251755	451304
Individual Energy Intensity, [BTU/(lb_f nmi)]	13.71	16.60	NA	NA	8.76	8.48
E_I Standard Deviation, [BTU/(lb_f nmi)]	15.32	22.31	NA	NA	9.40	9.20
Network Energy Intensity, [BTU/(lb_f nmi)]	9.15 (-22.36%;[1] -7.85%[2])					
Total Fuel Required, [Billion lb_f]	15.45 (-22.40%;[1] -7.88%[2])					
Total Operating Cost, [Billion 2014 US$]	35.56 (-6.75%;[1] -5.48%[2])					
Total Acquisition Cost, [Billion 2014 US$]	13.38 (-14.79%;[1] -17.27%[2])					

[1] Relative difference w.r.t. reference aircraft solution.
[2] Relative difference w.r.t. robust aircraft solution.

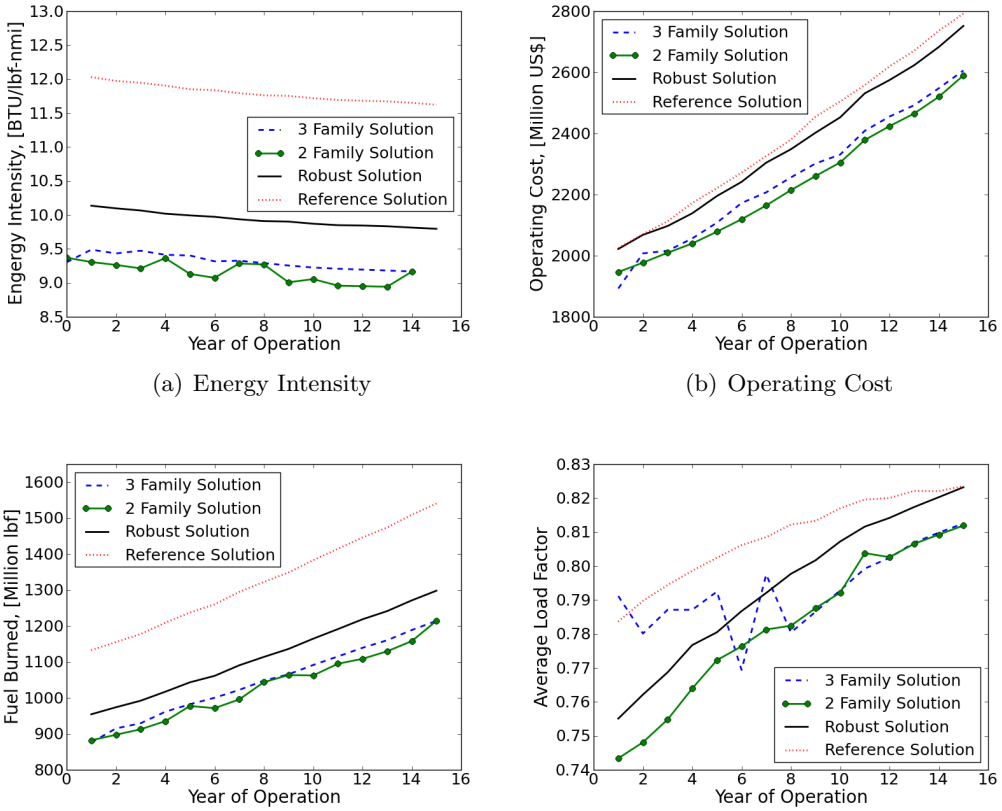

(a) Energy Intensity

(b) Operating Cost

(c) Fuel Burn

(d) Average Load Factor

Figure 6.6: Performance comparison of all solutions for operating the North American route network for 15 years

and 37.7%, respectively. Both these relative increases are higher than for the robust solution, but due to the overall higher efficiency of the allocated aircraft the fuel burn does exceed the fuel burn of year one by the reference aircraft only in years 13 and 14, respectively. The average load factors are lower for both cases. The main contribution to these lower load factors comes from the regional jet type aircraft whose capacity is better suited to the European network, discussed below. The operating cost of the two family cases increases more slowly compared to all the other cases at an average of 2.06% per year, which results in an overall lower operating cost. Even though the yearly increases are generally higher than for the reference and robust solution, they

still fall below the increases in passenger demand and revenue passenger miles. It can be noted that in both cases the largest capacity aircraft are used extensively and that the design of the aircraft families provides increased flexibility in the allocation, especially in the three aircraft family case.

European Routes

Table 6.6 provides a summary of the performance of the three family solution on the European network operated for 15 years with the given passenger demand profiles from the discrete time simulation. For the three family cases all aircraft except the high capacity Aircraft C2 are assigned to the network. As for the previous cases the route structure of the network results in low average ranges and corresponding lower annual utilization for all of the assigned aircraft, especially for the the two regional jet type aircraft and the larger Aircraft C1. The aircraft assigned the most number of flights is the second medium sized Aircraft B2, followed by the second regional jet type Aircraft A2. Aircraft C1 is only used starting in the eighth year to cope with the increase in passenger demand, especially on the very short, high demand routes between the hubs and Berlin. The total network energy intensity and fuel burn are significantly lower than the reference and robust solution, with a reduction in both of 19.9% and 7%, respectively. Operating and acquisition costs are also reduced, the operating cost by 4% and 8% and the acquisition cost by 12% and 17% compared to the two previous solutions.

The performance of the two family solution on the European route network is given in Table 6.7. The reduction in total fuel burn and energy intensity is slightly lower for the two family case compared to the three family case with a total reduction in both of 19.3% compared to the reference solution and 6.4% compared to the robust solution. The only aircraft not assigned to any of the days of operation in the network are the small region jet, Aircraft D1 and, like the three family solution, the largest aircraft, which is designed for longer ranges, Aircraft E3. Different from the three family case, the largest number of flights is assigned to the second regional jet type aircraft, Aircraft D2, followed by the first two members of the larger capacity Family E, where a switch between aircraft occurs around year eight from Aircraft E1 to Aircraft E2. The average ranges and annual utilization are again comparable to previous results. The operating costs follow the same trend as the fuel burn and energy intensity, with slightly lower reductions than the three family case, at 3.7% compared to the reference solution and 7.8% compared to the robust case. The acquisition cost, on the other hand, are significantly lower than

Table 6.6: Three families results for operating the European network for 15 years

	Aircraft Family A		Aircraft Family B		Aircraft Family C	
	Aircraft A1	Aircraft A2	Aircraft B1	Aircraft B2	Aircraft C1	Aircraft C2
Average Load Factor, [%]	84.0	80.4	84.7	83.5	87.5	NA
Average Route Range, [nmi]	204	239	463	378	212	NA
Average Annual Utilization, [hr]	1629	1562	1822	2176	1497	NA
Max. Number of Aircraft	23	78	87	148	44	0
Number of Flights	74997	248023	45844	1162288	36341	0
Individual Energy Intensity, [BTU/(lb_f nmi)]	22.13	17.87	12.75	13.02	22.56	NA
E_I Standard Deviation, [BTU/(lb_f nmi)]	27.90	21.61	16.11	15.59	23.97	NA
Network Energy Intensity, [BTU/(lb_f nmi)]	13.66 (-19.89%[1], -7.01%[2])					
Total Fuel Required, [Billion lb_f]	9.79 (-19.84%[1], -7.17%[2])					
Total Operating Cost, [Billion 2014 US$]	30.28 (-3.91%[1], -8.01%[2])					
Total Acquisition Cost, [Billion 2014 US$]	12.62 (-12.46%[1], -17.23%[2])					

[1] Relative difference w.r.t. reference aircraft solution.
[2] Relative difference w.r.t. robust aircraft solution.

Table 6.7: Two families results for operating the European network for 15 years

	Aircraft Family D			Aircraft Family E		
	Aircraft D1	Aircraft D2	Aircraft D3	Aircraft E1	Aircraft E2	Aircraft E3
Average Load Factor, [%]	NA	82.5	88.1	84.7	84.4	NA
Average Route Range, [nmi]	NA	328	280	380	393	NA
Average Annular Utilization, [hr]	NA	2261	1241	1532	1814	NA
Max. Number of Aircraft	0	118	32	91	99	0
Number of Flights	0	1140979	14291	300624	245456	0
Individual Energy Intensity, [BTU/(lb_f nmi)]	NA	13.81	15.27	14.59	12.74	NA
E_I Standard Deviation, [BTU/(lb_f nmi)]	NA	16.92	16.07	17.56	14.69	NA
Network Energy Intensity, [BTU/(lb_f nmi)]	13.76 (-19.33%[1] -6.37%[2])					
Total Fuel Required, [Billion lb_f]	9.86 (-19.25%[1]; -6.50%[2])					
Total Operating Cost, [Billion 2014 US$]	30.34 (-3.71%[1]; -7.82%[2])					
Total Acquisition Cost, [Billion 2014 US$]	11.76 (-18.45%[1]; -22.90%[2])					

[1] Relative difference w.r.t. reference aircraft solution.
[2] Relative difference w.r.t. robust aircraft solution.

for the three family case, due to the higher commonality shared between the assigned aircraft and the lower number of higher capacity aircraft required to meet the given demand.

The total values of the performance of the family solutions indicate a slightly better performance of the three family case over the two family case. Comparing the yearly change in overall values for operating the European network, Figure 6.7, shows higher fluctuations in the values from the two family case. As for the North American network, both family solutions remain

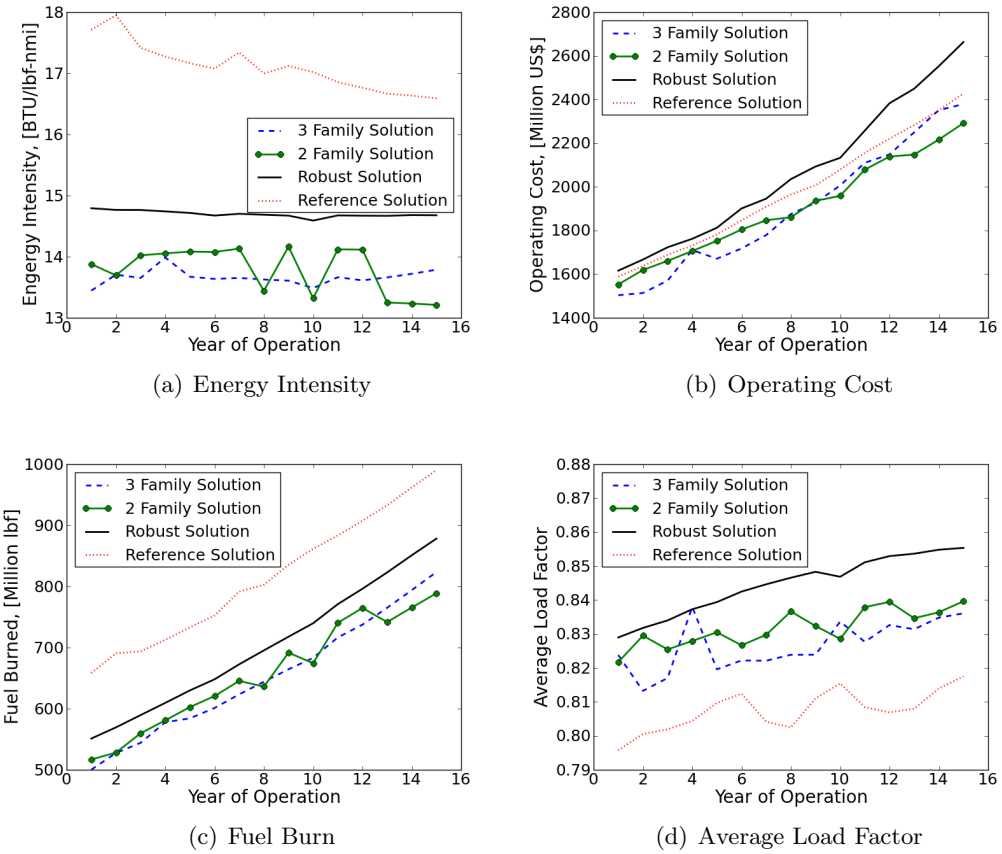

(a) Energy Intensity

(b) Operating Cost

(c) Fuel Burn

(d) Average Load Factor

Figure 6.7: Performance comparison of all solutions for operating the European route network for 15 years

below the values of the robust solution, also in the case of the average load

factor, which falls between the reference solution and the robust solution. The better performance of the three family case does not extend when examining the trends over the years. The energy intensity increases at an average rate of 0.19% a year, while the energy intensity of the two family solution decreases by 0.29% a year resulting in a total increase of 2.54% for the three family case and a total decrease of 4.8% for the two family case. Similarly the fuel burn increases at a higher rate for the three family case, at 3.63%, to a total increase of 64.67%, which is higher than the growth in passenger demand. The two family case increases its fuel burn at a slower rate of 3.31% a year to a total of 52.6%, which is much lower than any of the other solutions. In both cases the fuel burn exceeds the year one level of the reference solution around the tenth year of operation. The same can be observed in the operating cost, where the difference between the three family solution and the reference solutions shrinks from 5.4% in the first year to 2.0% in the final year, while the difference in cost is negligible in year 14. In case of the two family solution, the trend is reversed with a 2.3% difference in the first year that increases to 5.6% lower operating cost in the final year, compared against the reference solution.

The given total values for the networks was for an operational period of 15 years, but many aircraft are in service significantly longer. Hence, to assess the sustainability of any solution not only the overall performance of each but also the yearly trends must be considered. Since the rate of change of fuel burn per year of the three family solution is higher than the growth in passenger demand, this would indicate that the two family solution is preferable in terms of the long term environmental impact of operating these aircraft. The ratios of the route range to the design range of the performed departures on the North American and European network by three family aircraft can be seen in Figure 6.8 and Figure 6.9, respectively. In both networks the performed departures are distributed towards higher range ratios, compared to the reference and robust case. A significant number of departures also occur at range ratios which are greater than one. The higher the range ratio is above one the lower the number of passengers that can be carried and the possible load factor for these longer routes. This explains why the design ranges of the coupled solutions are not as low as would be expected from the data of the two networks alone. Although the performed departures are distributed over higher range ratios in the North American network, the average range ratio is essentially the same as for the reference case with a value of 43.3% of the design ranges. The same is not the case for the European network, where a large number of departures is shifted to higher range ratios, resulting in an higher average range ratio 26.5% compared to the reference and robust case.

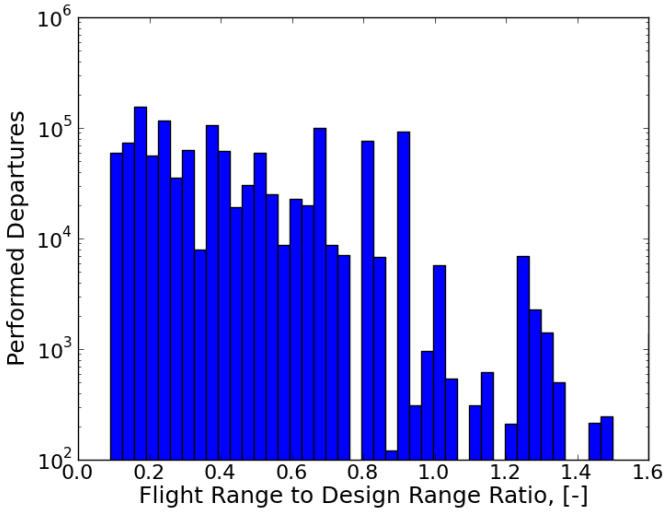

Figure 6.8: Route range to design range ratio of performed departures by the three family aircraft on the North American network (43.3% average ratio)

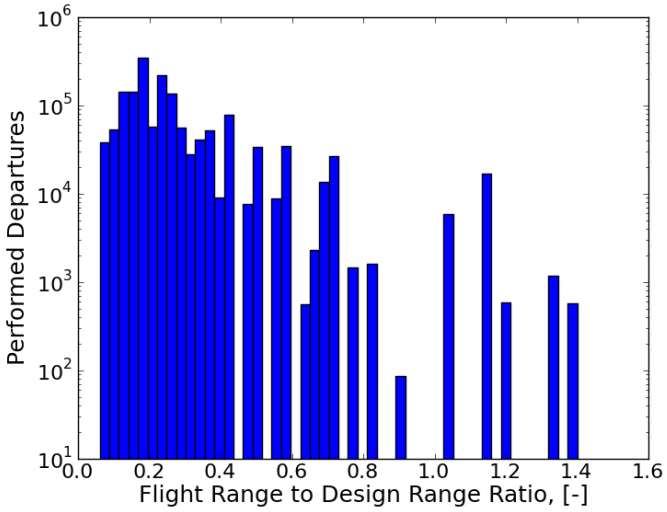

Figure 6.9: Route range to design range ratio of performed departures by the three family aircraft on the European network (26.5% average ratio)

This shift towards higher range ratios results in a decrease in operational inefficiencies as the aircraft are operated closer to their respective design points as is discussed below.

The performed departures are even more distributed towards higher range ratios for the two family case, as can be seen in Figure 6.10 for the North American network, and in Figure 6.11 for the European network. The average range ratio for this case for the North American network was 48.7% and 30.3% for the European network, which are the highest average values for all the different cases in both networks, which is due to the shorter design ranges of the aircraft. The reason the two family cases does not exhibit significantly higher performance in both networks combined when compared to the three family case is that these higher average range ratios are partially due to a higher number of performed departures at range ratios greater than one. At a range ratio greater than one the payload that can be carried by the aircraft is lower than the maximum payload, while the highest efficiency points are at maximum payload, as described below. This again shows the reason for the higher than expected design ranges of the aircraft and the benefit of coupling the design with the allocation of the aircraft.

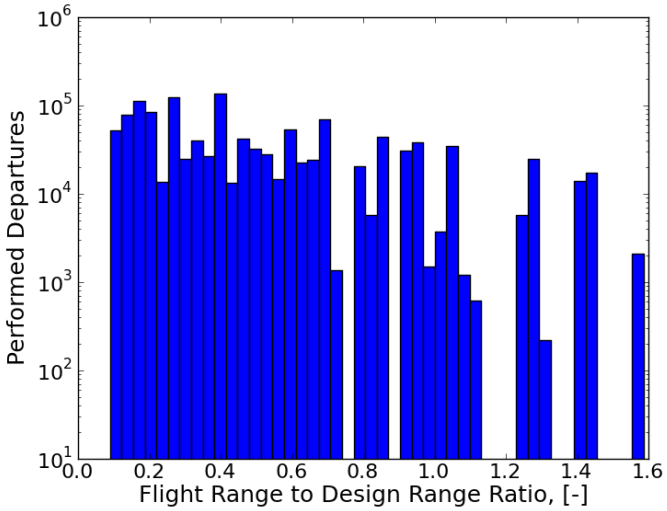

Figure 6.10: Route range to design range ratio of performed departures by the two family aircraft on the North American network (48.7% average ratio)

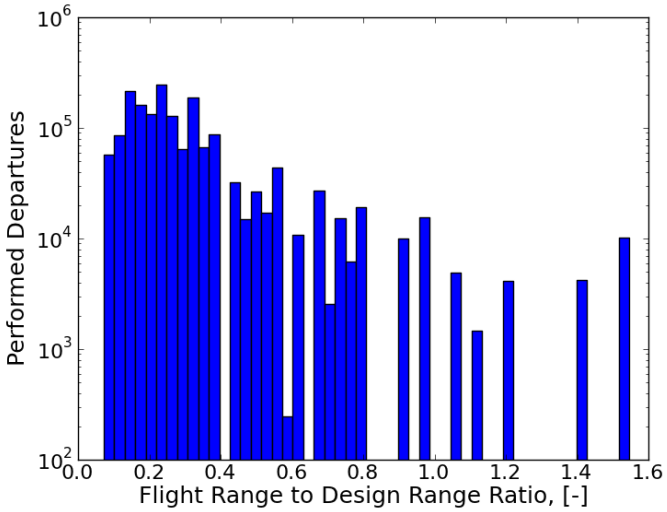

Figure 6.11: Route range to design range ratio of performed departures by the two family aircraft on the European network (30.3% average ratio)

Both cases show significant reductions in fuel consumed, energy intensity as well as cost compared to the reference and robust solutions. Figure 6.12 and Figure 6.13 show the payload range diagram for the three aircraft family case with an overlay of the energy intensity contours. The departures performed show the frequency of flight for each aircraft when operating both networks for 15 years. The payload range diagrams of the two family aircraft are shown in Figure 6.14 and Figure 6.15.

The lower design ranges of all the coupled aircraft and the design for high efficiency in climb shifts the constant energy intensity contours to lower ranges. This shift results in larger portions of the performed flights falling into lower energy intensity regions of the respective payload range envelopes, providing the overall reductions in fuel burn. As was noted before, a significant number of departures by most of the aircraft occur at ranges higher than the design range and high load factors, which also corresponds to low energy intensity regions of the respective payload range envelopes. A further reduction in the design ranges of these aircraft would shrink of the payload range envelopes and the longer range routes could only be performed at lower payloads, which would result in higher energy intensities for these routes. It can be noted that Aircraft D3 is used for a very limited number of routes in the European

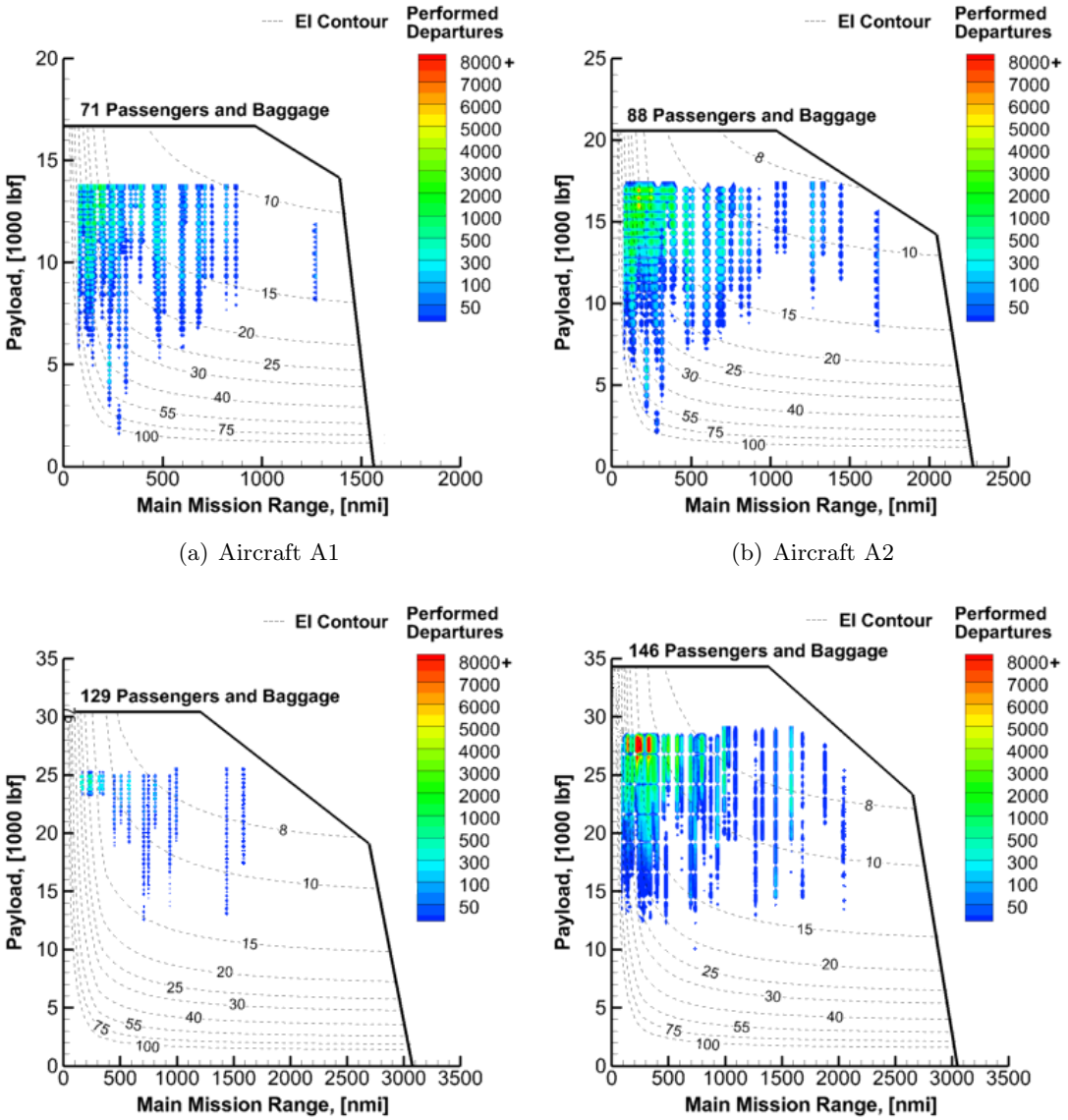

(a) Aircraft A1

(b) Aircraft A2

(c) Aircraft B1

(d) Aircraft B2

Figure 6.12: Frequency of flights performed on payload range diagram for the aircraft families A and B designs and operating both networks for 15 years

network, compared to the other aircraft.

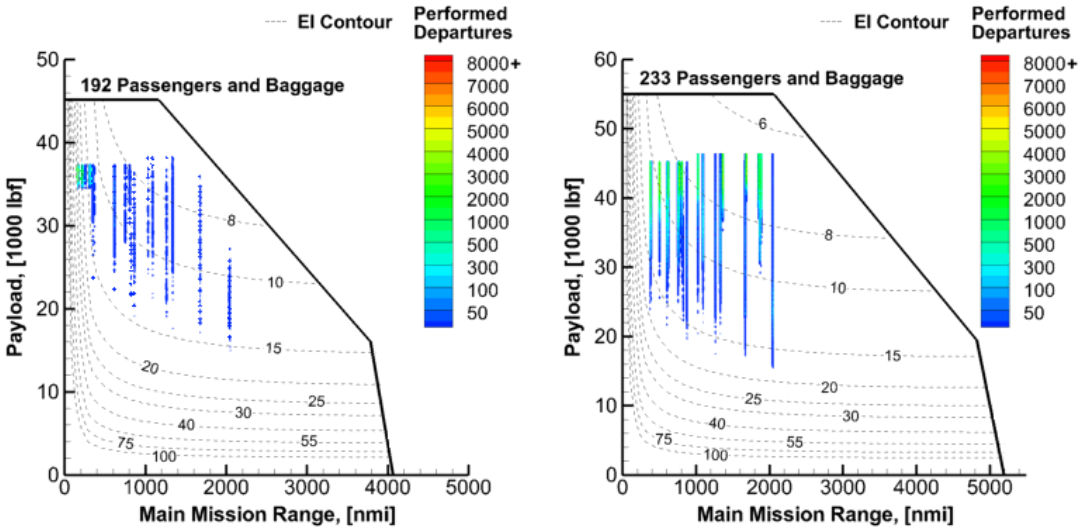

(a) Aircraft C1

(b) Aircraft C2

Figure 6.13: Frequency of flights performed on payload range diagram for the three aircraft family C designs and operating both networks for 15 years

The increase in efficiency for shorter ranges by family case aircraft can also be illustrated by considering the payload range efficiency envelopes of the two test cases compared to the robust aircraft. Payload range efficiency is given by the inverse of the energy intensity multiplied by the lower heating value of fuel. It represents how many miles one pound of payload can be transported by one pound of fuel. Figure 6.16 shows the payload range efficiency envelopes of the three family aircraft and the robust aircraft, Aircraft R1, R2 and R3, as comparison. The peak value of payload range efficiency for any aircraft occurs at the design range and design payload point. The lower design ranges and the design for short ranges of the three family aircraft results in a shift of this peak to lower ranges for all the aircraft compared to the robust aircraft. With the exception of the low capacity Aircraft A1 the peak values are also higher than the robust aircraft with similar capacities. As was seen in the range ratios of the performed departures, more departures occur closer to the design point of the payload range efficiency of the three family aircraft. Additionally, the aircraft of Family A show a steeper increase in payload range efficiency at very low ranges. The increase in the peak values and steeper increase in efficiency result in the increased performance of these aircraft on the networks compared to the robust aircraft and reference, which were designed for longer

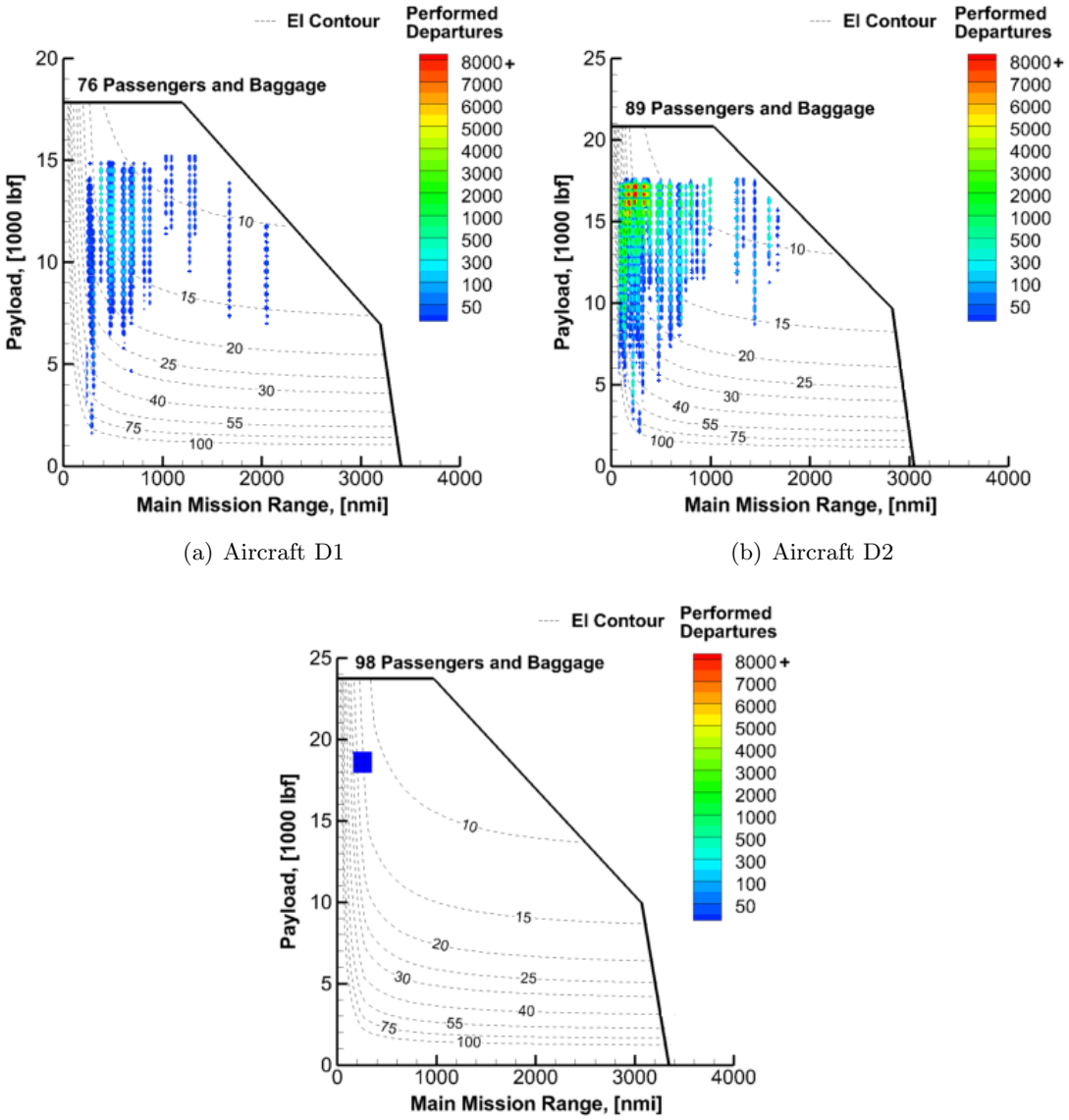

(a) Aircraft D1

(b) Aircraft D2

(c) Aircraft D3

Figure 6.14: Frequency of flights performed on payload range diagram for the aircraft family D designs and operating both networks for 15 years

ranges.

The same trend can also be observed in the payload range efficiency en-

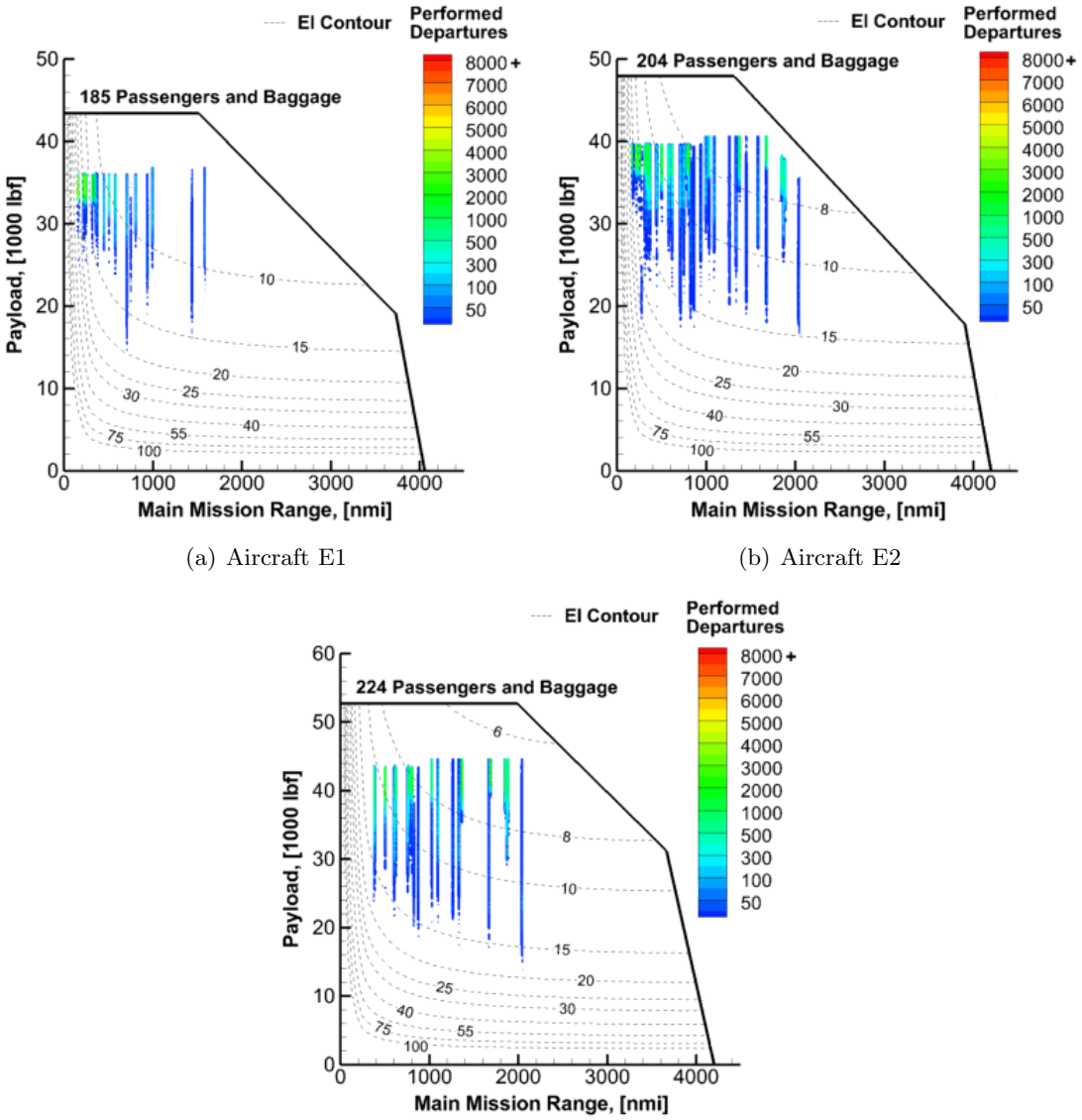

(a) Aircraft E1

(b) Aircraft E2

(c) Aircraft E3

Figure 6.15: Frequency of flights performed on payload range diagram for the aircraft family E designs and operating both networks for 15 years

velopes for the two family case, which are shown in Figure 6.17. The peak efficiencies are at higher values and shorter ranges compared to the robust aircraft, due to the design for shorter ranges of the aircraft. As was noted

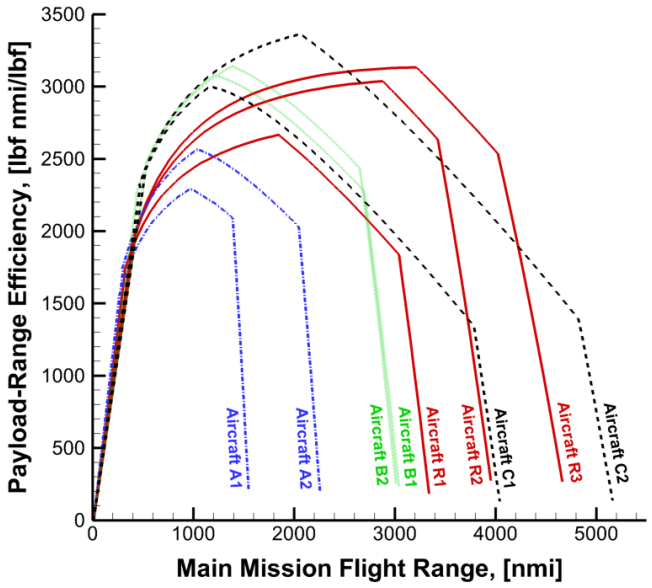

Figure 6.16: Payload range efficiency of three family and robust aircraft

above, a significant number of departures occur at range ratios greater than one, which indicate lower than maximum payloads. But due to the higher peak values of the payload range efficiency envelopes for these aircraft even operations past the design range and at lower payloads can have a higher payload range efficiency than the robust aircraft at maximum payload. Reducing the design ranges further would result in lower efficiencies for these longer range routes.

For both networks the performance of the two solutions is very similar, with the three family case having slightly better performance on the European network and the two family solution having a slight advantage on the North American network. This shows the multi-modality and complexity of the coupled optimization problem. Even with the flexibility provided by designing six aircraft for the two networks, trade-offs exist between the two markets. On the other hand, the performance of both family test cases is significantly better than the performance of the robust solution for both networks. Hence, the closer coupling in the design of these aircraft, including the selection of the capacities and design ranges, with the operational use does

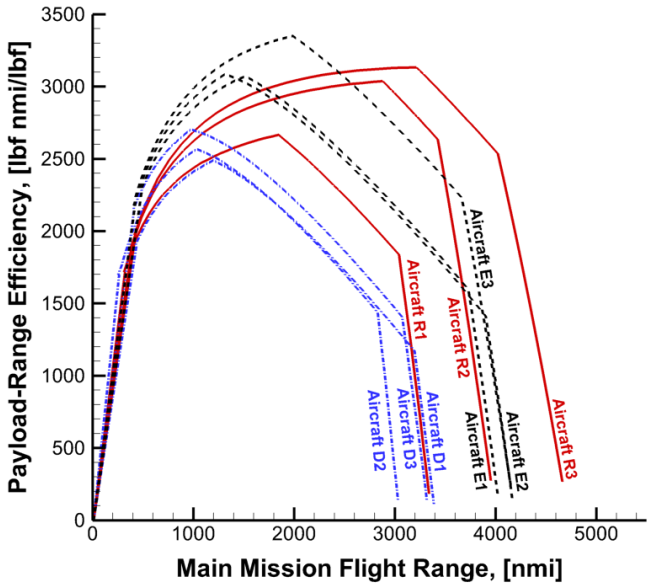

Figure 6.17: Payload range efficiency of two family and robust aircraft

provide further reductions in energy intensity, fuel burn and operating cost at the same technology level as a robust design optimization. The design of the aircraft as part of a family provides additional advantages in terms of the required acquisition cost for operating these networks.

7 Conclusions and Recommendations

The environmental impact of aviation is becoming of increasing importance in the design and development of new commercial transport aircraft. Predictions indicate that air traffic will continue to grow at a fast pace in the foreseeable future. At the same time, it is also predicted that the development and deployment of new technologies for the reduction of the climate impact of aviation will be outgrown by the growth in air transport activity. Therefore, the goal of carbon neutral growth of aviation in the near future will require continued research and development. One way, besides the development of new technologies, to reduce the climate impact of modern commercial aircraft is to integrate the use of aircraft by operators more closely with the design process. Most aircraft are not operated at their design range, which can lead to significant performance penalties. Combining better aircraft performance through the design of new aircraft with the optimization of operational performance can result in better economic performance and lower emissions. Additionally, the cost of developing and producing new aircraft is substantial, but requirements for different markets can very significantly. Using a product family approach in the design of an aircraft family can significantly reduce the total investment cost associated with new aircraft programs, while also providing reductions in operating cost due to lower training and maintenance cost.

The goal of this research was to develop a conceptual aircraft design framework that allows combining the multidisciplinary conceptual design optimization of aircraft families with the allocation of these aircraft on routes of multiple markets for extended periods of operation.

7.1 Conclusions

A methodology to account for the effects of aircraft sharing common components was introduced into a conceptual aircraft design framework using a weight–based design commonality index and cost reduction factors. The modeling of sustained operations, including daily and monthly variations in the passenger demand for any given route, and varying growth in passenger demand was done using a discrete time simulation. The solution of the fleet allocation problems allowed investigation into how different designs of aircraft are going to be employed to meet varying passenger demand and provide an indication of the robustness of the performance of these aircraft for sustained operations. A decoupled robust optimization approach for individual aircraft was also formulated as a reference case for the coupled optimization. Optimizations were performed on a set of 48 domestic routes in North America and Europe representative of routes flown by existing narrow-body aircraft.

The robust aircraft optimization results showed significant reductions in fuel burn and energy intensity compared to existing aircraft, by 15.8% for the North American network and 13.8% for the European network. The operating costs were similar to the existing aircraft with a reduction of 1.3% for the North American network and an increase of 4.5% for the European network. The reductions in fuel burn were less significant for the European routes showing a higher sensitivity to the growth in this market, which is dominated by short range routes. The designs exhibit higher aspect ratios and lower wing loadings than existing aircraft, which improves their efficiency in climb and allows for smaller engines. The bypass ratios were also allowed to be higher than for the existing aircraft, further improving the overall efficiency of these aircraft. The objective of the robust design optimization was the energy intensity and its robustness, and not the operating cost of the aircraft. One drawback of the robust optimization test case is that the design of the aircraft is still decoupled from the fleet allocation problem and the design range and capacity for each aircraft must be selected beforehand.

In the coupled optimization the optimizer was given flexibility to select the level of commonality between members of each family. Two test cases were performed, one case of three aircraft families, where each family had two aircraft, and a case of two aircraft families, where each family had three aircraft. In both cases the design of the aircraft reduced the design ranges and followed a similar design as the robust cases with higher aspect ratio wings, lower wing loadings and lower initial climb speeds. The combination of the

lower design ranges and more efficient aircraft resulted in lower takeoff weights allowing for smaller engines and more efficient aircraft for short ranges. For both networks the performance of the two solutions of families showed higher reductions in fuel burn, energy intensity and operating cost compared to the robust case. On the North American routes fuel burn and energy intensity were reduced by 6.3% and 7.9% for the two test cases, while operating costs were reduced by 4.5% and 5.5%, respectively compared to the robust solution. For the European routes fuel burn and energy intensity were reduced by 7.0% and 6.5% for the two test cases, while operating costs were reduced by 8.0% and 7.8%, respectively. Additionally, the acquisition costs were also reduced significantly. For the three family case, the acquisition cost were 11.0% and 17.2% lower compared to the robust aircraft for North American and European network respectively. For the two family case, the acquisition cost were 17.8% and 22.9% lower compared to the robust aircraft for North American and European network respectively. These reductions in acquisition cost are due to the closer selection of the required capacity, the lower maximum takeoff weights and the commonality between the aircraft.

In all of the performed test cases, the solutions showed yearly increases in fuel burn and operating costs generally lower than the growth in passenger demand and increases in revenue passengers miles for both networks under consideration. These increases were still sufficiently high to have the fuel burn exceed that of the existing aircraft within the 15 years of operation. For the robust design case this occurred at year nine and seven for the North American and European networks, respectively, while for the three and two family cases, this occurred at year 13 and 14 for the North American network and year 10 for the European network. The closer coupling between the design of aircraft and their operational use can significantly reduce the energy intensity and the fuel required for operating these aircraft, but these reductions are not sufficient to achieve carbon neutral growth at the current technology levels.

7.2 Recommendations for Future Developments

A number of potential areas for further development can be identified and if implemented would contribute to improve the overall objective of the coupled aircraft design and fleet allocation framework for sustainable aviation. One improvement would be to extend the number of routes and markets analyzed during the fleet allocation problems. For example, the investigation of aircraft required to meet demands in the fast growing Asian markets, such as

the Chinese and Indian domestic markets, would provide important insights into the types of aircraft and aircraft families required to significantly reduce future emissions of commercial aviation. Such an analysis would require detailed data for flights performed in these markets. The current work used representative hub-and-spoke route networks; a further area of development would be to include a network system optimization. In this case the routes would not be fixed but rather passenger demand for certain city pairs would be used to design the actual route network together with the aircraft used to operate it. Further reductions in fuel burn and emission may be realized by this close coupling of design and operations.

Several other environmental concerns, besides the emission of carbon dioxide from burning carbon based fuel, are of growing concern to the public, especially around airports. These include the noise and NO_x emissions during takeoff and landing. Hence, a more detailed propulsion module and a noise model should be implemented in the framework to assess the full environmental impact of each aircraft. Noise and NO_x emissions limits could then either be added as additional constraints with maximum allowable limits, or possible objectives during the optimization. Another aspect to consider, with respect to noise, is the possibility of extending operations at airports with night time takeoff and landing restrictions.

It was shown that even with close coupling between the design of aircraft and the operations on a network, the increases in passenger demand resulted in increased fuel burn in the future. To further reduce the environmental impact of commercial aviation, a move towards non-typical aircraft configurations, such as joint–wing configurations, truss–braced wings and blended-wing body concepts will most likely be required. But the feasibility of these concepts in improving efficiency and reducing the climate impact of aviation strongly depends on the type of routes they are operated on, for example the joint wing concepts seems to be more advantageous for regional jet type aircraft, which gain more from the reduced structural weight of a doubly supported wing structure, while maintaining a low induced drag during climb, than larger aircraft. Therefore, the presented design framework should be extended to analyze and optimize non-conventional configurations.

Bibliography

[1] M. Mane, W.A. Crossley, and Nusawardhana. System-of-system inspired aircraft sizing and airline resource allocation via decomposition. *Journal of Aircraft*, 44(4):1222–1235, July–August 2007.

[2] R.E. Perez and K. Behdinan. A multidisciplinary design optimization approach to aircraft family design. In *Canadian Aeronautics and Space Institute Annual General Meeting*, Toronto, ON, 2007.

[3] E.S. Dallara and I.M. Kroo. Aircraft design for reduced climate impact. In *49th AIAA Aerospace Sciences Meeting Including the New Horizons Forum and Aerospace Exposition*, Orlando, Florida, January 2011. AIAA.

[4] D.S. Lee, G. Pitari, V. Grewe, K. Gierens, J.E. Penner, A. Petzold, M.J. Prather, U. Schumann, A. Bais, T. Berntsen, D. Iachetti, L.L. Lim, and R. Sausen. Transport impacts on atmosphere and climate: Aviation. *Atmospheric Environment*, 44(37):4678 – 4734, 2010.

[5] International Civil Aviation Organization (ICAO). 37th session of the assembly, resolution a37-19: Consolidated statement of continuing ICAO policies and practices related to environmental protection climate change. `http://legacy.icao.int/icao/en/env2010/A37_Res19_en.pdf`, 2010. [accessed: June 2014].

[6] International Air Transport Asscociation (IATA). *IATA Technology Roadmap 2013*. International Air Transport Association, 4th edition, June 2013.

[7] R. del Rosario, J. Koudelka, R. Wahls, and N. Madavan. NASA subsonic fixed wing project overview. In *NASA Fundamental Aeronautics Program 2012 Technical Conference*, Cleveland, OH, March 2012.

[8] K. Franz, K. Risse, and E. Stumpf. Framework for sustainability-driven aircraft design. In *2013 Aviation Technology, Integration and Operations Conference*, Los Angeles, CA, August 2013. AIAA.

[9] H. Pfaender, H. Jimenez, J. Schutte, E. Garcia, and D. Mavris. Enhanced system-wide fuel estimates for n+2 aircraft technologies and concepts towards carbon neutral growth. In *AIAA/3AF Aircraft Noise and Emissions Reduction Symposium*, Atlanta, GA, June 2014. AIAA.

[10] S. Andrews and P.E. Ruben. Stability and control effects on the design optimization of a box-wing aircraft. In *14th AIAA Aviation Technology, Integration, and Operations Conference*, Atlanta, GA, June 2014. AIAA.

[11] T. Nam, I. Chakraborty, J. Gross, and D.N. Mavris. Multidisciplinary design optimization of a truss-braced wing concept. In *14th AIAA Aviation Technology, Integration, and Operations Conference*. AIAA, 2014.

[12] I. Chakraborty, J. Gross, T. Nam, C. Perullo, and D.N. Mavris. Analysis of the effect of cruise speed on fuel efficiency and cost for a truss-braced wing concept. In *14th AIAA Aviation Technology, Integration, and Operations Conference*. AIAA, 2014.

[13] M. Mane and W.A. Crossley. Allocation and design of aircraft for on-demand air transportation with uncertain operations. *Journal of Aircraft*, 49(1):141 – 150, January–February 2012.

[14] C. Barnhart, A. Farahat, and M. Lohatepanont. Airline fleet assignement with enhanced revenue modeling. *Operations Research*, 57(1):231–244, 2009.

[15] K.A. Moolchandani, D.B. Agusdinata, M. Mane, W.A. Crossley, and D. DeLaurentis. Impact of development rates of future aircraft technologies on fleet-wide environmental emissions. In *11th AIAA Aviation Technology, Integration, and Operations (ATIO) Conference*, Virginia Beach, VA, September 2011. AIAA.

[16] R. Birrenbach. Regional aircraft family design. In *2000 World Aviation Conference*, SAE technical paper series, San Diego, CA, October 2000. Society of Automotive Engineers and American Institute of Aeronautics and Astronautics, SAE International.

[17] K. Willcox and S. Wakayama. Simultaneous optimization of multiple-aircraft family. *Journal of Aircraft*, 40(4):616–622, July–August 2003.

[18] J.K.D. Morrison, R.J. Hansman, and S. Sgouridis. Game theory analysis of the impact of single-aisle aircraft competition for emissions. *Journal of Aircraft*, 49(2):483–494, Marcg–April 2012.

[19] C. Werner-Westphal, W. Heinze, and P. Horst. Multidisciplinary integrated preliminary design applied to unconventional aircraft configurations. *Journal of Aircraft*, 45(2):581–590, March–April 2008.

[20] S.G. Lehner, L.B. Luratiy, G.C. Bowerz, E.J. Cramer, W.A. Crossley, F. Engelsen, I.M. Kroo, S.C. Smith, and K.E. Willcox. Advanced multidisciplinary optimization techniques for efficient subsonic aircraft design. In *48th AIAA Aerospace Sciences Meeting Including the New Horizons Forum and Aerospace Exposition*, Orlando, Florida, January 2010. AIAA.

[21] I. Kroo and M. Takai. A quasi-procedural method for aircraft design. In *AIAA/AHS/ASEE Aircraft Design, Systems and Operations Meeting*, Atlanta, Georgia, September 1988. AIAA.

[22] R.P. Henderson, J.R.R.A. Martins, and R. Perez. Aircraft conceptual design for optimal environmental performance. *The Aeronautical Journal*, 116(1175):3712–3733, January 2012.

[23] M. Mane and W.A. Crossley. Concurrent aircraft design and trip assignment under uncertainty: Fractional operations. In *9th AIAA Aviation Technology, Integration, and Operations Conference (ATIO)*, Hilton Head, South Carolina, September 2009. AIAA.

[24] M. Mane and W.A. Crossley. Concurrent aircraft design and resource allocation under uncertainty for on–demand air transportation. In *The 26th Congress of International Council of the Aeronautical Sciences (ICAS)*, Anchorage, Alaska, September 2008. AIAA.

[25] N. Davendralingam and W.A. Crossley. Concurrent aircraft design and airline network design incorporating passenger demand models. In *9th AIAA Aviation Technology, Integration, and Operations Conference*, Hilton Head, South Carolina, September 2009. AIAA.

[26] N. Davendralingam, W.A. Crossley, and A. Nusawardhana. An approximate dynamic programming approach to aircraft allocation incorporating passenger demand models. In *10th AIAA Aviation Technology, Integration, and Operations (ATIO) Conference*, Fort Worth, Texas, September 2010. AIAA.

[27] Nusawardhana and W.A. Crossley. Concurrent aircraft design and variable resource allocation in large scale fleet networks. In *9th AIAA Aviation Technology, Integration, and Operations Conference (ATIO)*, Hilton Head, South Carolina, September 2009. AIAA.

[28] P. Govindaraju and W.A. Crossley. Profit motivated airline fleet allocation and concurrent aircraft design for multiple airlines. In *2013 Aviation Technology, Integration, and Operations Conference (ATIO)*, Los Angeles, CA, August 2013. AIAA.

[29] J.H. Choi, P. Govindaraju, N. Davendralingam, and W.A. Crossley. Platform design for fleet-level efficiency under uncertain demand: Application for air mobility command (AMC). In *2013 Aviation Technology, Integration, and Operations Conference*, Los Angeles, CA, August 2013. AIAA.

[30] C. Taylor and O.L. de Weck. Coupled vehicle design and network flow optimization for air transportation systems. *Journal of Aircraft*, 44(5):1478–1486, September–October 2007.

[31] S. Lehner, T. Zill, and Go. Using aircraft requirements as variables: An integrated optimization approach for air transportation system. In *12th AIAA Aviation Technology, Integration, and Operations (ATIO) Conference*, Indianapolis, IN, 17 - 19 September 2012.

[32] G. Marwaha and M. Kokkolaras. System-of-systems approach to air transportation design using nested optimization and direct search. *Structural and Multidisciplinary Optimization*, pages 1–17, 2014.

[33] G.C. Bower and I. Kroo. Multi-objective aircraft optimization for minimum cost and emissions over specific route networks. In *26th Congress of International Council of the Aeronautical Sciences (ICAS)*, Anchorage, Alaska, September 2008. AIAA.

[34] S. Ferguson, K. Lewis, and J. Donndelinger. Vehicle family optimization using integrated engineering and marketing tools. In *11th AIAA/ISSMO Multidisciplinary Analysis and Optimization Conference*, Portsmouth, Virginia, September 2006. AIAA.

[35] O. Asikoglu and T.W. Simpson. A new method for evaluating design dependencies in product architectures. In *12th AIAA Aviation Technology, Integration, and Operations (ATIO) Conference and 14th AIAA/ISSMO Multidisciplinary Analysis and Optimization Conference*, Indianaplois, Indiana, September 2012. AIAA.

[36] J. Allison, B. Roth, M. Kokkolaras, I. Kroo, and P. Y. Papalambros. Aircraft Family Design Using Decomposition-based Methods. In *11th AIAA/ISSMO Multidisciplinary Analysis and Optimization Conference*, Portsmouth, Virginia, September 2006. AIAA.

[37] R. Perez and J.R.R.A. Martins. pyACDT: An object-oriented framework for aircraft design modelling and multidisciplinary optimization. In *12th AIAA/ISSMO Multidisciplinary Analysis and Optimization Conference*, Victoria, BC, September 2008. AIAA.

[38] D.P. Raymer. *Aircraft Design: A Conceptual Approach*. AIAA Education Series. American Institute of Aeronautics and Astronautics, 3rd edition, 1999.

[39] E. Torenbeek. *Synthesis of Subsonic Airplane Design*. Delft University Press and Kluwer Academic Publishers, 6th edition, 1990.

[40] J. Roskam. *Airplane Design, Part VIII: Airplane Cost Estimation: Design, Development, Manufacturing, Operating*. DARcorporation, 2006.

[41] S. Chai, P. Crisafuli, and W.H. Mason. Aircraft center of gravity estimation in conceptual design. In *1st Aircraft Engineering, Technology, and Operations Congress*, Los Angeles, CA, September 1995. AIAA.

[42] F.T. Johnson, E.N. Tinoco, and N.J. Yu. Thirty years of development and application of CFD at Boeing commercial airplanes, Seattle. In *AIAA Computational Fluid Dynamics Conference*, Orlando, FL, June 23–26 2003.

[43] S.F. Hoerner. *Fluid-Dynamic Drag: Practical Information on Aerodynamic Drag and Hydrodynamic Resistance*. Hoerner, S.F., 1965.

[44] O. Gur, W.H. Mason, and J.A. Schetz. Full configuration drag estimation. In *27th AIAA Applied Aerodynamics Conference*, San Antonio, TX, June 2009. AIAA.

[45] Anym. *USAF Stability and Control DATCOM*. Douglas Aircraft Company, November 1965.

[46] T. Cebeci and P. Bradshaw. *Momentum Transfer in Boundary Layers*. McGraw-Hill, 1977.

[47] F.M. White. *Viscous Fluid Flow*. McGraw-Hill, 1974.

[48] E.J. Hopkins and M. Inoye. An evaluation of theories for predicting trubulent skin friction and heat transfer on flat plates at supersonic and hypersonic numbers. *AIAA Journal*, 9(6):993–1003, June 1971.

[49] E.J. Hopkins. Charts for predicting turbulent skin friction from the van Direst method (II). Technical Report TN D-6945, NASA, October 1972.

[50] L.M. Nicolai and G.E. Carichner. *Fundamentals of Aircraft and Airship Design*, volume 1—Aircraft Design. AIAA, 2010.

[51] R.S. Shevell. *Fundamentals of Flight*. Prentice-Hall, Englewoods-Cliffs, 2nd edition, 1989.

[52] O. Samoylovitch and D. Strelets. Determination of the Oswald efficiency factor at the aeroplane design preliminary stage. *Aircraft Design*, 3:167–174, 2000.

[53] M. Bartel and T.M. Young. Simplified thrust and fuel consumption models for modern two–shaft turbofan engines. *Journal of Aircraft*, 45(4):1450–1456, 2008.

[54] J.D. Mattingly, W.H. Heiser, and Pratt D.T. *Aircraft Engine Design*. AIAA Educational Series. AIAA, 2 edition, 2002.

[55] Engineering Sciene Data Unit. Estimation of windmilling drag and airflow of turbo-jet and turbo-fan engines. Technical Report ESDU 81009, ESDU International, London, UK, 1981. Performance, Vol. 4.

[56] M. E. Eshelby. *Aircraft Performance: Theory and Practice*. AIAA Education Series. AIAA, 2000.

[57] S.A. Powers. Critical field length calculations for preliminary design. *Journal of Aircraft*, 18(2):103–107, February 1981.

[58] Engineering Sciene Data Unit. Effect of cabin pressure on climb and descent rates. Technical Report 94040, ESDU International, London, UK, November 1994.

[59] A.J. Keane and P.B. Nair. *Computational Approches for Aerospace Design: The Pursuit of Excellence*. John Wiley & Sons, 2005.

[60] R.W. Hess and H.P. Romanoff. Cost-estimating relationships for aircraft airframes. Technical Report RAND Report R-3255-AF, RAND Corporation, Santa Monica, CA., 1987.

[61] J. Markish. Valuation techniques for commercial aircraft program design. M.Sc. thesis, Massachusetts Institute of Technology, 2002.

[62] R. F. Stossel. A proposed standard method for estimating airplane indirect operating cost. Technical Report LW70-500R, Lockheed-Georgia Company, 1970.

[63] J.R.R.A. Martins and A.B. Lambe. Multidisciplinary design optimization: A survey of architectures. *AIAA Journal*, 51(9):2049–2075, September 2013.

[64] R. Fellini, M. Kokkolaras, and P.Y. Papalambros. Quantitative platform selection in optimal design of product families, with application to automotive engine design. *Journal of Engineering Design*, 17(5):429 – 446, 2006.

[65] H.J. Thevenot and T.W. Simpson. Commonality indices for product family design: A detailed comparison. *Journal of Engineering Design*, 17(2):99 – 119, 2006.

[66] P. Jackson, editor. *Jane's All the World's Aircraft.* Jane's Information Group, 2004.

[67] M. Lohatepanont. *Airline Fleet Assignment and Schedule Design: Integrated Models and Algorithms.* PhD thesis, Massachusetts Institute of Technology, March 2002.

[68] Ki-Hwan Bae Bae. *Integrated Airline Operations: Schedule Design, Fleet Assignment, Aircraft Routing, and Crew Scheduling.* PhD thesis, Virginia Polytechnic Institute and State University, Blacksburg, Virginia, November 2010.

[69] Research and Innovative Technology Administration: Bureau of Transportation Studies. Transtats. `http://www.transtats.bts.gov/`, 2013. [accessed: November 2013].

[70] A. Hagenbring, A.K. Brodowski, and C. Schmidt. Shaping the future together: Annual report 2012. Annual report, Lufthansa Group, 2012.

[71] J. Fuchte, B. Nagel, and V. Gollnick. Twin aisle aircraft for short range operations - an economically attractive alternative? In *12th AIAA Aviation Technology, Integration, and Operations (ATIO) Conference and 14th AIAA/ISSMO Multidisciplinary Analysis and Optimization Conference*, Indianapolis, Indiana, September 2012. AIAA.

[72] Loo Hay Lee, Huei Chuen Huang, Chulung Lee, Ek Peng Chew, W. Jaruphongsa, Yean Yik Yong, Zhe Liang, Chun How Leong, Yen Ping Tan, K. Namburi, E. Johnson, and J. Banks. Discrete event simulation model for airline operations: Simair. In *Simulation Conference, 2003. Proceedings of the 2003 Winter*, volume 2, pages 1656–1662, December 2003.

[73] Airbus. Global market forecast: Future journeys 2013–2032. Blagnac Cedex, France, September 2013.

[74] M. Warner. Boeing current market outlook 2013–2032. Seattle, WA, September 2013.

[75] Bombardier. Commercial aircraft market forecast 2012-2031, 2012.

[76] Embraer. Market outlook 2012-2031, 2012.

[77] M Bazargan. *Airline Operations and Scheduling.* Ashgate Publishing, 2004.

[78] Hane C.A., Barnhart C., Johnson E.L., Marsten R.E., Nemhasuer G.L., and Sigismondi G. The fleet assignment problem: Solving a large-scale integer program. *Mathematical Programming*, 70:211–232, 1995.

[79] I. Tetzloff and W.A. Crossley. Incorporating fleet assignement with aircraft allocation to measure fleet-level metrics. In *2013 Aviation Technology, Integration and Operations Conference*, Los Angeles, CA, August 2013. AIAA.

[80] F.D. Harris. An economic model of U.S. airline operating expenses. Technical Report CR–2005-213476, NASA, College Park, Maryland, December 2005.

[81] P.M. Peeters, J. Middel, and A. Hoolhorst. Fuel efficiency of commercial aircraft: An overview of historical and future trends. Technical Report NLR-CR-2005-669, National Aerospace Laboratory NLR, November 2005.

[82] E. Schwartz and I.M. Kroo. Aircraft design: Trading cost and climate impact. In *47th AIAA Aerospace Sciences Meeting Including The New Horizons Forum and Aerospace Exposition*, Orlando, Florida, January 2009. AIAA.

[83] K. Boopathy and M.P. Rumpfkeil. Robust optimizations of structural and aerodynamic designs. In *15^{th} AIAA/ISSMO Multidisciplinary Analysis and Optimization Conference*, Atlanta, GA, June 2014. AIAA.

[84] G. Taguchi. *System of Experimental Design*. UNIPUB/Kraus International Publications, 1987.

[85] W.L. Oberkampf, J.C. Helton, C.A. Joslyn, S.F. Wojtkiewicz, and S. Ferson. Challenge problems: Uncertainty in system response given uncertain parameters. *Reliability Engineering and System Safety*, 85:11–19, 2004.

[86] D.A. DeLaurentis and D.N. Mavris. Uncertainty modeling and management in multidisciplinary analysis and synthesis. In *38th Aerospace Sciences Meeting & Exhibit*, Reno, NV, January 2000. AIAA.

[87] Federal Aviation Administration. Advisory circular: Airport design. Technical Report AC 150/5300-13A, U.S. Department of Transportation, September 2012.

[88] Ruben E. Perez, Peter W. Jansen, and Joaquim R. R. A. Martins. pyOpt: A Python-based object-oriented framework for nonlinear constrained optimization. *Structures and Multidisciplinary Optimization*, 45(1):101–118, 2011.

[89] P. W. Jansen and R.E. Perez. Coupled optimization of aircraft family design and fleet assignment for minimum cost and fuel burn. In *12th AIAA Aviation Technology, Integration, and Operations (ATIO)*

Conference and 14th AIAA/ISSMO Multidisciplinary Analysis and Optimization Conference, Indianapolis, Indiana, September 2012. AIAA.

[90] P.J. Angeline. *Evolutionary Programming VII, 7th International Conference, EP98*, volume 1447 of *Lecture Notes in Computer Science*, chapter Evolutionary Optimization versus Particle Swarm Optimization: Philosophy and Performance Differences, pages 601–611. Springer Berlin / Heidelberg, San Diego, California, March 1998. ISBN 978-3-540-64891-8.

[91] X. Hu, R.C. Eberhart, and Y. Shi. Engineering optimization with particle swarm. In *IEEE Swarm Intelligence Symposium 2003 (SIS 2003)*, pages 53–57, Indianapolis, IN, 2003.

[92] R. Hassan, B. Cohanim, O.L. de Weck, and G. Venter. A comparison of particle swarm optimization and the genetic algorithm. In *1st AIAA Multidisciplinary Design Optimization Specialist Conference*, Austin, TX, April 18-21 2005.

[93] R.C. Eberhart and J.A. Kennedy. New optimizer using particle swarm theory. In *Sixth International Symposium on Micro Machine and Human Science*, pages 39–43, Nagoya, Japan, 1995.

[94] J. Kennedy and R.C. Eberhart. Particle swarm optimization. In *IEEE International Conference on Neural Networks*, volume IV, pages 1942–1948, Piscataway, NJ, 1995.

[95] Y. Shi and R.C. Eberhart. A modified particle swarm optimizer. In *IEEE International Conference on Evolutionary Computation*, pages 69–73, Piscataway, NJ, 1998. IEEE Press.

[96] R. Perez and K. Behdinan. Particle swarm approach for structural design. *Computers & Structures*, 85:1579–1588, 2007.

[97] G. Venter and J. Sobieszczanski-Sobieski. Particle swarm optimization. *AIAA Journal*, 41(8):1583–1589, 2003.

[98] P.C. Fourie and A.A. Groenwold. The particle swarm optimization algorithm in size and shape optimization. *Structural and Multidisciplinary Optimization*, 23(4):259–267, May 2002.

[99] K.E. Parsopoulos and M.N. Vrahatis. Particle swarm optimization method for constrained optimization problems. In *Euro–International Symposium on Computational Intelligence 2002*, pages 214–220. Press, 2002.

[100] K. Sedlaczek and P. Eberhard. Using augmented Lagrangian particle swarm optimization for constrained problems in engineering. *Journal of Structural and Multidisciplinary Optimization*, 32(4):277–286, October 2006.

[101] A.I.F. Vaz and E.M.G.P. Fernandes. Optimization of nonlinear constrained particle swarm. *Technological and Economic Development Of Economy*, 1:30–36, 2006.

[102] G. Venter and R.T. Haftka. Constrained particle swarm optimization using a bi-objective formulation. *Structural and Multidisciplinary Optimization*, 40:65–76, 2010.

[103] Z.D. Richards. Constrained particle swarm optimisation for sequential quadratic programming. *International Journal of Modelling, Identification and Control*, 8(4):361–367, 2009.

[104] P.W. Jansen and R.E. Perez. Constrained structural design optimization via a parallel augmented Lagrangian particle swarm optimization approach. *Computers & Structures*, 89(13–14):1352 – 1366, 2011.

[105] G.N. Vanderplaats. An efficient feasible directions algorithm for design synthesis. *AIAA Journal*, 22(11):633–640, November 1984.

[106] G. Venter and J. Sobieszczanski-Sobieski. A parallel particle swarm optimization algorithm accelerated by asynchronous evaluations. In *Sixth World Congresses of Structural and Multidisciplinary Optimization*, Rio de Janeiro, Brazil, June 2005. AIAA.

[107] B. Koh, A.D. George, R.T. Haftka, and B.J. Fregly. Parallel asynchronous particle swarm optimization. *International Journal for Numerical Methods in Engineering*, 67(4):578–595, 2006.

Appendices

A Route Characteristics

The discrete time simulation requires monthly average passenger demand values to estimate the daily passenger demand for each route, while the fleet allocation problem requires monthly minimum flight frequencies to evaluate the constraints. The characteristics of the selected routes in both the North American and European markets are detailed below.

A.1 North American Routes

The North American routes are based on routes flown by single-aisle aircraft by Delta Airlines and ExpressJet Airlines operating from Atlanta (ATL) as the hub. Table A.1 and Table A.2 list the distances and the mean number of passengers for each month to be transported along each route. The minimum flight frequency for each route and month is given in Table A.3 and Table A.4, respectively. The designations are represented by their respective IATA airport code and the city name. The average number of passengers for each route and each month was estimated based on the total number of passengers transported and the number of departures performed as obtained from the Research and Innovative Technology Administration (RITA) aviation database [69] for the year 2012. The minimum frequency for each month and route is two thirds of the currently performed daily departures, as estimated from the monthly departures averaged over each day.

Table A.1: Selected Delta Airline routes and average monthly number of passengers from Atlanta

Destination	Distance	Mean No. of Passengers per day											
	[nmi]	Jan.	Feb.	Mar.	Apl.	May	Jun.	Jul.	Aug.	Sep.	Oct.	Nov.	Dec.
CCS (Caracas)	1685	142	84	99	112	121	136	130	132	178	133	138	154
UIO (Quito)	2057	85	87	95	88	102	154	165	153	102	84	94	134
SEA (Seattle)	1894	762	812	886	945	976	1206	1331	1285	1244	924	903	822
PDX (Portland)	1886	356	379	409	380	455	553	575	509	455	445	450	442
SFO (San Francisco)	1856	988	1018	1052	1161	1272	1387	1480	1421	1310	1245	1076	1030
LAX (Los Angeles)	1689	1763	1711	1816	1949	1874	2093	2148	2056	1798	1756	1570	1554
SLC (Salt Lake City)	1380	1296	1457	1535	1290	1383	1228	1256	1257	1176	1325	1249	1358
PHX (Phoenix)	1377	846	909	1023	948	1036	1049	1056	950	927	988	997	947
TUS (Tucson)	1337	231	248	256	302	323	295	286	272	287	302	322	248
GDL (Guadalajara)	1277	146	120	148	161	196	260	280	192	106	133	133	143
ABQ (Albuquerque)	1101	238	259	303	361	470	473	465	446	404	415	381	333
DEN (Denver)	1041	1048	1236	258	1137	1184	255	1377	1314	1222	1216	1116	1177
GCM (Georgetown)	877	100	113	142	107	118	140	151	94	115	131	113	123
MHT (Manchester NH)	827	105	96	111	225	221	218	216	227	214	214	190	105
BOS (Boston)	822	1211	1199	1496	1652	1734	1722	1699	1615	1549	1499	1501	1225
MSP (Minneapolis)	789	1553	1653	1837	1836	1764	1720	1735	1718	1570	1581	1587	1500
CUN (Cancun)	768	458	643	732	642	692	773	826	661	457	416	430	592
DFW (Dallas-Fort Worth)	634	1089	1146	1306	1362	1488	1601	1585	1535	1418	1462	1517	1317
BUF (Buffalo)	620	412	436	562	575	637	614	642	640	593	572	516	462
MIA (Miami)	518	1229	1447	1516	1444	1440	1259	1264	1215	1219	1361	1443	1484
DTW (Detroit)	517	839	940	1006	957	1220	1237	1187	1267	1237	1240	1149	1203
MSY (New Orleans)	369	756	896	1016	1413	1403	1365	1255	1147	1201	1433	1310	1181
CMH (Columbus)	389	542	640	688	733	757	809	725	679	781	819	802	623
SAV (Savannah)	186	471	500	422	672	871	768	724	668	683	712	681	621

Table A.2: Selected ExpressJet Airlines routes and average monthly number of passengers from Atlanta

Destination	Distance	Mean No. of Passengers per day											
	[nmi]	Jan.	Feb.	Mar.	Apl.	May	Jun.	Jul.	Aug.	Sep.	Oct.	Nov.	Dec.
MGM (Montgomery)	127	205	213	245	263	281	317	331	337	332	349	331	285
CHA (Chattanooga)	92	305	355	325	366	386	362	340	368	361	365	338	352
GSP (Greenville)	133	202	228	218	191	186	192	206	174	117	153	176	201
ABY (Albany)	126	77	85	90	80	95	91	92	88	90	94	94	88
DHN (Dothan)	148	96	101	121	135	134	133	126	122	129	129	130	112
BHM (Birmingham)	116	294	307	383	111	153	122	124	84	92	86	54	136
CAE (Colombia)	166	368	419	415	350	344	346	318	333	283	277	274	209
VPS (Valparaiso)	217	311	375	449	497	508	534	545	438	303	306	311	330
TLH (Tallahassee)	194	260	300	345	258	334	299	347	259	229	288	300	327
MEM (Memphis)	288	75	75	92	141	152	99	61	65	55	67	32	10
LEX (Lexington KY)	264	223	265	359	344	370	264	264	266	250	254	244	221
LWB (Lewisburg)	320	21	24	24	28	34	40	39	40	37	36	29	26
BTR (Baton Rouge)	389	283	300	359	339	349	350	354	351	321	355	343	320
SDF (Louisville)	280	208	273	337	67	91	102	108	78	44	38	58	50
MEI (Meridian)	231	37	41	50	39	52	44	43	43	43	42	46	42
SHV (Shreveport)	478	125	130	158	165	184	192	193	190	166	176	184	178
BMI (Bloomington)	463	157	178	199	161	212	218	204	206	194	165	197	157
SGF (Springfield)	489	90	97	110	121	123	162	168	148	158	166	171	130
ABE (Allentown)	602	78	87	88	47	45	104	122	119	116	111	85	80
MSN (Madison)	615	46	47	41	45	46	54	78	88	110	127	120	75
XNA (Bentonville)	511	138	130	142	195	217	221	213	221	220	198	220	174
OMA (Omaha)	714	169	188	134	157	197	229	230	218	107	113	161	114
SWF (Newburgh)	681	57	53	111	98	103	97	100	102	106	98	97	97
GRK (Killeen)	697	91	88	102	100	105	100	101	100	82	88	95	87

Table A.3: Delta Airline routes minimum flight frequencies

Destination	Distance	Minimum Flight Frequency per day											
	[nmi]	Jan.	Feb.	Mar.	Apl.	May	Jun.	Jul.	Aug.	Sep.	Oct.	Nov.	Dec.
CCS (Caracas)	1685	1	1	1	1	1	1	1	1	1	1	1	1
UIO (Quito)	2057	1	1	1	1	1	1	1	1	1	1	1	1
SEA (Seattle)	1894	4	4	4	4	4	5	5	5	5	4	4	4
PDX (Portland)	1886	2	2	2	2	2	3	3	3	2	2	2	2
SFO (San Francisco)	1856	4	4	4	4	5	5	5	5	5	5	4	4
LAX (Los Angeles)	1689	7	7	7	7	7	7	7	7	7	6	6	5
SLC (Salt Lake City)	1380	6	6	6	6	6	5	5	5	5	6	5	5
PHX (Phoenix)	1377	4	4	4	4	4	4	4	4	4	4	4	4
TUS (Tucson)	1337	2	2	2	2	2	2	2	2	2	2	2	2
GDL (Guadalajara)	1277	2	2	2	2	2	2	2	1	1	1	1	1
ABQ (Albuquerque)	1101	2	2	2	2	2	3	2	2	2	3	2	2
DEN (Denver)	1041	6	6	2	6	6	2	6	6	6	6	6	5
GCM (Georgetown)	877	1	1	1	1	1	1	1	1	1	1	1	1
MHT (Manchester NH)	827	1	1	1	2	2	2	2	2	2	2	2	1
BOS (Boston)	822	7	7	8	8	8	8	8	8	8	7	7	7
MSP (Minneapolis)	789	7	8	9	8	9	9	9	8	8	8	8	8
CUN (Cancun)	768	3	4	5	4	3	4	4	3	3	2	2	3
DFW (Dallas-Fort Worth)	634	6	7	7	8	8	8	8	8	8	8	8	8
BUF (Buffalo)	620	3	4	4	4	4	4	4	4	4	4	4	3
MIA (Miami)	518	7	8	8	8	8	7	7	7	7	7	7	7
DTW (Detroit)	517	5	5	5	5	6	6	6	6	6	6	6	6
MSY (New Orleans)	369	6	6	6	8	8	7	7	7	7	7	7	7
CMH (Columbus)	389	4	4	4	4	4	5	4	4	5	5	5	4
SAV (Savannah)	186	4	4	3	5	6	5	5	5	5	5	5	5

Table A.4: ExpressJet Airlines routes minimum flight frequencies

Destination	Distance	Minimum Flight Frequency per day											
	[nmi]	Jan.	Feb.	Mar.	Apl.	May	Jun.	Jul.	Aug.	Sep.	Oct.	Nov.	Dec.
MGM (Montgomery)	127	5	5	5	5	5	6	6	6	6	6	6	6
CHA (Chattanooga)	92	6	7	6	7	6	6	6	6	6	6	6	6
GSP (Greenville)	133	4	4	4	3	3	3	4	3	2	3	3	4
ABY (Albany)	126	2	2	2	2	2	2	2	2	2	2	2	2
DHN (Dothan)	148	3	3	3	3	3	3	3	3	3	3	3	3
BHM (Birmingham)	116	5	6	7	2	2	2	2	2	2	2	1	2
CAE (Colombia)	166	7	7	7	6	5	5	5	6	5	5	5	4
VPS (Valparaiso)	217	6	7	7	7	7	7	8	6	5	5	5	6
TLH (Tallahassee)	194	6	6	6	5	5	5	6	4	4	5	5	5
MEM (Memphis)	288	1	2	2	2	2	2	1	2	1	1	1	1
LEX (Lexington KY)	264	4	5	6	6	6	5	5	5	4	4	4	4
LWB (Lewisburg)	320	1	1	1	1	1	1	1	1	1	1	1	1
BTR (Baton Rouge)	389	5	5	6	5	6	6	5	6	5	5	5	5
SDF (Louisville)	280	4	4	6	1	2	2	2	2	1	1	1	1
MEI (Meridian)	231	2	2	2	2	2	2	2	2	2	2	2	2
SHV (Shreveport)	478	3	3	4	3	4	4	4	4	3	3	3	3
BMI (Bloomington)	463	3	3	3	2	3	3	3	3	3	2	3	3
SGF (Springfield)	489	2	2	2	2	2	3	3	3	3	3	3	3
ABE (Allentown)	602	2	2	2	1	1	2	2	2	2	2	2	2
MSN (Madison)	615	1	1	1	1	1	1	2	2	2	2	2	2
XNA (Bentonville)	511	3	3	3	4	4	4	4	4	4	4	4	3
OMA (Omaha)	714	3	3	2	2	3	3	3	3	2	2	2	2
SWF (Newburgh)	681	1	1	2	2	2	2	2	2	2	2	2	2
GRK (Killeen)	697	2	2	2	2	2	2	2	2	2	2	2	2

A.2 European Routes

The European network is based on 48 distinct non-stop routes serviced by Lufthansa and CityLine from the hubs of Frankfurt (FRA) and Munich (MUC). The average demand and monthly variations are estimated based on the type of aircraft operated on each route and general data given by the the Federal Statistical Office of Germany and the annual report published by the Lufthansa Group [70]. As for the North American routes the minimum flight frequency was estimated as two thirds of the currently performed flights. Table A.5 and Table A.6 list the distances and the mean number of passengers for each month to be transported along each route, while Table A.7 and Table A.8 list the route minimum flight frequency for each month. The origin airport and designations are represented by their respective IATA airport code.

Table A.5: Selected Lufthansa routes and average monthly number of passengers from Munich (MUC) and Frankfurt(FRA)

Origin	Destination	Distance	Mean No. of Passengers per day											
		[nmi]	Jan.	Feb.	Mar.	Apl.	May	Jun.	Jul.	Aug.	Sep.	Oct.	Nov.	Dec.
FRA	DUS	101	295	264	336	349	378	387	406	386	379	356	317	298
FRA	ZRH	153	426	386	500	505	559	561	600	576	556	532	458	437
MUC	FRA	162	1459	1460	1672	1741	1839	1745	1866	1803	1776	1771	1498	1386
FRA	AMS	197	342	299	391	409	439	440	473	448	442	425	367	342
FRA	HAM	223	1269	1113	1456	1491	1620	1652	1733	1640	1620	1560	1349	1261
FRA	TXL	234	1466	1293	1639	1726	1846	1878	2010	1898	1886	1769	1546	1441
MUC	CGN	235	606	611	685	734	769	724	780	763	740	746	627	586
FRA	CDG	241	691	623	785	813	881	894	956	918	905	839	751	694
MUC	TXL	259	1297	1286	1458	1549	1630	1547	1654	1604	1571	1597	1309	1236
MUC	DUS	262	1171	1166	1353	1377	1484	1394	1506	1458	1411	1418	1214	1138
MUC	HAM	324	1290	1307	1487	1539	1646	1566	1671	1646	1564	1606	1349	1231
FRA	VIE	336	642	568	719	762	810	808	883	847	821	792	675	636
FRA	LHR	353	1186	1046	1334	1420	1532	1518	1637	1551	1526	1461	1256	1199
MUC	CDG	368	473	483	543	584	604	568	613	603	577	590	484	458
MUC	NAP	461	407	410	463	481	517	497	524	506	495	509	423	402
MUC	LHR	509	720	728	835	880	927	874	941	901	884	913	752	718
FRA	DUB	586	386	341	439	443	487	495	525	497	498	462	398	378
FRA	BCN	590	809	712	912	931	1032	1038	1112	1059	1045	1000	841	800
MUC	ARN	712	417	427	479	502	530	504	538	526	507	528	448	409
MUC	MAD	808	496	497	574	600	637	601	646	637	602	624	524	483
MUC	LED	941	179	175	208	215	227	215	230	224	219	222	186	171
FRA	IST	1007	371	326	422	442	477	482	512	481	487	447	398	369
MUC	TBS	1452	81	81	93	96	102	97	103	100	97	100	83	78
FRA	TLV	1596	239	216	272	285	312	312	330	311	313	293	254	237

Table A.6: Selected Cityline routes and average monthly number of passengers from Munich (MUC) and Frankfurt(FRA)

Origin	Destination	Distance	Mean No. of Passengers per day											
		[nmi]	Jan.	Feb.	Mar.	Apl.	May	Jun.	Jul.	Aug.	Sep.	Oct.	Nov.	Dec.
MUC	NUE	74	74	73	83	89	93	88	94	93	90	92	76	72
FRA	STR	84	104	92	116	121	133	135	142	135	133	127	108	103
FRA	FMO	130	116	102	133	136	146	150	158	151	148	138	122	116
MUC	PRG	143	284	276	326	342	361	343	366	361	344	350	295	269
FRA	FDH	146	91	80	101	107	117	116	124	119	117	110	98	89
FRA	BSL	151	160	142	183	189	205	204	221	210	208	195	174	161
FRA	BRU	163	224	196	250	265	283	285	303	289	289	278	237	219
MUC	DRS	183	239	247	277	286	307	292	311	301	298	298	247	234
MUC	VIE	192	328	328	379	400	419	395	425	412	400	403	349	320
MUC	LUX	232	77	78	89	94	100	93	101	97	95	100	82	76
FRA	LNZ	246	170	153	195	199	220	226	237	224	223	212	182	173
MUC	TRN	254	86	89	99	107	112	104	113	112	106	109	92	86
MUC	FMO	276	272	274	318	331	349	330	354	344	336	348	283	265
FRA	TRN	292	167	154	194	200	219	220	235	226	220	209	180	173
MUC	BRE	304	230	229	266	279	289	275	293	284	274	283	236	223
MUC	BRU	322	435	436	501	520	551	517	559	551	518	538	446	422
FRA	LCY	334	233	208	263	277	299	298	319	302	298	280	247	232
MUC	NCE	340	208	204	241	252	263	250	267	263	249	257	216	204
FRA	BLL	344	185	165	210	217	240	238	254	242	236	228	199	181
FRA	FLR	389	376	341	423	446	482	494	521	491	488	457	403	376
MUC	MRS	403	233	231	271	283	297	279	301	297	284	286	242	228
FRA	TLS	484	34	32	40	41	45	45	48	46	46	43	37	36
MUC	OSL	712	71	72	81	86	91	86	92	90	85	89	75	69
FRA	MSQ	755	129	119	149	154	169	167	179	171	171	161	139	131

Table A.7: Lufthansa routes minimum flight frequencies

Origin	Destination	Distance	Minimum Flight Frequency per da											
		[nmi]	Jan.	Feb.	Mar.	Apl.	May	Jun.	Jul.	Aug.	Sep.	Oct.	Nov.	Dec.
FRA	DUS	101	3	3	4	4	4	4	4	4	4	4	3	3
FRA	ZRH	153	4	3	4	4	4	4	4	4	4	4	4	4
MUC	FRA	162	8	8	9	10	10	10	10	10	10	10	8	8
FRA	AMS	197	3	3	4	4	4	4	4	4	4	4	3	3
FRA	HAM	223	8	7	9	9	10	10	11	10	10	10	8	8
FRA	TXL	234	8	7	9	9	10	10	10	10	10	10	8	8
MUC	CGN	235	5	5	6	6	6	6	6	6	6	6	5	5
FRA	CDG	241	6	5	6	6	7	7	8	7	7	6	6	6
MUC	TXL	259	8	8	8	9	9	9	10	9	9	9	8	7
MUC	DUS	262	7	7	8	8	8	8	9	8	8	8	7	7
MUC	HAM	324	8	8	9	9	10	10	10	10	10	10	8	8
FRA	VIE	336	4	4	4	5	5	5	6	5	5	5	4	4
FRA	LHR	353	6	6	7	8	8	8	9	8	8	8	7	6
MUC	CDG	368	3	3	4	4	4	4	4	4	4	4	3	3
MUC	NAP	461	2	2	2	2	2	2	3	2	2	2	2	2
MUC	LHR	509	5	5	6	6	6	6	6	6	6	6	5	5
FRA	DUB	586	2	2	2	2	2	2	2	2	2	2	2	2
FRA	BCN	590	4	4	4	4	5	5	6	5	5	5	4	4
MUC	ARN	712	3	3	3	3	3	3	4	3	3	3	3	3
MUC	MAD	808	3	3	3	3	3	3	4	3	3	3	3	2
MUC	LED	941	2	2	2	2	2	2	2	2	2	2	2	2
FRA	IST	1007	2	2	2	2	2	2	3	2	2	2	2	2
MUC	TBS	1452	1	1	1	1	1	1	1	1	1	1	1	1
FRA	TLV	1596	2	2	2	2	2	2	2	2	2	2	2	2

Table A.8: Cityline routes minimum flight frequencies

Origin	Destination	Distance	Minimum Flight Frequency per day											
		[nmi]	Jan.	Feb.	Mar.	Apl.	May	Jun.	Jul.	Aug.	Sep.	Oct.	Nov.	Dec.
MUC	NUE	74	2	2	2	2	2	2	2	2	2	2	2	2
FRA	STR	84	2	2	2	2	2	2	3	2	2	2	2	2
FRA	FMO	130	2	2	3	3	3	3	4	3	3	3	3	2
MUC	PRG	143	3	3	3	3	3	3	4	3	3	3	3	2
FRA	FDH	146	2	2	2	2	2	2	3	2	2	2	2	2
FRA	BSL	151	3	3	4	4	4	4	4	4	4	4	3	3
FRA	BRU	163	4	3	4	4	4	4	5	4	4	4	4	4
MUC	DRS	183	3	3	4	4	4	4	4	4	4	4	3	3
MUC	VIE	192	3	3	4	4	4	4	4	4	4	4	4	3
MUC	LUX	232	2	2	2	2	2	2	2	2	2	2	2	2
FRA	LNZ	246	2	2	3	3	3	3	4	3	3	3	3	2
MUC	TRN	254	2	2	2	2	2	2	2	2	2	2	2	2
MUC	FMO	276	3	3	3	3	3	3	4	3	3	3	3	3
FRA	TRN	292	2	2	3	3	3	3	4	3	3	3	3	2
MUC	BRE	304	3	3	3	3	3	3	4	3	3	3	3	3
MUC	BRU	322	4	4	5	5	5	5	6	5	5	5	4	4
FRA	LCY	334	2	2	3	3	3	3	4	3	3	3	3	2
MUC	NCE	340	3	3	3	3	3	3	4	3	3	3	3	3
FRA	BLL	344	2	2	3	3	3	3	4	3	3	3	3	2
FRA	FLR	389	4	3	4	4	4	4	5	4	4	4	4	4
MUC	MRS	403	3	3	4	4	4	4	4	4	4	4	4	3
FRA	TLS	484	1	1	1	1	1	1	1	1	1	1	1	1
MUC	OSL	712	1	1	1	1	1	1	1	1	1	1	1	1
FRA	MSQ	755	2	2	2	2	2	2	2	2	2	2	2	2

B Feasible Direction Inspired Particle Swarm Optimizer

In this research, a recent type of probabilistic global search algorithm, a particle swarm optimizer (PSO) was used to perform the aircraft design optimizations. A number of advantages with respect to other algorithms make the PSO an ideal candidate to be used in certain optimization tasks. The algorithm is robust and well–suited to handle non–linear, non–convex design spaces with discontinuities. It can handle continuous, discrete and integer variable types. Compared to other global design optimization methods, PSO is more efficient, requiring fewer numbers of function evaluations, while leading to better or equal quality of results for different optimization tasks [90, 91, 92]. The basic PSO algorithm including a modification for single objective constraint optimization is described below. The asynchronous parallelisation of the algorithm is also described.

B.1 The Particle Swarm Optimizer

The particle swarm process is based on the simplified social behaviour where a population of individuals, for example a flock of birds or a swarm of insects such as bees, adapts to its environment and was first described by Eberhart and Kennedy [93]. This adaptation process is stochastic in nature and depends on the local memory of each individual and the global memory of the population. The algorithm is generally related to evolutionary computation, hence it has ties to both genetic algorithms and evolutionary programming [94]. In the implementation of the simplified social model, the population is referred to as the swarm, which consists of individual particles. Each particle has a position within the design space and a velocity. The position is the location of the particle in the design space, as determined by the values of the design variables. The velocity is the rate of change of the position of the particle.

Over time the position and velocity of each particle gets repeatedly updated to simulate the adaptation to the given environment. To update the current position of each particle in the swarm, the algorithm makes use of the current velocity vector of that particle and a time interval. The update of the velocity vector, in turn, is based on the previous values, or "memory", recorded by the particle in its search path, conceptually resembling an autobiographical memory, and the knowledge of the best position found by the swarm as a whole [93, 94]. In the numerical implementation, the position $\mathbf{x}$ of a particle i at iteration $k+1$ is updated by:

$$\mathbf{x}_{k+1}^{i} = \mathbf{x}_{k}^{i} + \mathbf{v}_{k+1}^{i}\Delta t \tag{B.1}$$

where $\mathbf{v}_{k+1}^{i}$ is the corresponding updated velocity vector, and Δt is the time step value. Throughout the present work, a unit time step is used. Several different formulations for updating the velocity vector of each particle exist, depending on the specific PSO algorithm in question. The standard formulation used in the literature was introduced by Shi and Eberhart [95]. In this formulation, the velocity vector of each particle is calculated and shown in Equation (B.2) by:

$$\mathbf{v}_{k+1}^{i} = w\mathbf{v}_{k}^{i} + c_1 r_1 \frac{\left(\mathbf{p}_{k}^{i} - \mathbf{x}_{k}^{i}\right)}{\Delta t} + c_2 r_2 \frac{\left(\mathbf{p}_{k}^{g} - \mathbf{x}_{k}^{i}\right)}{\Delta t} \tag{B.2}$$

where $\mathbf{v}_{k}^{i}$ is the velocity vector at iteration k, r_1 and r_2 represent random numbers between 0 and 1; $\mathbf{p}_{k}^{i}$ represents the best particle position particle i has achieved so far, and $\mathbf{p}_{k}^{g}$ corresponds to the global best position found in the swarm up to iteration k so far. The remaining three terms are problem–dependent parameters, with w representing the inertia weight and c_1 and c_2 representing "trust" parameters, which can affect the convergence behaviour of the PSO algorithm [96]. The inertial weight scales the current velocity of each particle, with large values resulting in a more global search pattern, while small inertia values concentrate the velocity updates and each particle's movement to nearby regions of the design space. The inertial weight is usually reduced over time to allow the swarm to converge. Figure B.1 shows the velocity and position update of a single particle graphically.

The updated position is affected by the social communication of the global best position found so far and also by the individual memory of each particle redirecting the particle from the current path. Thus, each particle is influenced by the behaviour of the swarm and its adaptation to its environment, which allows the return to promising regions of the space previously discovered and searching for better positions over time.

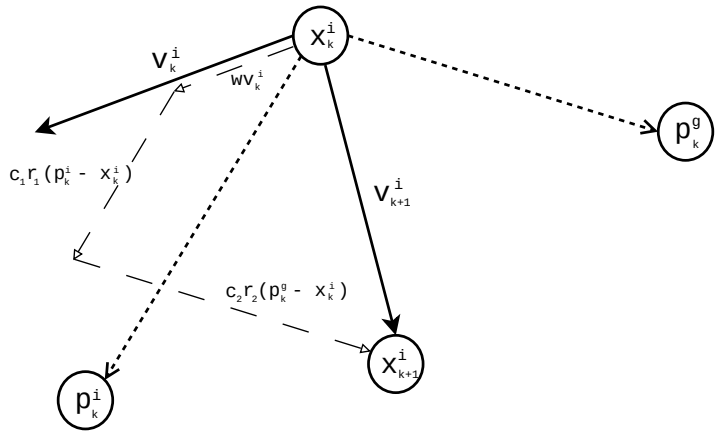

Figure B.1: PSO particle position and velocity update

Based on the particle and velocity updates as explained above, the steps of the algorithm can be outlined as follows:

1. Create an initial set of particle positions $\mathbf{x}_o^i$ and velocities $\mathbf{v}_o^i$ randomly distributed throughout the design space bounded by specified limits on each design variable and maximum velocities.
2. Evaluate the objective function values $f\left(\mathbf{x}_k^i\right)$ of each particle based on its position $\mathbf{x}_k^i$ in the design space.
3. Update the optimum particle position $\mathbf{p}_k^i$ at current iteration (k), if applicable, and global optimum particle position $\mathbf{p}_k^g$.
4. Update the position of each particle using its previous position and updated velocity vector as specified in Equations (B.1) and (B.2).
5. Repeat steps 2-4 until the specified convergence criteria is met.

B.2 Constraint Handling

The basic PSO algorithm is formulated as an unconstrained single objective optimizer. Different methods have been proposed to handle constraint optimization problems with the PSO algorithm [97, 98, 99, 100, 101, 102, 103]. One of the most common approaches is to transform the constraint optimization problem into an unconstrained problem by adding a penalty function to the objective function for violated constraints[98]. This approach requires the careful tuning of the penalty function, since a too low penalty can result in infeasible solutions while a too high penalty can overemphasize the satisfaction of constraints to the optimality of the solution. The fixed penalty

can be replaced by an adaptive penalty method [99], but constraint feasibility is still not directly enforced by these methods. Another approach is to reformulate the problem into a sequence of unconstrained problems using a dynamic augmented Lagrangian Multiplier [104]. This method enforces the Karush–Kuhn–Tucker conditions of optimality, which ensures both feasibility and optimality at convergence. The structure of the augmented Lagrangian multiplier algorithms generally results in a higher number of function evaluations and only allows for an acceleration through synchronous parallelization. One general drawback of these methods is that the feasibility of constraints is not addressed directly but by modifying the objective function. The feasibility of the solution can only be "guaranteed" at absolute convergence of the algorithms, while the feasibility of the solution during the optimization process can vary significantly. The design of aircraft is driven by constraints and the feasibility of the solution is paramount.

Hence, a different approach, inspired by the method of feasible direction [105], was recently implemented in the `pyOpt` framework (`pyFDPSO`). Feasibility of constraints is handled directly through a change in the particle velocity vector inspired by the method of feasible directions and the selection of best solutions based on constraint dominance similar to multi-objective optimization. The algorithm addresses the feasibility of the solution first and when achieved maintains it throughout the optimization process. In the current algorithm, the velocity update of each particle includes an additional term added to the inertia weight:

$$\mathbf{v}_{k+1}^{i} = \left(w - f_{dg} dg_k^i\right) \mathbf{v}_k^i + c_1 r_1 \left(\mathbf{p}_k^i - \boldsymbol{x}_k^i\right) + c_2 r_2 \left(\mathbf{p}_k^g - \mathbf{x}_k^i\right) \tag{B.3}$$

where dg_k^i is a measure on whether the change of the particle's previous position, $\mathbf{x}_{k-1}$, to the current position $\mathbf{x}_k$ by velocity $\mathbf{v}_k$ resulted in the particle to enter the infeasible design space or approach the feasible design space, f_{dg} is a user defined weighting parameter. The value of dg_k^i is calculated by:

$$dg_k^i = \left[\sum_{le} \frac{\left|h_k^{i,le}\right| - \left|h_{k-1}^{i,le}\right|}{\left|h_k^{i,le}\right| + \left|h_{k-1}^{i,le}\right|} + \sum_{li} \frac{g_k^{i,le} - \max\left(g_{k-1}^{i,le}, 0\right)}{g_k^{i,le} + \left|g_{k-1}^{i,le}\right|} \right] \frac{1}{n_{ifc}} \tag{B.4}$$

where $h_k^{i,le}$ is the value of the le^{th} equality constraint violation of particle i for iteration k and $k-1$, respectively, and $g_k^{i,li}$ is the value of the li^{th} inequality constraint. The sums are normalized by the number of infeasible constraints, n_{ifc}. Additionally, each constraint is only added in the sums above if they

are infeasible at the current position of the particle. Given the definition in Equation (B.4) the additional term in the velocity update will either accelerate a particle in the previous direction if the sum of all constraint violations was reduced, decelerate or even reverse the direction of the particle if the the sum of constraint violations increased from step $k-1$ to k. The change in the velocity update alone is not sufficient to steer the swarm towards a feasible optimum.

The update of the particle best and global best reference solution is important to ensure that the swarm does not converge to an infeasible optimum, which, in case of minimization, may have a significantly lower objective function value. Therefore, the best solution found by each particle so far is updated by the following rule: The update of the particle best and global best reference solution is important to ensure that the swarm does not converge to an infeasible optimum, which, in the case of minimization, may have a significantly lower objective function value. Therefore, the best solution found by each particle so far is updated by the following rule:

1. If both solutions are infeasible, but the constraint violation of solution $\mathbf{x}_k^i$ is lower:
   $\tau_k^i < \tau_k^{pbest,i}$ and $\tau_k^{pbest,i} > 0 \rightarrow \mathbf{p}_k^i = \mathbf{x}_k^i$
2. If a new solution is almost feasible or both solutions are feasible:
   $\tau_k^i \leq \text{tol } f_p k_{max}/k$

   If $f_k^i < f_k^{pbest,i} \rightarrow \mathbf{p}_k^i = \mathbf{x}_k^i$

where f_k^i is the objective function value, k_{max} is the maximum number of iterations, f_p is a user–defined parameter governing the relaxation of the constraint bounds and τ_k is the sum of all constraint violations at iteration k, calculated by:

$$\tau_k^i = \sum_{le} \max\left(\left|h_k^{i,le}\right|, tol_e\right) + \sum_{li} \max\left(g_k^{i,li}, tol_i\right) \tag{B.5}$$

where tol_e and tol_i are the user–defined tolerances for equality and inequality constraints, respectively. In the first step, if the best solution found so far is infeasible the current solution will replace the best solution if the sum of constraint violations is lower. In the second step, if the best solution is feasible and the current solution falls within a relaxed constraint boundary, the current solution will replace the best solution if the objective function value is lower. As the algorithm progresses, the relaxation on the constraint boundary

becomes smaller, moving the selection of the best solution towards the feasible design space. Relaxing the constraint bound in earlier iterations allows the swarm to search the design space close to the constraint bounds. The update of the global best solution follows the same procedure as for the particle best solution with the exception that the constraint bounds are not relaxed. Relaxing the constraint bounds for the particle solutions but not the global best solution allows individual particles to explore the design space close to active constraints, while the global best solution remains fully feasible.

B.3 Algorithm Parallelization

One drawback of the PSO algorithm is the high computational cost as measured by elapsed time, but it is ideally suited for a coarse–grained parallel implementation on a parallel or distributed computing network [106]. Each particle is independent of any other particle at each iteration and can therefore be analyzed independently in parallel. This allows for a task parallel implementation, where multiple code segments are run concurrently on different processors. Different parallel implementations have been developed for the PSO algorithm [104]. These implementations can be grouped into two main categories, synchronous and asynchronous approaches. The synchronous approach follows the algorithm described above, with the exception that the particle evaluations at each iteration are distributed over available processes. The current implementation employs a master–slave algorithm allowing for a dynamic distribution of the particles and can be seen in Figure B.2. In this master–slave algorithm, the master assumes the task of communicating the particle location to each free process. The slave process evaluates the particle and sends the objective and constraints values back to the master. The master sends particles to each free process until all particles in the swarm are evaluated for the given iteration. The master then proceeds to update the particle and global best location for the given iteration and to update the iteration based values, such as the inertial weight, and check for convergence. The iteration counter is increased by one and the next round of particles is send to the slave process if the solution is not yet converged.

The asynchronous implementations removes the distinct synchronization point of the iteration when each particle in the swarm is evaluated. Instead, the particle's new search direction, new sets of design variables and the global best location are updated continuously as the particles are evaluated following a master–slave allocation, as can be seen in Figure B.3. Hence, the algorithm

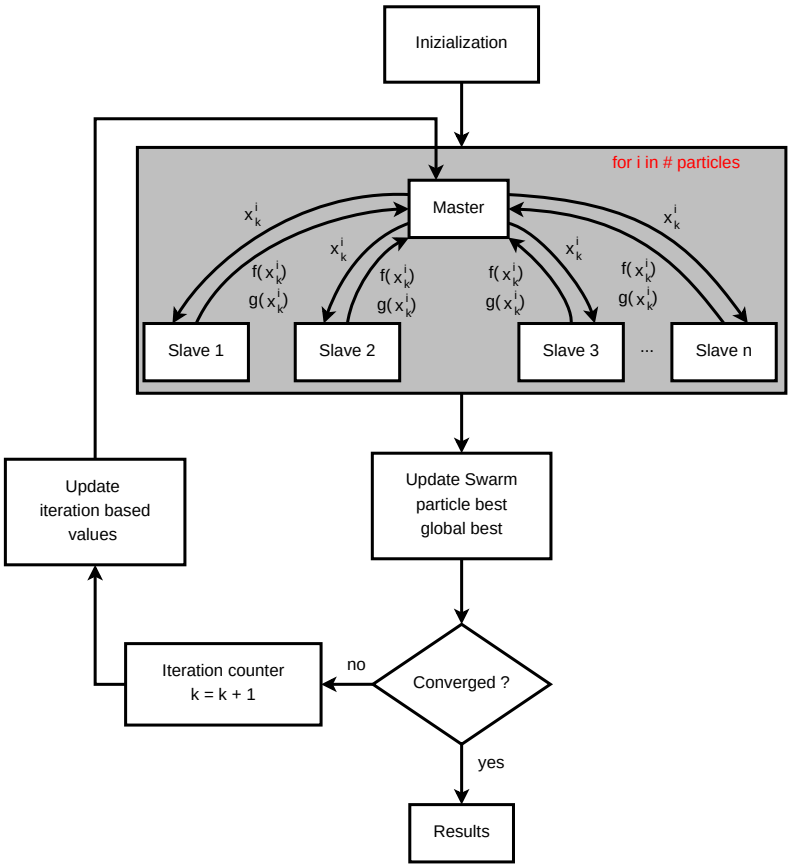

Figure B.2: Dynamic process management PSO parallelization

can proceed without waiting for the completion of all function evaluations for a current iteration. This in turn can significantly reduce the problem of load imbalance from which the synchronous implementations suffer and increase the parallel efficiency and provide better speed-up for problems where the analysis time depends on the design point being analyzed [107]. For example, during the design optimization of an aircraft a set of design variables is possible where the thrust of the engines is too low to let the aircraft takeoff or climb and such a set of design variables would throw an exception during the objective function evaluation. This usually occurs at the beginning of the sizing process and the objective function returns its values significantly faster to the master process. In a synchronous approach this slave node would be idle until all particles of

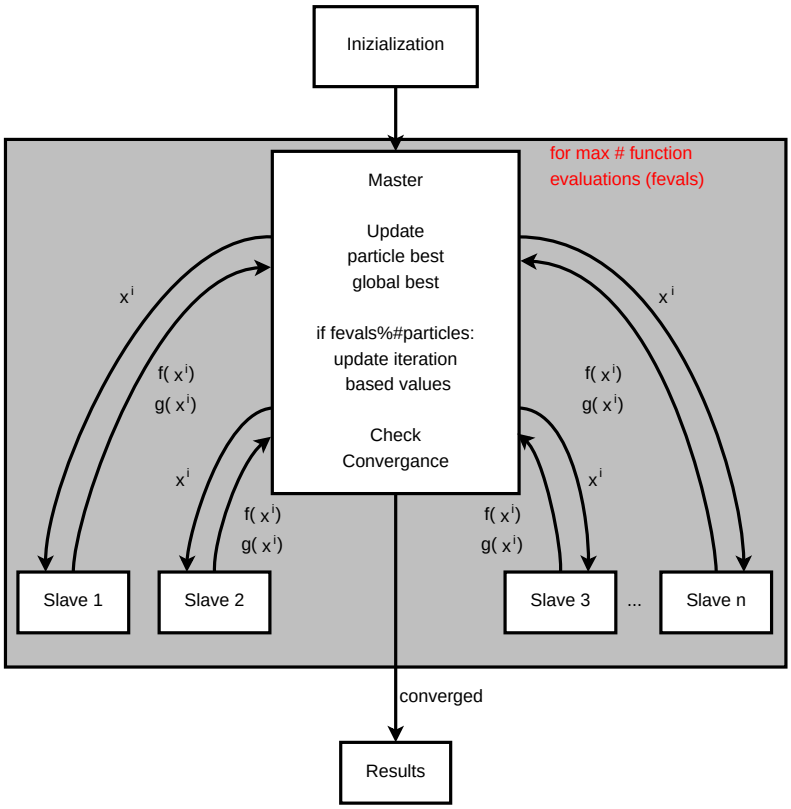

Figure B.3: Asynchronous PSO parallelization

the swarm are evaluated, while in the asynchronous approach the position and velocity of that particle is updated based on the current information available and sent to the slave process for evaluation. Some of the parameters, such as the inertial weight, may be updated based on the current number of iterations; to maintain the updating process pseudo–iterations are used, which count the number of function evaluations when the number reaches a multiple of the swarm size advances the number of iterations by one and updates values such as the interial weight.

C Quality of Performance Response Surface

The evaluation of the performance of each aircraft on each route of the two networks for each day of operation results in 525600 route performance evaluations of different payloads and ranges for each aircraft. To determine the required fuel and hence the takeoff weight for each route range and payload the performance module uses a 2D Newton method, which in turn requires several performance evaluations. This results in a higher computational burden when these evaluations are performed during the objective function evaluations in the coupled aircraft design case. To reduce the computational time two types of response surfaces can be used, the generation of aircraft polars to reduce the time required to perform the aerodynamic evaluations of each aircraft and a bi–quadratic response surface for performance. The use of these response surfaces can only be warranted if the resulting error in the performance analysis is small.

Following is an evaluation of the errors and computational time resulting from using the aerodynamic polars and quadratic response surfaces for Aircraft A1 and Aircraft C2 of the three family test case solution. The errors of Aircraft A1 are representative for the other solution aircraft, while Aircraft C2 shows the highest error values for all solution aircraft. The relative errors were calculated with respect to using the full performance and aerodynamics evaluation as described in Section 3.1.5 and Section 3.1.3, respectively.

C.1 Performance with Aerodynamic Polars

The performance evaluation uses numerical simulation during climb, cruise and descent, which combined with the analytical equations used for the takeoff and landing ground runs requires on the order of 100 calls to the aerodynamics

module. The aerodynamics module provides the aerodynamic performance of the aircraft with respect to drag for different flight conditions, Mach numbers and altitudes, and trimmed lift coefficients. The computational time for a single aerodynamics evaluation is low, since the module uses analytical and semi-empirical expressions, but the high number of calls allows for significant time savings by generating aerodynamic polars for different Mach numbers and altitudes and interpolating between those polars. Figure C.1 shows the relative errors introduced by using the aircraft polars instead of the full aerodynamics calculation in the performance evaluation over the payload range envelope for the two aircraft. The points shown within the payload range envelope are the performed departures for both networks. Table C.1 summa-

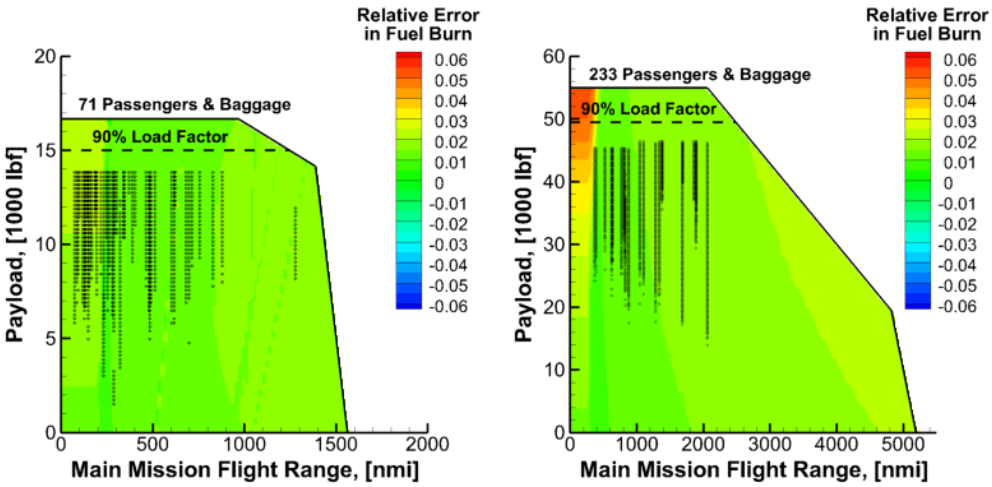

(a) Aircraft A1

(b) Aircraft C2

Figure C.1: Relative error in fuel burn over the payload range envelope when using the aircraft polars in the performance evaluation

rizes the computational time required to setup the aircraft polars and for each performance evaluation on a single core of the Beowulf cluster and the mean relative error as well as the minimum and maximum relative errors in fuel burn.

Using the aircraft polars during the performance evaluation introduces a relatively constant error of 1.5% over the payload range envelope for Aircraft A1. For Aircraft C2 the error is significantly higher in the region of zero cruise

Table C.1: Timings and error summary when using the aircraft polars in the performance evaluation

	Aircraft A1		Aircraft C2	
	Full Aero.	Aircraft Polars	Full Aero.	Aircraft Polars
Required Setup Time, [sec]	NA	1.71017	NA	2.14173
Average Time per Evaluation, [sec]	116.968	103.152 (1.134)[1]	44.141	22.633 (1.950)[1]
Relative Errors (Fuel Burn), [%]				
Mean Error	1.502		1.807	
Minimum Error	-0.249		0.677	
Maximum Error	2.384		5.525	

[1] Speed–up factor of time w.r.t. full performance and aerodynamics calculation.

range, when the range of the mission is too short for the aircraft to reach the initial cruise altitude before descending. In this region the error increases with increasing payload up to maximum of 5.52% at the maximum capacity of the aircraft. In the remaining region of the payload range envelope the relative error in fuel burn is comparable to Aircraft A1. In both cases the relative error is generally positive, hence the fuel required for the mission is over-predicted. The setup time for the aircraft polars is negligible, at around 2 seconds for each of the aircraft. The performance evaluation time for Aircraft A1 is approximately 2.5 times higher than for Aircraft C2, which can be explained by higher number of iterations during the Newton search. The speed–up provided by the aircraft polars is also very minor for Aircraft A1 at only 11% less time required for each payload range point. For Aircraft C2 the speed–up is more noticeable with a factor of almost two.

C.2 Bi-quadratic Performance Response Surface

Generating the bi-quadratic performance response surface requires only the evaluation of nine points on the payload range diagram. These points are then used to fit a two dimensional quadratic surfaces for fuel burn and flight time based on the main mission flight range and payload. When cruise range is used instead of flight range as the independent variable in generation of the response surface the 2D Newton methods reduces to a 1D method with respect to takeoff weight only. The cruise range points can then be directly related to the flight range. Figure C.2 shows the relative errors introduced by using the bi-quadratic response surface, when generated using the performance

evaluation based on the full aerodynamics calculations, on the payload range envelopes for the same two aircraft discussed above. Table C.2 summarizes relative errors and the computational time required to set up the response surfaces and the average time required for each evaluation of a payload and main mission flight range point on a single core of the Beowulf cluster.

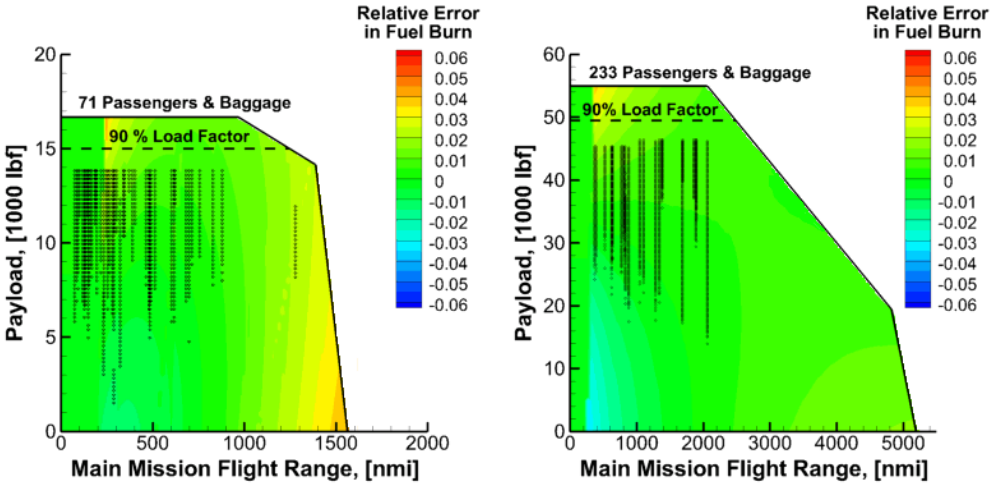

(a) Aircraft A1 (b) Aircraft C2

Figure C.2: Relative error in fuel burn over the payload range envelope when using the bi–quadratic performance response surface

Table C.2: Timings and error summary when using the bi–quadratic performance response surface

	Aircraft A1		Aircraft C2	
	Full Aero.	Response Surface	Full Aero.	Response Surface
Required Setup Time, [sec]	NA	305.216	NA	328.265
Average Time per Evaluation, [sec]	116.968	1.375×10^{-4} $(85.07\times10^{4})^{1}$	44.141	1.406×10^{-4} $(31.37\times10^{4})^{1}$
Relative Errors (Fuel Burn), [%]				
Mean Error	0.981		0.405	
Minimum Error	-1.293		-3.267	
Maximum Error	4.377		3.777	

[1] Speed–up factor of time w.r.t. full performance and aerodynamics calculation.

In both cases the region of the highest errors is just after the interface with

the region of zero cruise range at high and low payload values. In this case the response surface over-predicts the fuel burn close to the maximum payload and under-predicts close to zero payload. The overall relative errors are low with a mean value less than 1%. The maximum error for Aircraft A1 is higher than for the previous case, while it is lower for Aircraft C2. It can be noted, that most of the regions with highest absolute errors falls outside of routes that are being analyzed for the two networks, due to the 90% maximum and 30% minimum load factor constraints in the fleet allocation problem. As for using the aircraft polars, the response surface generally over-predicts the fuel required at most of the points in the payload range envelope, which results in a conservative estimation.

The setup time for each of the response surfaces is significant, especially when considering that for each set of design variables a response surface must be generated for each of the six aircraft during an objective function call in the coupled optimization cases. In the quoted setup time the sizing point of each aircraft was already calculated and was not included in the values above. The time required to evaluate a route for a given payload was only a fraction of a second in both cases, since the response surface is a simple quadratic expression compared to the iterative solution of the full performance calculation. This results in speed ups on the order of 10^5.

C.3 Aircraft Polars and Bi-quadratic Performance Response Surface

To further increase the computational speed for each objective function evaluation, the two methods can be combined. In this case, the aerodynamic polars are generated and then used during the performance evaluation of the nine points required for the response surfaces to reduce the setup time required for each aircraft. Figure C.3 shows the relative errors over the payload range envelopes when this combined approach is used and Table C.2 summarizes relative errors and timings. The setup times includes the time required to generate the aircraft polars and the time required to set up the response surfaces.

The combined approach increases the overall errors, since the error from using the aircraft polars affects the points calculated for the response surface generation. The mean errors are lower than the combined errors of the two previous approaches, with both being below 3%. The maximum and minimum

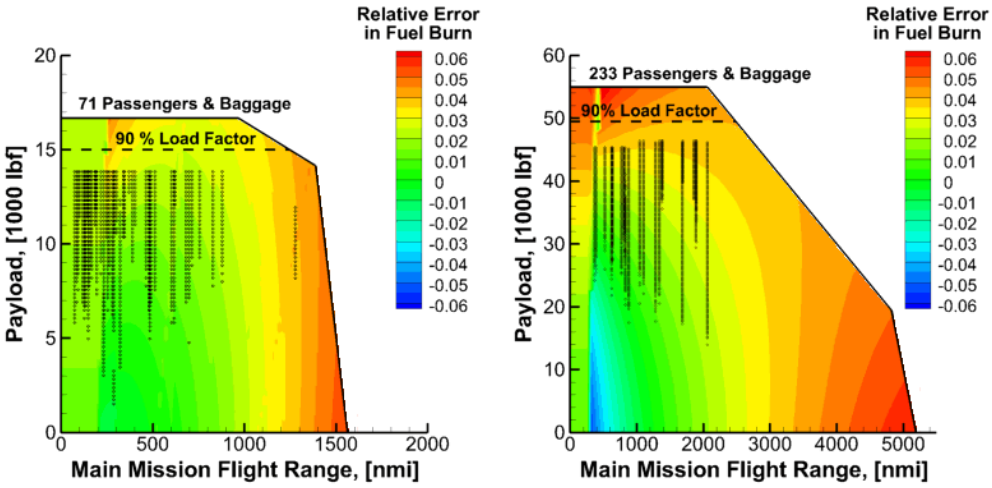

(a) Aircraft A1 (b) Aircraft C2

Figure C.3: Relative error in fuel burn over the payload range envelope when using the aircraft polars and the response surface

Table C.3: Timings and error summary when using the aircraft polars and the response surface

	Aircraft A1		Aircraft C2	
	Full Aero.	Polars and Response Surface	Full Aero.	Polars and Response Surface
Required Setup Time, [sec]	NA	30.310(10.07)[1]	NA	21.137(15.53)[1]
Average Time per Evaluation, [sec]	116.968	1.162×10^{-4} $(100.64\times10^{4})^{1}$	44.141	1.210×10^{-4} $(36.48\times10^{4})^{1}$
Relative Errors (Fuel Burn), [%]				
Mean Error		2.506		2.836
Minimum Error		-0.770		-5.380
Maximum Error		5.894		6.619

[1] Speed–up factor of time w.r.t. full performance and aerodynamics calculation.

errors are also increased. The regions of highest errors are at high payloads and at the boundaries of the payload range envelope. The majority of the routes analyzed still fall within regions of lower average errors, and even considering the maximum values, the errors are within acceptable limits during the conceptual design optimization of these aircraft. As noted before, for the majority of points the fuel required is over-predicted resulting in conservative

values during the optimization.

The increase in the errors comes at significantly lower setup times for each aircraft, on the order of 10 to 15 times faster, compared to the full performance setup, while the functional calls are on an equivalent order of magnitude as for the full performance response surface. For this work the combined approach is used during the coupled design optimization of the aircraft families and fleet allocation, due to the significantly reduced time for the setup of the polars and response surfaces and the acceptable levels of errors in the analysis.

C.4 Error Propagation

The main concern in propagating errors introduced by the performance response surfaces is in the evaluation of the direct operating cost of each aircraft on each route. The direct operating cost are one of the main deciding factor in allocating a specific aircraft type to operate the given routes in the networks, as described in Section 4.2. The direct operating cost depend on the fuel and the flight time required to perform each specific mission. Both these values can be computed using one of the performance evaluation approaches described above and each value can introduce an error in the direct operating cost calculations. The relative errors in direct operating cost calculated using fuel required and flight time values obtained from each of the response surface models over the payload range envelope of Aircraft A1 and Aircraft C2 can be found in Table C.4. The relative errors are with respect to the direct operating cost calculated using the fuel and flight time values obtained from running the full performance and aerodynamics models. The mean, minimum

Table C.4: Errors in direct operating cost when using the performance response surfaces for Aircraft A1 and Aircraft C2

	Aircraft A1			Aircraft C2		
Relative Error, [%]	Aircraft Polars	Response Surface	Polars and Response Surface	Aircraft Polars	Response Surface	Polars and Response Surface
Mean	0.485	0.779	1.261	0.643	0.315	1.471
Minimum	-0.444	-0.675	-0.667	0.217	-2.351	-4.417
Maximum	1.102	3.085	3.746	3.174	2.007	3.547

and maximum relative errors are lower than for the fuel burn alone for all the cases. The combination of errors in fuel burn and flight time does not result in increased errors in direct operating cost over the payload range envelopes.

The values of the errors follow the same trends and distributions as for the performance values, with the exception of the mean error for Aircraft A1 from using the aerodynamic polars, which has the lowest mean error in operating cost of all the different approaches. The highest errors occur when combining the aerodynamic polars and the bi–quadratic performance response surfaces, as was expected from the values obtained for the fuel burn, with average errors of 1.3 to 1.5% for the two aircraft.